Universitat de Girona

APPLICATIONS OF HYDRODYNAMIC AND WATER QUALITY MODELS TO THE SAU AND BOADELLA RESERVOIRS

Saddek TAKKOUK

ISBN: 978-84-694-5169-4
Dipòsit legal: GI-772-2011
http://hdl.handle.net/10803/31853

Application of a hydrodynamic and water qaulity models to the Sau and Boadella Reservoirs

Saddek Takkouk

Thesis work supervised by
Xavier Casamitjana Vila

January 2011

Acknowledgments

This work was supported by the former International Graduate School of Catalonia of the Government of Catalonia (IGSOC).

First of all, I would like to thank my supervisor, Xavier Casamitjana, for providing me with this opportunity and for his guidance along the way. Likewise, thanks to the Environmental Physics group members, Jordi Colomer, Teresa Serra and Marianna Soler.

I would like to thank Jörg Imberger for providing me with the model (CWR DYRESM-CAEDYM) and also Jason Antenucci for teaching me the online DYRESM-CAEDYM course.

My thanks also go to Joan Armengol of the Ecology Department of Barcelona University for providing me with Sau Reservoir data and to the Meteorologic Service of Catalonia and the Catalan Water Agency, represented by Carlos Baserba, for providing me with Boadella Reservoir data.

Also, I would like to thank the entire staff of the Physics Department for contributing to and helping me complete this thesis, especially Elena Roget, Josep Calbo, Josep González, Xisco, Eduard and Toni.

In addition, I would like to thank my wife, for her unwavering support, and my children, Mohamed Abdel Mouiz, Anfel, Afnane and Alaa Ayat Errahmane.

També vull donar les gràcies a la Universitat de Girona per haver-me acceptat en el Programa de doctorat, i a la Generalitat de Catalunya per donar-me aquesta oportunitat de finançament de l'estudi. Finalment, vull donar les gràcies a tots els catalans de la UdG, a l'associació de pares i mares de l'Escola Cassià Costal i al Grup Excursionista i Esportiu Gironí (GEiEG).

INDEX

Figure list **Pages**

Table list **Pages**

SUMMARY

Density stratification is crucial for the hydrodynamics as well as for the ecosystems functioning in almost all lakes. Most important for stratification is the temperature dependence of the water density. Stratification might change due to the meteorological effects, inflow and outflow producing the so-called ecological response of the reservoir. In recent years many physical limnology studies have been carried out in many reservoirs in the world; most of them are specifically related to water quality issues.

This PhD thesis therefore, aims to highlight an assessment of the main physical mechanisms of two medium-sized reservoirs situated in Catalonia. The focus is on the Sau and Boadella reservoirs located in Catalonia, in northeast Spain, but some of the results obtained here can be extended to other medium-sized reservoirs situated in the same region and climate. The Sau and Boadella reservoirs are both quite eutrophic in nature and supply drinking water to the area of Barcelona and Girona (Figueres). Therefore, having a better understanding of the main physical processes and the ecological response of the reservoir to such processes might be of significant help to the water management authority.

We intend to use a 1D hydrodynamic model linked with water quality (DYRESM-CAEDYM) if the conditions of application of such model which will be checked in chapter three are met. In order to characterize the dynamical regimes for the Sau and Boadella reservoirs, it is important to estimate the Wedderburn number, the Lake number, the Burger number and the inflow/outflow Froude numbers. the Wedderburn number is an indicator of the upwelling of metalimnetic water, the Lake number is an indicator of upwelling of hypolimnetic water, the Burger number characterizes the influence of the earth's rotation on the water movement in reservoirs and the inflow/outflow Froude numbers are related to the river when it enters the reservoirs and water that flows out of the reservoirs.

Sau is a canyon type reservoir, with only one tributary, the Ter River, while the Boadella has two tributaries, the Arnera and the Muga rivers. It should be mentioned that the Boadella Reservoir is used for comparison purposes. For both reservoirs, there were two years (2000-2001) available input data for the DYRESM-CAEDYM model. Simulated parameters are temperature, dissolved oxygen, dissolved inorganic phosphorus and chlorophyll. However, significant unknown river data are daily dissolved oxygen, nutrients and chlorophyll. We therefore suggest a hypothesis based on the available reservoir water quality profiles. For every month's water quality profile we take the mean concentrations of each of them and use the most repeated one as the daily river concentration input over the simulation period.

The DYRESM-CAEDYM model needs to be calibrated to get simulated values well adjusted to observed ones. The calibration process is the most difficult task due to time consuming and the large number of hydrodynamic and water quality parameters to be calibrated. For both reservoirs, the calibration process was done by trial-and-error adjustment of the most sensitive parameters in different calibration periods. The calibration process has to be done in this order: temperature, dissolved oxygen, phosphorus and chlorophyll. The last one, however, is the most difficult to calibrate because it depends on the previous calibrated parameters. Therefore, errors in the calibration process have to be accepted.

During the spring-summer season of 2000 and 2001 the Sau Reservoir stratifies and a thick metalimnion is formed. DYRESM-CAEDYM simulates temperature stratification very well. For dissolved oxygen the model gives a good simulation, indicating an anoxic zone at the bottom during the stratification period. Also, simulated soluble inorganic phosphorus has the same trend as in the field. Nevertheless, the measured inorganic phosphorus is much higher, and the reason might be the loading discharge of the phosphorus source at the bottom of reservoir, or it could be the river inflow. Even with calibration, chlorophyll simulation is the most difficult task to achieve. The simulated chlorophyll is far from the measured value in the mixed surface layer. This can be due to the fact that some phytoplankton species were not taken into consideration or to the limitation of a one dimensional model.

Meanwhile, for Boadella Reservoir the modelling exercise, for the same simulation length 2000-2001, shows that for the temperature stratification period (from spring-summer) and overturn period (through the autumn and winter), the simulated dissolved oxygen is quite similar to that predicted in the Sau Reservoir. Unfortunately, in the Boadella Reservoir there was a lack of observed data of phosphorus to comparing it with the simulated one. But simulated chlorophyll is better than in the Sau Reservoir.

In general, DYRESM-CAEDYM is a good water quality management tool since it can make accurate predictions of temperature, dissolved oxygen, and, with less confidence, phosphorus and chlorophyll.

CHAPTER 1

Introduction

1. 1 GENERAL FRAME

The eutrophication of lakes and reservoirs attributable to increase of nutrients loading particularly of nitrogen and phosphorus that can be increased algal bloom formation, which is a major water quality issue worldwide. Eutrophication is the naturally occurring process by which water bodies become more productive, changing from oligotrophic (low nutrient supply) to eutrophic (rich in nutrients) (Bayly & William 1973). This nutrient enrichment is coupled with an increase in phytoplankton growth. The most important factors controlling the growth are availability of nutrients, light and mixing conditions. Excessive abundance of phytoplankton generally has detrimental effects on the domestic, industrial and recreational uses of water bodies. During periods of algal blooms oxygen depletion occurs in the lower water column, often resulting in fish kills. Furthermore, as the algae grow and decompose, aesthetic and odour problems arise, due to the accumulation of scum on the water surface and shores (Soranno 1997). Potentially, toxic phytoplankton can be a serious health risk to humans and animals, and have been implicated with numerous poisoning incidents worldwide (Carmichael et al. 2001).

Therefore, in recent years, the study of the motion and mixing of water in lakes and reservoirs has been developed. Water hydrodynamics in these reservoirs are generated in response to surface wind stress, rotational effects, river inflow or outflow, and differential heating. The sophisticated machines with large processors made easier for us to run complex hydrodynamic models coupled with water quality models. The hydrodynamics in aquatic systems is connected with vertical stratification, that could be enhanced or weakened by chemical constituents, and depends on the interplay between the dominant disturbance forces, which are mechanisms energizing the water motion, and the restoring forces such as potential energy, sometimes the earth’s rotation, and reservoir bathymetry.

It is very important to understand the hydrodynamic of a reservoir because mixing and transport processes are of greatest importance to water chemistry and biology in reservoirs which reveals the ecological response of the reservoir to meteorological forcing, inflows and outflows (Imberger 1998) and (Imberger 1994, Imberger 1990, Fischer et al. 1979).

For this reason, evaluating aquatic management strategies for lakes and reservoirs is necessary. Several hydrodynamical and water quality models have been developed to study the seasonal dynamics amid these model, a simple empirical models that have been developed since the mid-1960's to predict eutrophication on the basis of the phosphorous (P) loading concept (Vollenweider, 1968) (see reviews by Mueller, 1982, and Ahlgren et al., 1988).

Afterward, several models have been developed following this approach. Examples include AQUASYM (Reichert, 1994), GIRL (Kmet and Straskraba, 1989) and MONOD (Karagounis et al., 1993). Finally, an approach that has been developed for 1D hydrodynamic model to include water quality parameters such as DLM-WQ , CE-QUAL-R1 (USCE, 1995), MINILAKE (Riley and Stefan, 1988), DYRESMWQ (Hamilton and Schladow, 1997), and (CE-QUALR1, MINILAKE, DYRESM-WQ, and 1-D, 3-D Dynamic Reservoir Simulation Model DYRESM, ELCOM coupled with ecological model CAEDYM these last two models were developed in the water center of the western university of Australia. Our focus is on the one dimensional hydrodynamic model DYRESM coupled with ecological model CAEDYM which is worldwide used model especially for lakes and reservoirs. Therefore, DYRESM model has been applied for Sau reservoir by (Vidal et Om. 1993), (Armengol. et al. 1994 and 2003) and (Han et al 2000) who have studied the effect of river on the longitudinal process and thermal structure in Sau reservoir. (Casamitjana. et al. 2003) used another hydrodynamic model (DLM) to study the effect of withdrawal in Boadella reservoir. (Andrew. et al. 2007) have used calibrated DYRESM to simulate boreal lake. (Louise. et al. 2006) have used DYRESM-CAEDYM to simulate seasonal dynamics of nutrient in Lake Kinneret. Also (Romero. et al. 2004) have applied DYRESM-CAEDYM and ELCOM-CAEDYM to simulate underflow through Lake Barrgorang. (Schladow et al. 1997) have employed DYRESM-CAEDYM to predict water quality in lakes and Reservoirs in part I and II. (Hmilton. et al. 1995) have applied (DYRESM-CAEDYM)

model to control the indirect effect on water quality in an Australian Reservoir. (Antenucci. et al. 2003) have examined DYRESM-CAEDYM to study the effect of artificial destratification in management strategies for a eutrophic water supply reservoir San Roque, Argentina

The present study focuses on the criteria of using such one dimensional hydrodynamic model DYRESM linked to water quality model CAEDYM. if, this criteria was checked Then could be applied to Sau and Boadella reservoirs. The major goal is to contribute to a better understanding of the main physical-ecological processes interaction and the water quality consequences affecting both of these reservoirs. Therefore, DYRESM-CAEDYM model was used to simulate water temperature, dissolved oxygen, phosphorus and chlorophyll.

1.2 STUDY SITE

1.2.1 Sau Reservoir

The Sau Reservoir was selected as the main study site and the focus of this PhD for three reasons: first, it is a good representative example of Spanish and Mediterranean reservoirs; second, it has been widely studied since it was first filled in 1964; and last, it is one of the chain of reservoirs reservoir supplying water to the capital of Catalonia. In Chapter 5 I will also study the Boadella Reservoir, which is smaler than the Sau Reservoir.

Sau is an eutrophic reservoir with incoming nutrients from the River Ter, polluted due to human activity in the watershed (Vidal and Om 1993, Armengol et al. 1994). Its eutrophication process and evolution since it was first filled have been described by Vidal (1977).

River valley reservoirs, such as the Sau Reservoir, are often large and narrow, and only receive water from a single river inflow. These reservoirs have important longitudinal changes controlled by the river intrusions across them (Hejzlar & Straškraba, 1989). Thus these reservoirs could be considered as hybrid systems between inflowing rivers and lakes (Margalef, 1983), with a progressive transformation from a river to a lake system, not only in terms of environmental variables, but also in their morphology and hydrodynamic characteristics. In general, a reservoir can be divided

along the longitudinal axis into three zones (Kimmel et al., 1990): the riverine zone, where it characterised by relatively high flow velocity; the transition zone, with moderate flow velocity; and the lacustrine zone, where the water is stagnant and the flow velocity is negligible. The riverine zone is characterized by a higher flow and consequently high Froude numbers, which is the report of inertia and gravity, short residence time and high values of nutrients and suspended solids. The transition zone, where the river meets the reservoir, is characterized by moderate velocity, moderate Froude and dissymmetric Froude numbers, high phytoplankton productivity and relatively large sedimentation. Finally, the lacustrine zone, consisting of the area near the dam, is characterised by low Froude numbers and considerable dissymmetric Froude numbers corresponding to long residence time, lower available nutrients and lower suspended matter. In response to inflow characteristics, the canyon-type morphology of the Sau Reservoir (Fig. 1.1) results in a marked longitudinal heterogeneity in the community populations (Armengol et al. 1999, Comerma 2003) and also affects the hydrodynamics. The main body of the reservoir, where the dam is located, corresponds roughly to the lacustrine zone; this zone behaves like a lake because the wind is the main forcing mechanism influencing the hydrodynamics. However the riverine and transition zones are narrow and meandering and sheltered from the wind forcing. The hydrodynamics in these zones is mainly affected by the river inflow. Of course, no strict boundaries between the zones exist and the hydrodynamics generated in one zone can affect the rest of the reservoir. Nevertheless, separating the reservoir into these zones will be useful in studying the main processes taking place in each one.

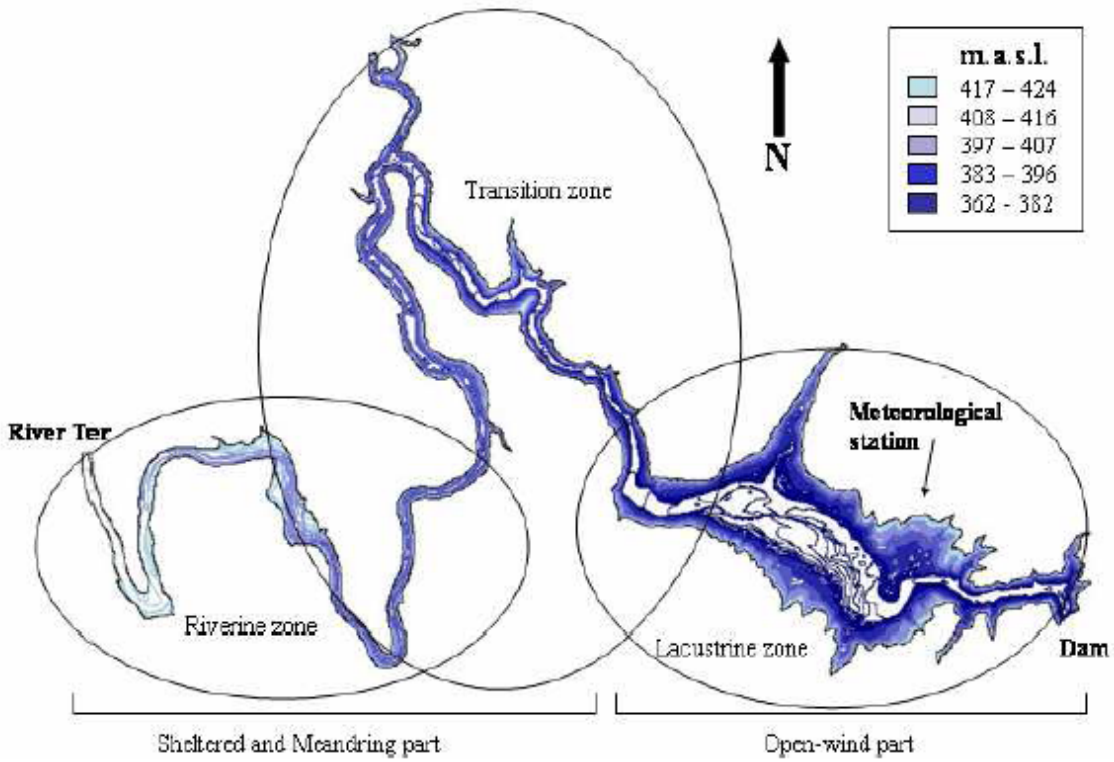

Figure 1.1 Bathymetric map of the Sau Reservoir

1.2.2 Boadella Reservoir

The Boadella Reservoir is located in the north-east of Spain in the eastern pre-pyrenees was built in response to urban growth, tourist development, intensive agriculture and the demand for drinking water is relatively small compared to Sau Reservoir. However, this last was selected in this thesis serving as a comparative one to Sau reservoir in terms of water quality. Boadella Reservoir is used for supplying water and energy power to Figueres and other small towns downstream as well was for irrigation purposes. The eutrophication of Boadella Reservoir is due the main tributary inflow in the reservoir which is polluted River Muga and the secondary inflow occurs through the Arena River (Casamitjana et al. 2003).

The difference between Boadella Reservoir (Fig. 1.2) and Sau Reservoir (Fig. 1.1) is that riverine zone of Boadella is characterised by two rivers Muga and Arena and its intersection, thus flow conditions might be differ from Sau Reservoir. Consequently, hydrodynamics in Boadella reservoir may also differ from Sau Reservoir because it is mainly affected by two river inflow.

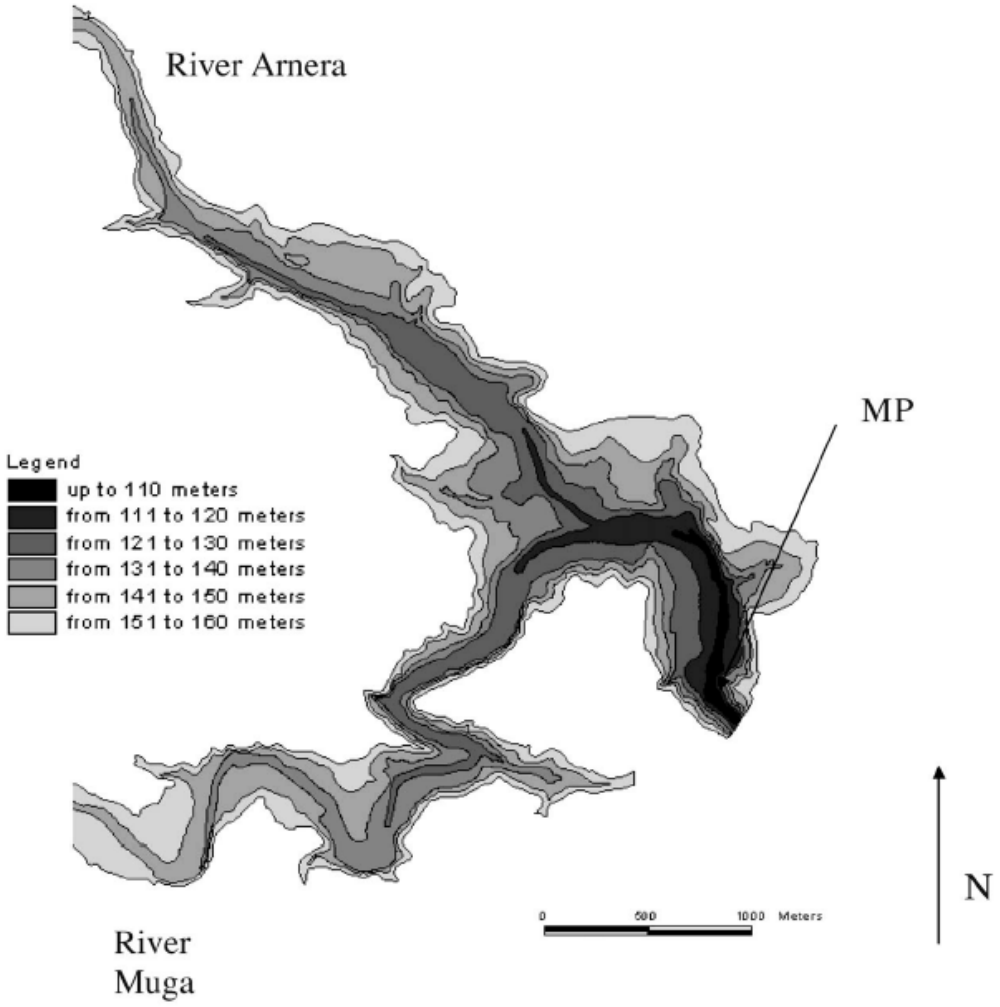

Figure 1.2 Boadella Reservoir bathymetry

1.3 SEASONAL THERMAL STRUCTURE

In general, temperate lakes and reservoirs such as those in the Mediterranean region develop thermal stratification and their water columns can be divided into three main layers: the epilimnion, the metalimnion and the hypolimnion. The hydrodynamics are directly constrained by this stratification, which tends to vertically stabilize the system and therefore reduce vertical motion and mixing processes to the extent that the input energy can overcome the internal dissipation and potential energy associated with the stratification. The main process affecting the seasonal evolution of the thermal structure is the differential heating of the water reservoir. Thus, solar radiation and longwave radiation tend to heat the water, while evaporation, sensible heat transfer and radiation from the water surface mostly cool the water. The net balance of heat sources depends not only on the season, but also on the changing meteorological conditions so that the balance can even change from hour to hour. Other dominant disturbances, such as wind, inflows and outflows, also affect the stratification. The wind and convection are the main mechanisms for mixing at the water surface, with the thickness of the epilimnion being a factor of such mechanisms (Imberger 1985, Imberger and Parker, 1985). The presence of river inflows and outflows is responsible for the main differences in the hydrodynamics and stratification of lakes and reservoirs, although some lakes are also influenced by inflows. The degree of the stratification can be affected by the inflow temperature (Straškraba 1993, Armengol et al. 1994).

The resultant stratification is the product of the surface heating/cooling and all the mixing processes occurring in the reservoir/lake. The main mechanisms of mixing are due to the effect of internal waves, inflows, outflows, wind-momentum, shear, diffusion, etc (see Fischer et al. 1979, Imberger and Patterson 1990 or Wüest and Lorke 2003). These processes are summarized in Fig. (1.3).

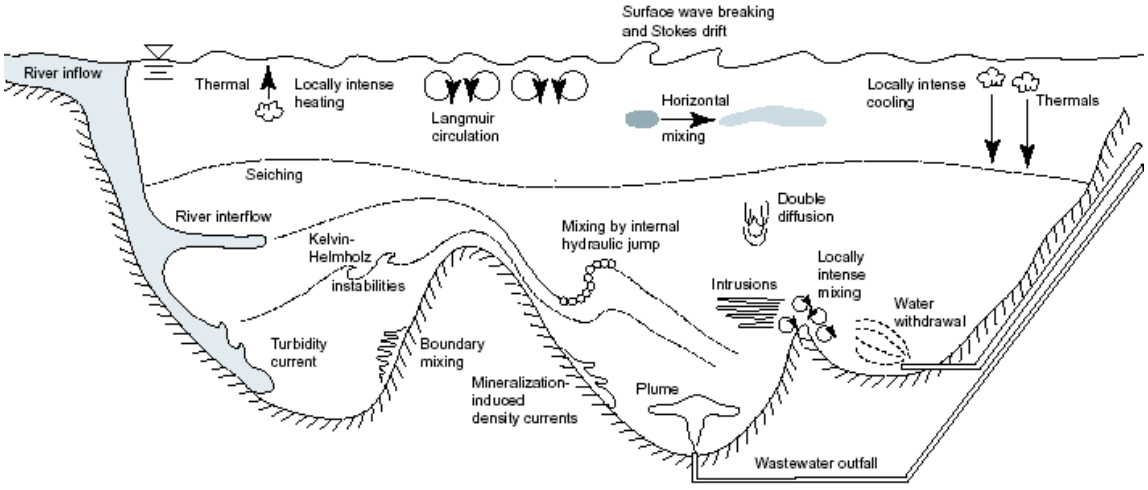

Figure 1.3 Schematic representation of mixing processes in a lake. Taken from Imboden and Wüest (1995).

Sau, like many other Spanish reservoirs, can be defined as a warm monomictic reservoir with a sharp metalimnion during the summer stratification (Armengol 1994). A description of the seasonal evolution of the thermal structure in the Sau Reservoir can be found in Han et al. (1999) where it was also simulated by the one dimensional model, DYRESM.

1.4 INFLOWS AND OUTFLOWS

1.4.1 Inflows

The action of the inflow and outflow is to cause vertical displacement of the horizontal water slabs. Since, incoming nutrients or contaminants come from rivers. Thus, river inflow entering a lake, reservoir, or coastal region often has a different density than that of the receiving ambient water. The main differences in the density are due to temperature as well as the concentration of dissolved and suspended solids. When the inflowing water has a different density than the ambient water, the water flows into the receiving ambient water until a balance is reached between the momentum of the inflowing water and the baroclinic pressure that results from the density difference. When the inflowing water is less dense than the ambient water, it separates from the bottom up and goes over the surface of the ambient water, generating an overflow. In the case of inflows with a higher density than the ambient water, the inflow plunges under the surface to form a gravity-driven density current, along the bottom, downward up to the level of neutral buoyancy where it inserts (interflow) or to the bottom of the basin (underflow) (See Fig. 1.4). The region previous to the overflow or underflow plunge is momentum-dominated while in the region after the plunge

occurs the density current becomes buoyancy-dominated. On the way towards the dam, mixing occurs and water of the ambient body entrains into the inflow, a process defined as entrainment; at the same time, water from the inflow entrains into the ambient water, a process defined as detrainment. Entrainment implies a flow of ambient water into the turbulent layer generated in the boundary of the inflow and the ambient layer, as in a free shear region. Ellison and Turner (1959) suggested that the velocity of the inflow into the turbulent region must be proportional to the velocity of the layer, with the constant of proportionality being the so called entrainment constant.

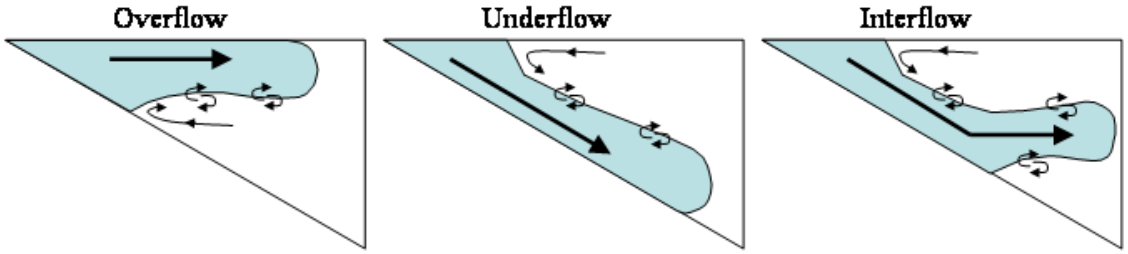

Figure 1.4 Inflow dynamics

1.4.2 Outflows

Outflows constitute the main difference between a lake and a reservoir. Commonly, reservoirs are provided with outlets at different levels so that the reservoir can be used to control the temperature of the outflowing water and/or other water quality parameters. Such control allows the operators to select the type of water for specific necessities, for example, cold water for fish or warm water for irrigation.

The effect of selective withdrawal also directly affects the stratification by sharpening the thermocline where the outlet is located (Casamitjana et al. 2003, Martin and Arneson, 1978). When the fluid is stratified, the outflow is influenced by the buoyancy force. When the outlet structure is open, it generates pressure that instantaneously sets up a radial flow pattern towards the outlet. However, such radial convergence near the sink quickly distorts the isopycnals. Buoyancy forces initiate a set of internal waves that propagate upstream (Kataoka et al. 2001) and adjust the isopycnals back to a horizontal neutral position and the initial radial flow collapses into a jet-like structure (Fig. 1.5).

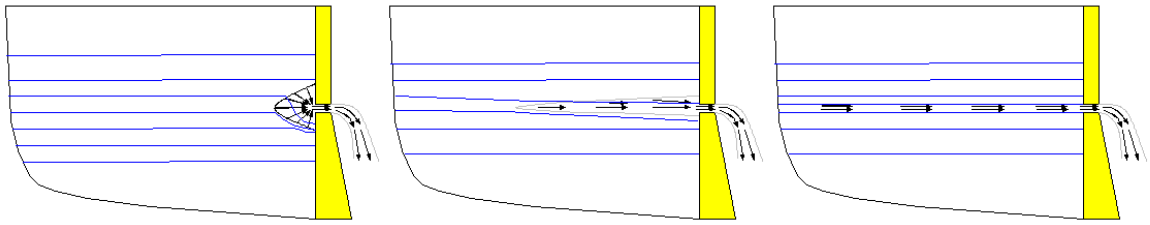

Figure 1.5 Evolution of the outflow from the opening of the outlet to the generation of the jet flow. Blue lines represent isopycnals.

Selective withdrawal also depends on the outlet characteristics (line or point sink) and stratification type (linear, two-layered, etc). A review of such processes can be found in Imberger and Paterson (1990). However, we will focus on the effect of the withdrawal on the stratification. The Sau Reservoir usually presents a thick thermocline, so the outlet structure affects such a stratification by sharpening the gradient at the level at which the outlet is placed (Fig. 1.6).

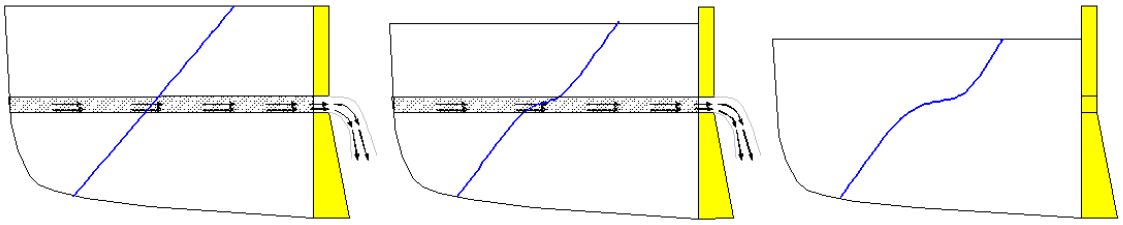

Figure. 1.6 Stratification process due to the water withdrawal from a selective outlet. The blue line indicates the temperature profile evolution and the shadowed area indicates the sink line.

1.5 LAKE REGIME CLASSIFICATION

The thermal regimes of the lake are classified as a function of altitude, latitude and bathymetry such as mean depth and surface area. However in recent years the classification schemes have been developed with a help of non-dimensional parameters such as Froude, Wedderburn, and lake number. Froude number estimated as inertia and gravity ratio. Wedderburn number defined as baroclinic restoring force and disturbance wind force ratio. Lake number which is given as the ratio of gravity and wind force. In terms of water quality, the lake number provides an excellent variable against which dissolved oxygen and metals may be correlated (Robertson and Imberger 1994) and the inflow Froude number can be related to algal growth species. The weakness of such non-dimensional parameters is that they are based on a steady state scenario, which of course is rarely the case; the wind, the inflow and outflow are all functions of time and the resulting dynamical regimes are strongly dependent on this time variability. However, these numbers do serve to put into context the relative strengths of competing influences. Such a comparison leads to an understanding of whether a particular lake is strongly or weakly influenced by particular external meteorological conditions. For more details of non-dimensional numbers, see Chapter 3.

1.6 OBJECTIVES

The aim of this PhD thesis is to model the hydrodynamic processes and water quality behaviours of the Sau and Boadella reservoirs.

This thesis focuses on how hydrodynamics affects nutrients and phytoplankton community dynamics. The resultant thermal stratification in a reservoir can be related to physical processes, and, therefore, the importance of such processes is obvious. The aim of this PhD thesis is to give better understanding the response of two reservoirs with special emphasis on those that affect into the water quality. Essentially, this thesis focuses on examining the ecological response of the Sau and Boadella reservoirs by using a 1D hydrodynamic model (DYRESM) combined with a water quality model (CAEDYM). The chapters are arranged in a logical order, starting with an introduction, data analysis and field experiments, checking criteria for using the 1D hydrodynamic model for the two reservoirs, applying the DYRESM-CAEDYM to the Sau Reservoir, and finally trying to use the same models to another reservoir which is Boadella Reservoir.

- **Chapter 1** in this chapter we introduce one important reservoir which is Sau Reservoir and another small Reservoir which is Boadella Reservoir. A short description of DYRESM and CAEDYM models and equations that has been used in both of them. The purpose of the models is to provide a quantitative description of the interactions that occur between physical and ecological processes, and the water quality consequences of these interactions.

- **Chapter 2** describes the available data that has been used as input to the hydrodynamic and water quality models for both reservoirs. These data are meteorological data, daily inflow/outflow data, bathymetry data, temperature profiles and water quality profiles such as dissolved oxygen, nutrients, and chlorophyll. The entire data field has been analysed to see how the lack of such data might complicate the calibration process.

- **Chapter 3** evaluates the possibilities and limitations of using a one dimensional hydrodynamic model to the Sau and Boadella reservoirs, investigating numbers such as the Lake number, the Wedderburn number, the Burger number, and the inflow and outflow Froude numbers. The objective of this chapter is to evaluate these numbers and identify their magnitude compared to critical values, thereby establishing the difference between these numbers for the two investigated reservoirs and observing the influences on the diagnostic regime of each one.

- **Chapter 4** describes the application of Dynamic Reservoir Model (DYRESM) linked with Computational Aquatic Environmental Dynamic Model (CAEDYM) to the Sau reservoir. The simulation length is a two year period (2000-2001). The simulations parameters are temperature, dissolved oxygen, inorganic phosphorous, and chlorophyll. The specific objective is to see how the Sau Reservoir behaves in response to the one dimensional hydrodynamic model linked with the water quality model, comparing the simulated parameters with field values. Also, the DYRESM and CAEDYM models have been calibrated to diminish the gap between simulated and field values.

- **Chapter 5** is an attempt to apply and validate the same DYRESM-CAEDYM model to the Boadella Reservoir, located in the same region. The main objective here was to compare the simulation results for the Boadella Reservoir with those of the Sau Reservoir. However, there was a big gap in the data sets for the Boadella Reservoir, especially for the soluble reactive phosphorus. Therefore, the phosphorus case will be dropped and the simulation comparison restricted to temperature, dissolved oxygen, and chlorophyll.

All in all, this PhD thesis aims to provide the reader with a global vision of the dynamic regime of a reservoir by applying 1D dimensional hydrodynamic models (DYRESM) linked with a water quality model (CAEDYM) to two Mediterranean reservoirs such as Sau and Boadella.

1.7 METHODS

1.7.1 DYRESM description

A brief description of the models that will be used throughout this thesis: the DYRESM 1D model, the CAEDYM water quality model. However, for further details, the reader is referred to the corresponding science manuals (Antenucci and Imerito 2000), (Romero et al. 2004), and (Hodges and Dallimore 2006 and Hipsey et al. 2005) available at the CWR web page (www.cwr.uwa.edu.au/~ttfadmin/). Thus,

DYRESM (Dynamic Reservoir Simulation Model) is a one-dimensional hydrodynamic model for lakes and reservoirs. The DYRESM was developed in Australia by the CWR (Center for Water Research) of the UWA (University of Western Australia). The model is used to predict the variation of water temperature and salinity with depth in space and time. The DYRESM model is based on an assumption of one dimensionality; that is, the variations in the vertical direction play a more important role than those in the horizontal direction. The reservoir is therefore represented by a series of horizontal water layers. The lateral or longitudinal variation in the layers is neglected. The mixed-layer approach for the DYRESM model is based on the mixing energy budgets developed by Imberger and Patterson (1981), Spigel et al. (1986), and Imberger and Patterson (1990). In DYRESM three mechanisms are available for surface layer mixing: stirring (energy from wind stress), convective overturn (decrease in potential energy), and shear (transfer of kinetic energy from the upper to the lower layer). Additionally, DYRESM can be linked to the CAEDYM water quality model. The coupled DYRESM-CAEDYM model is used in reservoirs to predict temperature, salinity, and water quality indicators such as dissolved oxygen, nutrients, and chlorophyll. For more details see the DYRESM Science Manual. The data preparation and simulation process for the DYRESM model (see Chapter 2) are meteorological, morphometry, Inflow/ Outflow, initial profile, parameters data file, and configuration data file. The major governing equations and symbols used for one dimensional hydrodynamic model are grouped in Table 1.1 and Table 1.2 and described below.

Surface flux of momentum

$$\tau = \rho_A C_E U^2$$

Surface flux of sensible heat

$$H = -\rho_A C_P C_H \left(T_A - T_S\right)$$

Surface flux of evaporative heat

$$E = -\rho_A C_W U \left(q_A - q_S\right)$$

Shortwave radiation distribution over depth

$$Q(h) = Q_0 e^{-\eta h}$$

Longwave radiation input to surface layer

$$LW0 = \zeta T_K^4$$

Available kinetic energy of surface layer

$$KE_A = \frac{C_K}{2}\left(w_*^3 + \psi^3 u_*^3\right)\Delta t + \frac{C_S}{2}\left[u_{1_1}^2 + \frac{u_1^2}{6}\frac{d\delta}{dh} + \frac{u_1 \delta}{3}\frac{du_1}{dh}\right]h'$$

Required potential energy of surface layer

$$PE_R = \left[\frac{C_T}{2}\left(w_*^3 + \psi^3 u_*^3\right)^{2/3} + \frac{\Delta\ \rho g h}{\rho_0} + \frac{g\delta 2}{24\rho_0}\frac{d(\Delta\rho)}{dh} + \frac{g\Delta\rho\delta}{12\rho_0}\frac{d\delta}{dh}\right]h'$$

River inflow entrainment

$$En = \frac{3}{4}\left[\frac{5\tan\phi}{F_i^2} - \frac{5C_D}{\sin\beta}\right]\frac{F_i^2}{\left(3F_i^2 + 2\right)}$$

Grashof number

$$Gr = N^2 L^4 / \nu^2$$

Froude number

$$F = Q/\ \ NL^2$$

Outflow withdrawal velocity

$$u = 0.5u_0(1 - \frac{x}{L})\left[1 + \cos\pi\frac{\left(z - z_0\right)}{\lambda}\right]$$

Hypolimnetic diffusivity

$$D_z = \frac{\alpha\varepsilon}{N^2 + k_0^2 u_*^2}$$

Brunt- Väisälä frequency

$$N^2 = -\frac{g\partial\rho}{\rho\partial z}$$

Dissipation

$$\varepsilon = \langle\varepsilon\rangle for \quad z \geq H_t - h_1$$

$$\varepsilon = \langle\varepsilon\rangle \exp\left[-\frac{H_t - h_1 - z}{\sigma}\right]^2 for\ z\ \langle\ H_t - h_1$$

Table 1.1 Summary of the governing equations in DYRESM.

A	layer surface area
C_E, C_H, C_w	process-specific bulk aerodynamic transfer coefficients
C_D	stream drag coefficient
$\mathbf{C}_p$	specific heat capacity of water
D_z	turbulent diffusivity coefficient
E	evaporative heat flux
En	inflow entrainment coefficient
F_i	internal Froude number
F	Froude number
g	acceleration due to gravity
Gr	Grashof number
h	layer thickness
h’	depth of layer immediately below surface layer
h_1	depth from the lake bottom to the centre of area of the N^2 distribution
H	sensible heat flux
H_1	total depth of water
ko	wave number of the largest eddies
KE_A	available turbulent kinetic energy in the surface layer
L	length of lake at inflow insertion height
LW_o	incoming longwave radiation
N	buoyancy frequency of stream inflow
N	Brunt-Väisälä frequency
PE_R	required potential energy for mixing in the surface layer
q_A	specific humidity of air
q_s	specific humidity of water surface
Q	volume flux of the insertion
Q_0	shortwave radiation flux at the top of a layer
ρ	water density
ρ_0	reference density
T_A	air temperature
T_S	surface water temperature
τ	wind shear stress
μ	withdrawal velocity
μ_1	shear velocity at the bottom of the surface layer
μ_*	turbulent velocity scale for wind shear
μ_0	maximum withdrawal velocity
U	wind speed
w_*	turbulent velocity scale for penetrative convection
x	horizontal distance relative to the centre of the offtake
z	vertical distance relative to the centre of the offtake
z_0	height of the offtake

Table 1.2 List of Hydrodynamic symbols

α	constant related to the mixing efficiency of the turbulence
β	half angle of river cross-section
δ	Kelvin-Helmholtz billow thickness scale
$\Delta\rho$	density jump across bottom of surface layer
Δt	time step
ε	dissipation
ϕ	river bed slope
η	light extinction coefficient
λ	withdrawal layer thickness
σ	first moment distance of the N^2 distribution below h_l
ν	kinematic viscosity
ψ, C_K, C_T *and* C_S	process-specific parameters for mixing efficiency
ζ	Stefan-Boltzmann constant

Table 1. 2 (continued) List of Hydrodynamic symbols

Surface thermodynamics and mass fluxes

The surface exchanges include heating due to shortwave radiation penetration into the lake and the fluxes at the surface due to evaporation, sensible heat (i.e. convection of heat from the water surface to the atmosphere) and longwave radiation. Shortwave radiation (280nm to 2800nm) is usually measured directly. Longwave radiation (greater than 2800nm) emitted from clouds and atmospheric water vapour can be measured directly or calculated from cloud cover, air temperature and humidity.

Solar (shortwave) radiation flux - The depth of penetration of shortwave radiation depends on the net shortwave radiation that penetrates the water surface and the extinction coefficient. The net solar radiation penetrating the water can be written as:

$$Q_{sw} = Q_{sw(total)}(1 - r_a^{(sw)}), \tag{1.1}$$

where $Q_{sw(total)}$ is the shortwave radiation that reaches the surface of the water, Q_{sw} is the net shortwave radiation penetrating the water surface, and $r_a^{(sw)}$ is the shortwave albedo. Once the shortwave radiation has penetrated the water surface, it penetrates deeper following the Beer-Lambert law, such that

$$Q(z) = Q_{sw} e^{-\eta_a z}, \tag{1.2}$$

where z is the depth below the water surface and η_a is the attenuation coefficient. Thus the shortwave energy per unit area entering layer k through its upper surface is

$$\Delta Q_k = Q_k - Q_{k-1} \tag{1.3}$$

Long wave energy flux - The longwave radiation is calculated by one of three methods, depending on the input data. Three input measures are allowed: (a) incident longwave radiation, (b) net longwave radiation, and (c) cloud cover. The net longwave radiation energy deposited onto the surface layer for a period Δt is calculated as:

$$\text{(a) } Q_{lw} = (1 - r_a^{(lw)}) Q_{lw(incident)} - .\varepsilon_w \sigma T_w^4, \tag{1.4}$$

by using incident longwave radiation; where $r_a^{(lw)}$ is the albedo for longwave radiation, which is taken as a constant = 0.03 (Henderson-Sellers, 1986), ε_w is the emissivity of the water surface (=0.96), σ is the Stefan-Boltzmann constant (σ = 5.6697x10 - 8Wm^{-2}K^{-4}), and *Tw* is the absolute temperature of the water surface (i.e. the temperature of the surface layer).

$$\text{(b) } Q_{lw} = (1 - r_a^{(lw)}) Q_{lw(net)}, \tag{1.5}$$

by using net longwave radiation, and

$$\text{(c) } Q_{lw} = (1 - r_a^{(lw)})(1 + 0.17C^2).\varepsilon_w(T_a)\sigma T_a^4 - .\varepsilon_w \sigma T_w^4, \tag{1.6}$$

where C is the cloud cover fraction ($0 \le C \le 1$), ε_w = 9.37x10-6K^{-2}, and $.\varepsilon_w(T_a) = C.\varepsilon_w T_a^2$.

Sensible heat flux - The sensible heat loss from the surface of the lake for the period Δt may be written as (Fischer et al. (1979))

$$Q_{sh} = C_s \rho_a C_P U_a (T_a - T_s) \Delta t , \tag{1.7}$$

where C_s is the sensible heat transfer coefficient for wind speed at a reference height of 10 m above the water surface (= 1.3×10^{-3}), ρ_a the density of air in kg m^{-3}, C_P the specific heat of air at constant pressure (= 1003 J kg^{-1} K^{-1}), U_a is the wind speed in m s^{-1} at the 'standard' reference height of 10 m, with temperatures either both in Celsius or both in Kelvin.

Latent heat flux - The evaporative heat flux is given by Fischer et al. (1979) as

$$Q_{lh} = \min\left(0, \frac{0.622}{P} C_L \rho_a L_E U_a (e_a - e_s(T_s)) \Delta t\right), \tag{1.8}$$

where P is the atmospheric pressure in pascals, C_L is the latent heat transfer coefficient (=1.3×10^{-3}) for wind speed at a reference height of 10m, ρ_a the density of air in kg m^{-3}, L_E the latent heat of evaporation of water (= 2.453x106 J kg^{-1}), U_a is the wind speed in ms^{-1} at the reference height of 10m, e_a the vapour pressure of the air, and e_s the saturation vapour pressure at the water surface temperature T_S. Both vapour pressures are measured in pascals.

Thus, the total non-penetrative energy density deposited in the surface layer during the period Δt is given by

$$Q_{non-pen} = Q_{lw} + Q_{sh} + Q_{lh} \tag{1.9}$$

Surface mass fluxes - The surface mass fluxes are based on a balance between evaporation and rainfall, changing the mass of the surface layer cells.

7.2 CAEDYM description

CAEDYM is an aquatic ecological model designed to be readily linked to hydrodynamic models, which currently include the 1D DYRESM model. The coupling between CAEDYM and the hydrodynamic driver is dynamic; specifically, the thermal structure of the water body is dependent on the water quality concentrations by feeding back through water clarity.

The model includes comprehensive process representation of the C, N, P, Si and DO cycles, several size classes of inorganic suspended solids, and phytoplankton dynamics. Numerous optional biological and other state variables can also be configured. Hence, CAEDYM is more advanced than traditional N-P-Z models, as it is a general biogeochemical model that can resolve species- or group-specific ecological interactions. CAEDYM operates on any sub-daily time step to resolve algal processes (diurnal photosynthesis and nocturnal respiration), and is generally run at the same time interval as the hydrodynamic model. Algorithms for salinity dependence are included so that a diverse range of aquatic settings can be simulated. The user can prescribe in water quality configuration file depending on whether the simulation is for freshwater, estuaries or coastal waters.

Fig. 1.7 represents the major biogeochemical state variables in CAEDYM. The existing configuration file allows users to customize the model elements needed in any simulation. Parameters are introduced as an input file, so users do not doesn't need to modify the source; but, inevitably, users may define variables not represented in CAEDYM, thus some modifications to the source may be needed. For a more detailed description, the reader is referred to the CAEDYM Science Manuals (Romero Hipsey, Antenucci, and Hamilton 2004) available on the CWR web page (www.cwr.uwa.edu.au/).

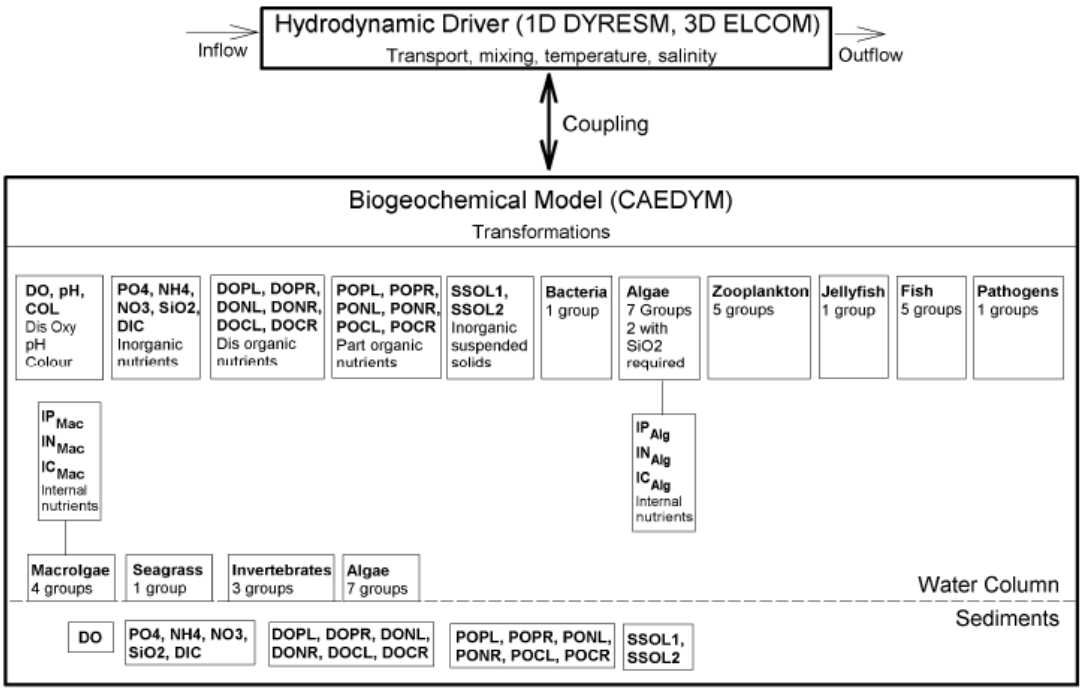

Figure 1.7 Summary of the biogeochemical paths simulated in CAEDYM.

CAEDYM simulates the *C, N, P, DO* and *Si* cycles with inorganic suspended solids, phytoplankton and optional biotic compartments such as zooplankton, fish, bacteria and others. The Model is divided into sub-routines or sections. Next we will see an overview of the main simulated variables.

Light

The shortwave incident radiation supplied by the hydrodynamic driver (DYRESM) is converted to the photosynthetically active component (*PAR*) based on the assumption that 45% of the incident spectrum lies between 400-700 nm (Jellison and Melack, 1993). *PAR* is assumed to penetrate into the water column according to the Beer-Lambert law with the light extinction coefficient dynamically adjusted to account for variability in the concentrations of algal, inorganic and detrital particulates, and dissolved organic carbon levels. The ultra-violet component of the incident light can also be used to look at pathogen inactivation and organic matter photolysis.

Inorganic Particles

Two inorganic particles groups (*SS*) can optionally be included within the simulation, with each group assigned a unique diameter and density, and modelled as a balance between resuspension and settling. Adsorption and desorption of aqueous-phase Fraction Reactive Phosphorous *FRP* , NH_4 , Particulate Inorganic Phosphorous (*PIP)* and Particulate Inorganic Nitrogen (*PIN*) can also be configured. Particle settling is modelled on the basis of Stokes law. The inorganic particles are now being updated to six groups.

Sediments and Resuspension

CAEDYM maintains the mass balance of all simulated variables in both the water column and a single sediment layer; providing a complete description of the dominant pools of sediments fluxes in the water column to maintain mass conservation. The sediment fluxes of dissolved inorganic and organic nutrients are based on empirical formulations that account for environmental sensitivities and require laboratory and field studies. (Taken from www.cwr.uwa.edu.au/).

Resuspension of inorganic (*SS*) and organic particles (*POM*) from the sediment-water interface require a number of parameters including the critical shear stress and the resuspension rate constant. The composition of the sediments is established in the CAEDYM initial conditions file.

Dissolved Oxygen

Dissolved Oxygen (*DO*) dynamics within CAEDYM are of forms of atmospheric exchange, the sediment oxygen demand (*SOD*), microbial use during organic matter mineralization and nitrification, photosynthetic oxygen production and respiratory oxygen consumption, and respiration by other optional biotic components. Microbial activity facilitates the breakdown of organic carbon (in particular, *DOC*) to CO_2, and a stoichiometrically equivalent amount of oxygen is removed. The process of nitrification also requires oxygen that is dependent on the stoichiometric factor for the

ratio of oxygen to nitrogen ($Y_{O2:N}$) and the half saturation constant for the effect of oxygen limitation (K_{NIT}). Photosynthetic oxygen production and respiratory oxygen consumption are summed over the number of simulated phytoplankton groups. (See Fig. 1.8.)

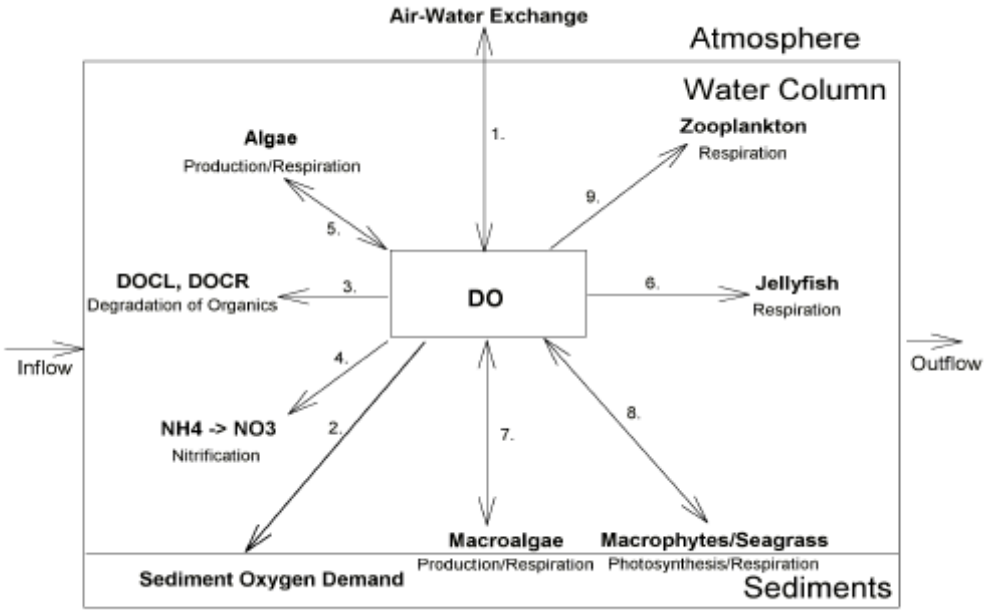

Figure 1.8 Simplified schematic of the DO Dynamic within CAEDYM

Carbon, Nitrogen, Phosphorus and Silica

The cycles of simulated nutrients account for both inorganic and organic, and dissolved and particulate forms of *C, N* and *P*, along the degradation pathway of *POM* to *DOM* to dissolved inorganic matter (*DIM*). Nitrogen includes denitrification, nitrification and N_2 fixation. *Si* is included for the uptake of diatoms into the dissolved form. The *C* cycle includes atmospheric fluxes of CO_2 based on the partial pressure of CO_2 differences (pCO_2). See Fig. 1.9 for the schematic representation of the generic configuration of CADEYM.

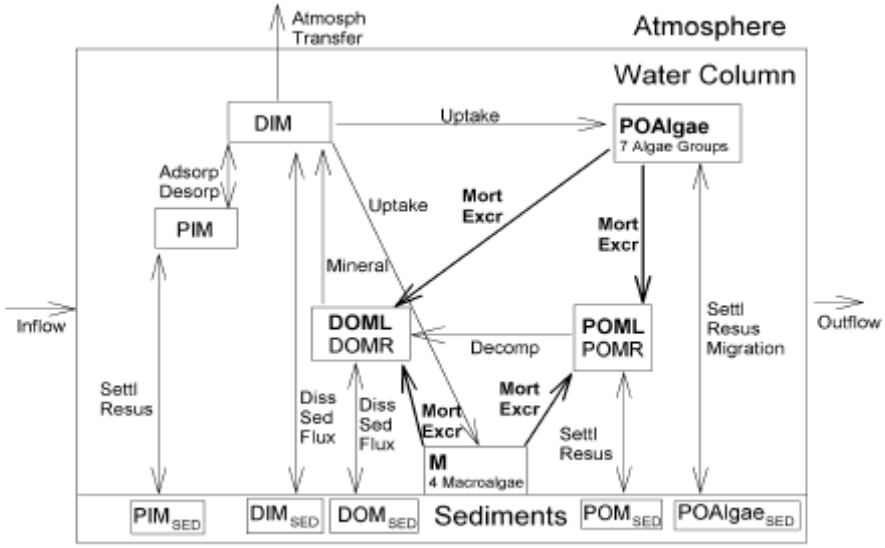

Figure 1.9 Generic schema of the nutrient dynamics with CAEDYM

Phytoplankton Dynamics

Up to seven phytoplankton groups can be simulated with CAEDYM. The algal biomass can be simulated either in *chla* (*μg chla* L^{-1}) or carbon (mg C L^{-1}). The growth rate is calculated based on the maximum growth rate for every species multiplied by the temperature factor and the minimum value of expressions for limitation by light or nutrients. Phytoplankton may be grazed by zooplankton, fish and clams. Light limitation on phytoplankton growth can be configured to be subject to photoinhibition or to be non-photoinhibited.

Nutrient dynamics within algae can be simulated by using a constant nutrient to *chla* ratio or by dynamic intracellular stores. The first is based on the simple Michaelis-Menten equation used to model nutrient limitation with the half saturation constant for the effect of external nutrient concentrations. The metabolic loss of nutrients from mortality and excretion is proportional to a constant multiplied by the loss rate and the fraction of excretion and mortality that returns to the detrital pool. The second model uses dynamic intracellular stores that can regulate growth. This model allows for the phytoplankton to have variable internal nutrient concentrations with dynamic nutrient uptake bounded by minimum and maximum values. Nutrient losses are calculated from internal nutrient concentrations.

Loss terms for respiration, natural mortality and excretion are modelled with a single respiration rate coefficient. This loss rate is then divided into the pure respiratory fraction and losses due to mortality and excretion. The constant f_{DOM} is the fraction of mortality and excretion going to the dissolved organic pool with the remainder going into the particulate organic pool. In (Fig. 1.10) is represented CAEDYM Phytoplankton dynamics

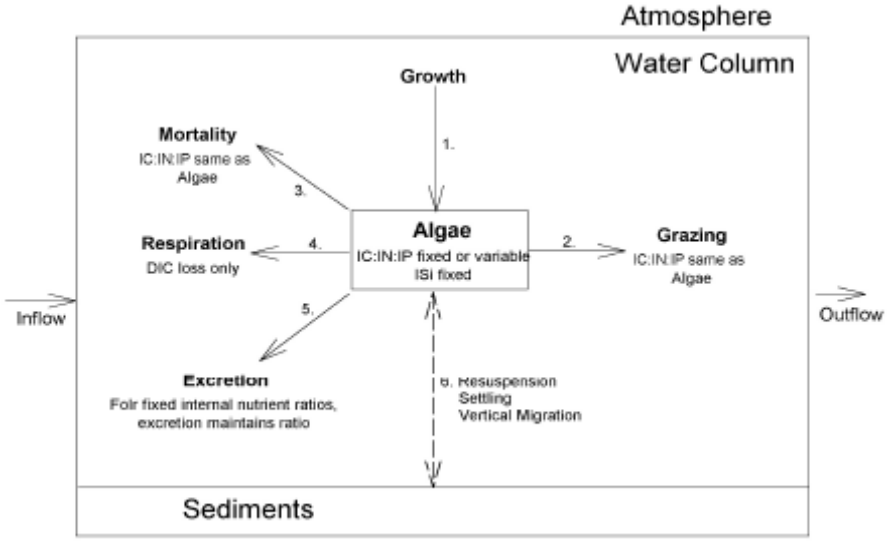

Figure 1.10 Phytoplankton dynamics within CAEDYM

Bacteria

Bacterial biomass and organic matter mineralization may also be simulated. The bacteria are prescribed a fixed C:N:P ratio that is constant over the course of simulation. The incoming nutrients, primarily received from a dissolved organic matter pool, are converted to CO_2, NH_4 and *FRP* and released back to the water column.

Zooplankton

CAEDYM assumes each zooplankton group has a fixed *C:N:P* ratio and, depending on the *C:N:P* ratio of the various food sources, the groups balance their internal concentration by excretion of labile dissolved organic matter. The grazing preference of each group is user defined, and can be for any of the simulated algal, zooplankton, bacterial or detrital groups. Faecal pellets can also be specified as either hard, soft or in between, and lost to the sediment or returned to the detrital pool.

Higher biology

CAEDYM is able to model higher organisms such as fish, jellyfish, and benthic organisms including macroalgae, benthic macroinvertebrates and clams/mussels.

Pathogens and Microbial Indicator Organisms

CAEDYM has an optional pathogen model for users interested in simulating microbial pollution in a lake, reservoir, estuary or coastal environment. The model was developed based on *Cryptosporidium* sp. dynamics and also contains variations for simulating indicator organisms such as coliform bacteria.

Governing Equations

The main equations used in CAEDYM for the biogeochemical paths are summarized in Table 1.3. Likewise a list of symbols and variables used are summarized in Table 1.4.

Table 1.3

Major equations used in CAEDYM

Rate of change of phytoplankton concentration (mg chl $a\,m^{-3}$ per day)	$\frac{\delta C_i}{\delta t} = (\mu_i - R_i)C_i + V_i + H_i$
Phytoplankton growth rate (per day)	$\mu_i = \mu_{\max i} f_i(T) f_i(S) \min\left[f_i(N), f_i(P), f_i(I), f_i(Si)\right]$
Phytoplankton respiration and mortality rate (per day)	$R_i = \frac{k_{Ri}\vartheta_i^{T-20}}{f_i(S)}$
Temperature limitation	$f_i(T) = \psi_i^{T-20} + \psi_i^{d_i(T-a_i)} + b_i$ (Griffin et al., 2001)
Light limitation	$f_i(I) = \begin{cases} (I/I_S)\exp(1 - I/I_S), & \text{photoinhibited(freshwaterdiatoms)} \\ 1 - \exp(-I/I_{ki}), & \text{non-photoinhibited(othergroups)} \end{cases}$
Nitrogen limitation	$f_i(N) = \frac{\mathrm{IN}_i}{\mathrm{IN}_{\max i} - \mathrm{IN}_{\min i}}\left(1 - \frac{\mathrm{IN}_{\min i}}{\mathrm{IN}_i}\right)$
Phosphorus limitation	$f_i(P) = \frac{\mathrm{IP}_i}{\mathrm{IP}_{\max i} - \mathrm{IP}_{\min i}}\left(1 - \frac{\mathrm{IP}_{\min i}}{\mathrm{IP}_i}\right)$
Silica limitation	$f_i(\mathrm{Si}) = \begin{cases} \frac{\mathrm{Si}}{\mathrm{Si} + K_{Si}}, & \text{diatoms} \\ 1, & \text{other groups} \end{cases}$
Salinity limitation (freshwater species: *M. aerugnosa*, chlorophytes and freshwater diatoms)	$f_i(S) = \begin{cases} 1, & S \le S_{\mathrm{opi}} \\ \frac{(S_{\max i} - S_{\mathrm{opi}})^2}{(S_{\max i} - S_{\mathrm{opi}})^2 - (\beta_i - 1)(2S_{\mathrm{opi}}S - S^2 - S_{\mathrm{opi}}^2)}, & S > S_{\mathrm{opi}} \end{cases}$
Salinity limitation (marine species: marine diatoms and dinoflagellates)	$f_i(S) = \begin{cases} 1, & S > S_{\mathrm{opi}} \\ \frac{S_{\mathrm{opi}}^2}{(S^2 - 2S_{\mathrm{opi}})(\beta_i - 1) + \beta_i S_{\mathrm{opi}}^2}, & S \le S_{\mathrm{opi}} \end{cases}$
Rate of change of nitrate concentration (mg N m^{-3} per day)	$\frac{\partial \mathrm{NO_3}}{\partial t} = -\sum((1 - P_{\mathrm{Ni}})U_{\mathrm{Ni}}) - D + \mathrm{Nit} + H_{\mathrm{NO_3}}$
Phytoplankton assimilation preference for NH_4 over NO_3	$P_{\mathrm{Ni}} = \left[\frac{\mathrm{NH_4} \cdot \mathrm{NO_3}}{(\mathrm{NH_4} + K_{\mathrm{Ni}})(\mathrm{NO_3} + K_{\mathrm{Ni}})}\right]\left[\frac{\mathrm{NH_4} \cdot K_{\mathrm{Ni}}}{(\mathrm{NH_4} + \mathrm{NO_3})(\mathrm{NO_3} + K_{\mathrm{Ni}})}\right]$
Rate of change of ammonium concentration (mg N m^{-3} per day)	$\frac{\delta \mathrm{NH_4}}{\delta t} = \sum(E_{\mathrm{Ni}} - P_{\mathrm{Ni}}U_{\mathrm{Ni}}) - \mathrm{Nit} + M_{\mathrm{N}} + X_{\mathrm{N}} + H_{\mathrm{NH_4}}$
Rate of change of organic nitrogen concentration (mg N m^{-3} per day)	$\frac{\delta \mathrm{ON}}{\delta t} = -M_{\mathrm{N}} + V_{\mathrm{ON}} + H_{\mathrm{ON}}$
Rate of change of internal (cellular) phosphorus concentration for phytoplankton group i (mg P (mg chl a)$^{-1}$ per day)	$\frac{\delta \mathrm{IP}_i}{\delta t} = \frac{U_{\mathrm{P}i} - E_{\mathrm{P}i}}{C_i} + V_i \mathrm{IP}_i + H_{\mathrm{IP}i}$
Rate of change of phosphate concentration (mg P m^{-3} per day)	$\frac{\delta \mathrm{PO_4}}{\delta t} = \sum(E_{\mathrm{P}i} - U_{\mathrm{P}i}) + M_{\mathrm{P}} + X_{\mathrm{P}} + H_{\mathrm{PO_4}}$
Rate of change of organic phosphorus concentration (mg P m^{-3} per day)	$\frac{\delta \mathrm{OP}}{\delta t} = -M_{\mathrm{P}} + V_{\mathrm{OP}} + H_{\mathrm{OP}}$
Rate of change of internal (cellular) nitrogen concentration for phytoplankton group i (μg N (mg chl a)$^{-1}$ per day)	$\frac{\delta \mathrm{IN}_i}{\delta t} = \frac{(U_{\mathrm{N}i} - E_{\mathrm{N}i})}{C_i} + V_i \mathrm{IN}_i + H_{\mathrm{IN}_i}$
Phytoplankton phosphorus uptake (mg P m^{-3} per day)	$U_{\mathrm{P}i} = \mathrm{UP}_{\max i} C_i \left[f_i(T)\left(\frac{\mathrm{IP}_{\max i} - \mathrm{IP}_i}{\mathrm{IP}_{\max i} - \mathrm{IP}_{\min i}}\right)\left(\frac{\mathrm{PO_4}}{K_{\mathrm{P}i} + \mathrm{PO_4}}\right)\right]$
Phytoplankton nitrogen uptake (mg N m^{-3} per day)	$U_{\mathrm{N}i} = \mathrm{UN}_{\max i} C_i \left[f_i(T)\left(\frac{\mathrm{IN}_{\max i} - \mathrm{IN}_i}{\mathrm{IN}_{\max i} - \mathrm{IN}_{\min i}}\right)\left(\frac{\mathrm{NO_3} + \mathrm{NH_4}}{K_{\mathrm{Ni}} + \mathrm{NO_3} + \mathrm{NH_4}}\right)\right]$
Release of phosphate through phytoplankton excretion (mg P m^{-3} per day)	$E_{\mathrm{P}i} = R_i f_i(S) \mathrm{IP}_i C_i$
Release of ammonia nitrogen through phytoplankton excretion (mg N m^{-3} per day)	$E_{\mathrm{N}i} = R_i f_i(S) \mathrm{IN}_i C_i$
Denitrification (mg N m^{-3} per day)	$D = k_{\mathrm{N_2}} \vartheta_{\mathrm{D}}^{T-20}\left(\frac{K_{\mathrm{DO}}}{K_{\mathrm{DO}} + \mathrm{DO}}\right)\mathrm{NO_3}$
Nitrification (mg N m^{-3} per day)	$\mathrm{Nit} = k_{\mathrm{NO}} \vartheta_{\mathrm{N}}^{T-20}\left(\frac{\mathrm{DO}}{K_{\mathrm{NIT}} + \mathrm{DO}}\right)\mathrm{NH_4}$

Table 1.3 (continued)

Mineralisation of organic phosphorus ($mg\,P\,m^{-3}$ per day)	$M_P = \left[k_{OAP}\upsilon^{T-20}\frac{K_{MIN}}{K_{MIN}+DO} + k_{OP}\upsilon^{T-20}\frac{DO}{K_{MIN}+DO}\right]OP$
Mineralisation of organic nitrogen ($mg\,N\,m^{-3}$ per day)	$M_N = \left[k_{OAN}\upsilon^{T-20}\frac{K_{MIN}}{K_{MIN}+DO} + k_{ON}\upsilon^{T-20}\frac{DO}{K_{MIN}+DO}\right]ON$
Release of phosphate from bottom sediments ($mg\,P\,m^{-3}$ per day)	$X_P = \begin{cases} \frac{S_P(K_{DOS}/(K_{DOS}+DO_b)+(\lvert pH_b-7\rvert)/(K_{pH}+\lvert pH_b-7\rvert))}{dz_b}, & \text{bottom layer} \\ 0, & \text{other layers} \end{cases}$
Release of ammonia nitrogen from bottom sediments ($mg\,N\,m^{-3}$ per day)	$X_N = \begin{cases} \frac{S_N(K_{DOS}/(K_{DOS}+DO_b)+(\lvert pH_b-7\rvert)/(K_{pH}+\lvert pH_b-7\rvert))}{dz_b}, & \text{bottom layer} \\ 0, & \text{other layers} \end{cases}$
Rate of change of dissolved oxygen ($g\,O_2\,m^{-3}$ per day)	$\frac{\delta DO}{\delta t} = F - U_b - U_{OC} - Y_{O:N}Nit + \sum P_i + H_{DO}$
Rate of change of dissolved oxygen due to exchange across the air–water interface ($g\,O_2\,m^{-3}$ per day)	$F = \begin{cases} \frac{wu^2(O_a-DO_s)}{dz_s\sqrt{Sc/660}}, & \text{surface layer} \\ 0, & \text{subsurface layer} \end{cases}$ (Wanninkhof, 1992)
Dissolved oxygen concentration in the air phase near the air–water interface, i.e., saturation concentration ($g\,O_2\,m^{-3}$)	$O_a = 1.42763\exp\left(-173.3292 + 249.6339\frac{100}{T} + 143.3483\log\left(\frac{T}{100}\right) - 21.8492\frac{T}{100} + S\left[-0.033096 + 0.014259\frac{T}{100} - 0.0017\left(\frac{T}{100}\right)^2\right]\right)$ (Riley and Skirrow, 1974)
Schmidt number (dimensionless)	$Sc = \left(0.9 + \frac{0.1S}{35}\right)[1953.4 - 128.0T + 3.9918T^2 - 0.050091T^3]$ (Wanninkhof, 1992)
Rate of change of dissolved oxygen concentration due to uptake by bottom sediments ($g\,O_2\,m^{-3}$ per day)	$U_b = \begin{cases} \left(\frac{K_F\upsilon^{T-20}}{dz_b}\right)\left(\frac{DO_b}{K_S+DO_b}\right), & \text{bottom layer} \\ 0, & \text{other layers} \end{cases}$
Net production of oxygen due to phytoplankton production and respiration ($g\,O_2\,m^{-3}$ per day)	$P_i = Y_{O:C}Y_{C:chla}C_i[\mu_i(1-k_p) - R_i]$
Utilisation of oxygen due to remineralisation of organic materials in the water column ($g\,O_2\,m^{-3}$ per day)	$U_{OC} = k_{OC}\vartheta_{OC}^{T-20}Y_{O:C}OC\left[\frac{DO}{K_{OC}+DO}\right]$
Rate of change of labile organic carbon concentration ($mg\,C\,m^{-3}$ per day)	$\frac{\partial OC}{\partial t} = \sum \chi_i - B_{OC} + H_{OC} + V_{OC}$
Breakdown of organic carbon in the water column ($mg\,C\,m^{-3}$ per day)	$B_{OC} = k_{OC}\vartheta_{OC}^{T-20}OC\left[\frac{DO}{K_{OC}+DO} + k_{an}\frac{K_{OC}}{K_{OC}+DO}\right]$
Contribution to labile organic carbon pool from phytoplankton mortality and excretion ($mg\,C\,m^{-3}$ per day)	$\chi_i = (1-j_i)R_iY_{C:chla}C_i$
Net change in concentration of substance Y due to settling and resuspension from bottom sediments ($mg\,m^{-3}$ per day) where $l-1$ is the layer above the current layer, l	$V_Y = \begin{cases} (\Re_Y - \upsilon_{YT(l)}Y_l)/dz_b + \upsilon_{YT(l-1)}Y_{l-1}/dz_{l-1}, & \text{bottom layer} \\ -\upsilon_{YT(l)}Y_l/dz_l + \upsilon_{YT(l-1)}Y_{l-1}/dz_{l-1}, & \text{bottom layers} \end{cases}$
Settling rate of substance Y at the current water temperature, T of layer l (m per day)	$\upsilon_{YT(l)} = \upsilon_{Y20}\left(\frac{\eta_{20}\rho_T}{\eta_T\rho_{20}}\right)$
Rate of change in concentration of substance Y due to resuspension ($mg\,m^{-3}$)	$\Re_Y = \begin{cases} \frac{\alpha_f((\tau-\tau_c)/\tau_{ref})}{dz_b}, & \text{diatoms and organic C, N and P} \\ 0, & \text{other substances} \end{cases}$ (Winterwerp, 1998)
Shear stress ($N\,m^{-2}$)	$\tau = \tau_s + \tau_w$
Shear stress due to steady currents ($N\,m^{-2}$)	$\tau_S = C_D\overline{U}^2\rho_T$ (Engelund and Hansen, 1972)

Table 1.3 (continued)

Drag coefficient of the bed (dimensionless)	$C_D = \frac{0.03}{\log^2(12h/k_d)}$ (Engelund and Hansen, 1972)
Oscillatory shear stress due to waves ($N\,m^{-2}$)	$\tau_w = 0.25 f_w U_m^2 \rho_T$ (Coastal Engineering Research Center, 1975)
Maximum orbital velocity ($m\,s^{-1}$)	$U_m = \frac{\pi H}{T_w \sinh(2\pi dz_1/L)}$ (Coastal Engineering Research Center, 1975)
Wave friction factor (dimensionless)	$f_w = \exp\left\lfloor 5.213(k_d/a_w)^{0.194} - 5.977 \right\rfloor$ (Swart, 1974)
Maximum bottom amplitude of shallow-water waves (m)	$a_w = \frac{H}{2\sinh(2\pi h/L)}$ (Coastal Engineering Research Center, 1975)
Wavelength (m)	$L = \frac{2\pi h \left\lfloor \tanh(4\pi^2 h/gT_w^2) \right\rfloor}{4\pi^2 h/gT_w^2}$ (Coastal Engineering Research Center, 1975)
Wave period (s)	$T_w = 2.40\pi u \left\lfloor \frac{\tanh[0.833(gh/u^2)^{0.375}]}{g} \right\rfloor \tanh \left\lfloor \frac{0.077(gF/u^2)^{0.25}}{\tanh[0.833(gh/u^2)^{0.375}]} \right\rfloor$ (Coastal Engineering Research Center, 1975)
Wave height (m)	$H = 0.283u^2 \left\lfloor \frac{\tanh[0.530(gh/u^2)]}{g} \right\rfloor \tanh \left\lfloor \frac{0.0125(gF/u^2)^{0.42}}{\tanh[0.530(gh/u^2)^{0.75}]} \right\rfloor$ (Coastal Engineering Research Center, 1975)

Table 1.4

List of symbols and units for variables

C_i	Chlorophyll *a* concentration of phytoplankton group i ($mg\,chl\,a\,m^{-3}$)
DO	Dissolved oxygen concentration ($g\,m^{-3}$)
DO_b	Dissolved oxygen concentration in the bottom layer ($g\,m^{-3}$)
DO_s	Dissolved oxygen concentration near the water surface ($g\,m^{-3}$)
dz_b	Thickness of the bottom layer of the water column (m), from the hydrodynamic model
dz_l	Thickness of layer l (m), from the hydrodynamic model
dz_s	Thickness of the surface layer of the water column (m), from the hydrodynamic model
F	Fetch length over which wind blows (m), determined from model grid
h	Depth of water (m), from the hydrodynamic model
H_i	Net flux of phytoplankton group i into the grid-cell due to advection and mixing ($mg\,chl\,a\,m^{-3}$ per day)
H_{INi}	Net change in intracellular nitrogen for phytoplankton group i due to advection and mixing ($mg\,N\,(mg\,chl\,a)^{-1}$ per day)
H_{IPi}	Net change in intracellular phosphorus stores for phytoplankton group i due to advection and mixing ($mg\,P\,(mg\,chl\,a)^{-1}$ per day)
H_{NH_4}	Net flux of NH_4 into the grid-cell due to advection and mixing ($mg\,N\,m^{-3}$ per day)
H_{NO_3}	Net flux of NO_3 into the grid-cell due to advection and mixing ($mg\,N\,m^{-3}$ per day)
H_{OC}	Net flux of labile organic matter into the grid-cell due to advection and mixing ($mg\,m^{-3}$ per day), calculated in the hydrodynamic model
H_{ON}	Net flux of organic nitrogen into the grid-cell due to advection and mixing ($mg\,N\,m^{-3}$ per day), calculated in the hydrodynamic model
H_{OP}	Net flux of organic phosphorus into the grid-cell due to advection and mixing ($mg\,P\,m^{-3}$ per day), calculated in the hydrodynamic model
H_{PO_4}	Net flux of PO_4 into the grid-cell due to advection and mixing ($mg\,P\,m^{-3}$ per day), calculated in the hydrodynamic model
H_Y	Net flux of substance Y into the grid-cell due to advection and mixing ($g\,O_2\,m^{-3}$ per day)
I	Irradiance ($\mu E\,m^{-2}\,s^{-1}$)
i	Phytoplankton group index
IN_i	Internal (cellular) nitrogen concentration ($mg\,N\,(mg\,chl\,a)^{-1}$) in phytoplankton group i
IP_i	Internal (cellular) phosphorus concentration ($mg\,P\,(mg\,chl\,a)^{-1}$) in phytoplankton group i
NH_4	Ammonium concentration ($mg\,N\,m^{-3}$)
NO_3	Nitrate concentration ($mg\,N\,m^{-3}$)
OC	Labile organic carbon ($mg\,C\,m^{-3}$)
ON	Organic nitrogen concentration ($mg\,N\,m^{-3}$)
OP	Organic phosphorus concentration ($mg\,N\,m^{-3}$)
pH_b	pH in the bottom layer
PO_4	Phosphate concentration ($mg\,P\,m^{-3}$)
S	Salinity
Si	Silica concentration ($mg\,Si\,m^{-3}$)
T	Water temperature (°C)
u	Wind speed 10 m above the water surface ($m\,s^{-1}$)
$\overline{U}$	Mean bottom layer current velocity ($m\,s^{-1}$), from the hydrodynamic model
Y	Concentration of substance Y (units as given for each substance)
ς_T	Dynamic viscosity of water at temperature T
$\tilde{n}_T$	Density water at temperature T ($kg\,m^{-3}$)

CHAPTER 2

Data Analysis and Field Experiments

2.1 Introduction

In this chapter we present field data from the Sau and Boadella reservoirs to be used as input into DYRESM and CAEDYM, two models which predict the thermal structure and water quality behaviour of reservoirs. DYRESM is a hydrodynamic one-dimensional model; CAEDYM is a water-quality model that can be linked to him. The field data used in the models consists of meteorological data (wind velocity, solar radiation, air temperature, vapour pressure and precipitation), bathymetric data from the reservoirs, water inflow (temperature, volume, salinity, concentrations of dissolved oxygen, nutrients and chlorophyll), water withdrawal (outflow discharge) and water quality constants. However, in terms of data availability Sau Reservoir is well monitored and has more data then Boadella reservoir.

2.2 Study sites

2.2.1 Sau Reservoir

Sau is the first of a cascade of reservoirs situated in the central part of the Ter River that was first filled in 1964. One of the most characteristic features of Sau is its canyon-shaped structure (Fig. 2.1). The Sau Reservoir is used to supply drinking water to the Barcelona metropolitan area. As Vidal & Om (1993) and Armengol et al. (1994) have shown, the trophic condition of Sau has evolved over time in response to human activity in the watershed, in particular in terms of the presence of soluble reactive phosphorus and inorganic dissolved nitrogen. However, since the construction of sewage treatment plants the presence of soluble reactive phosphorous has decreased.

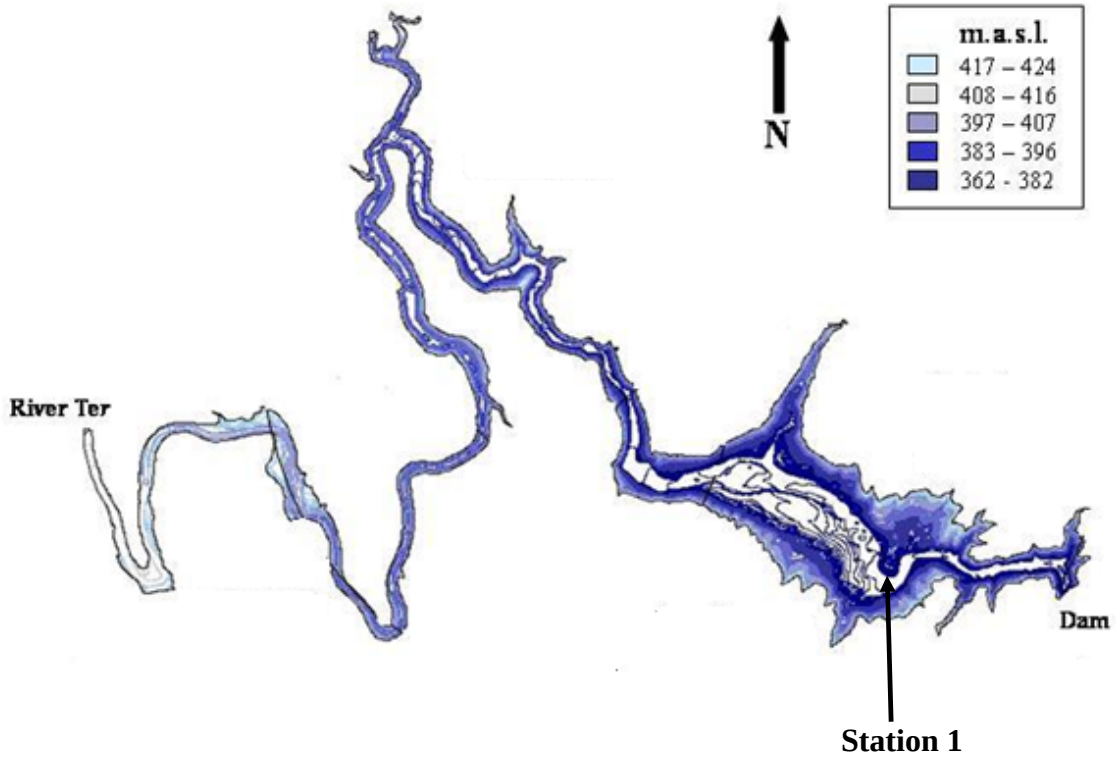

Figure 2.1 Sau Reservoir bathymetry.

2.2.2 Boadella Reservoir

The Boadella Reservoir (Fig.2.2) was built to meet the demands of urban, tourist, development of intensive agriculture, and to supply drinking water. Boadella is located in the north-east of Spain in the eastern Pre-Pyrenees. The average yearly total net inflow into the reservoir occurs through two main tributaries: the Muga and the Arnera. It has been estimated that the Muga contributes 65% and the Arnera 35% of the total inflow (Casamitjana et al., 2003). Water from the Boadella Reservoir is used mainly to supply drinking water to Figueres and other small towns downstream, as well for irrigation purposes. Formerly, it was used to run a hydroelectric power plant. The nutrient input into the reservoir is not very high, with average values of 3.2 μgNl^{-1} for nitrates and 0.2 μgPl^{-1} for total phosphorus (APHA, 1989).

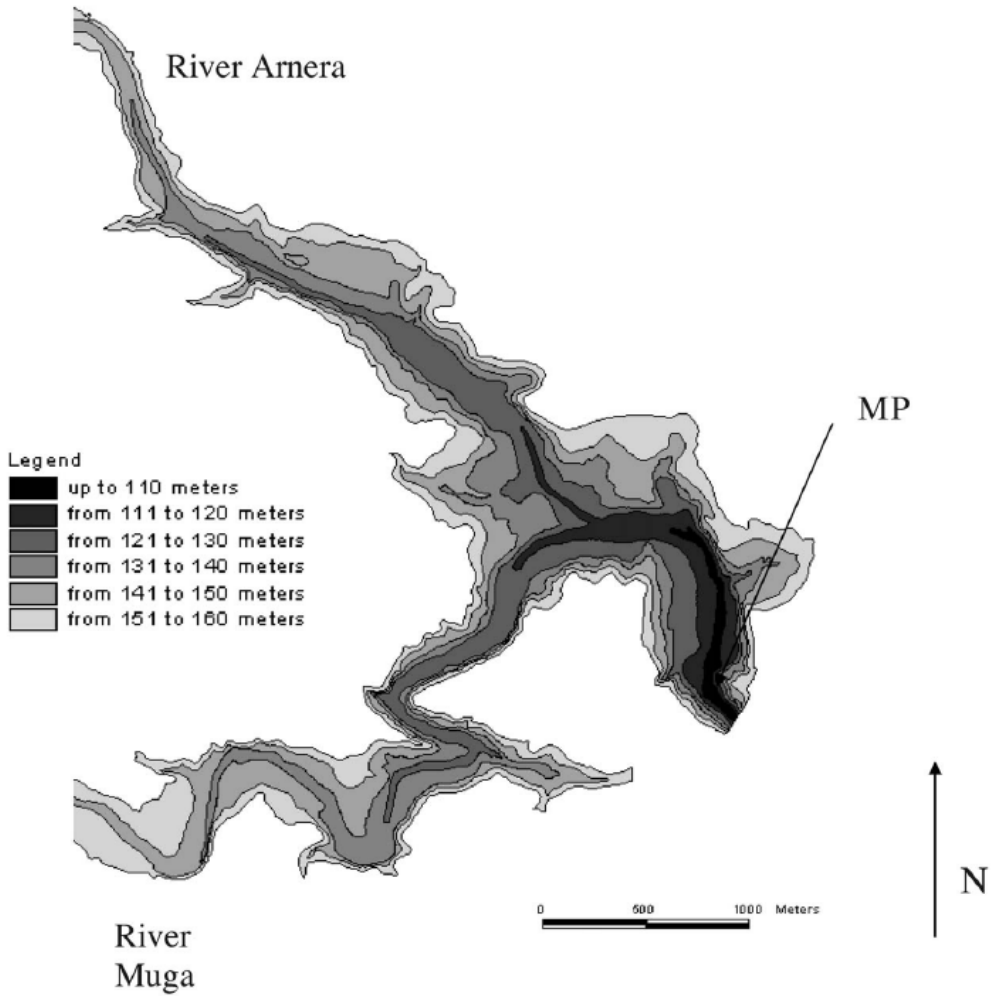

Figure 2.2 Boadella Reservoir bathymetry.

2.3. Data introduction

Sau Reservoir data for the period 2000-2001 were provided by a research team led by Professor Joan Armengol, from the Ecology Department of the University of Barcelona. The data provided consist of morphometric (section 2.4.1) and meteorological data, recorded at the Club Nàutic station (Station 1) (Fig. 2.1); these data consist of daily temperature, solar radiation, vapour pressure, wind velocity and precipitation (section 2.4.2). Monthly temperature, dissolved oxygen, soluble reactive phosphorous and chlorophyll profiles were also provided (section 2.4.5), as well as daily inflow and outflow (Fig. 2.10-B and Fig. 2.11). However, daily river concentrations of dissolved oxygen, reactive phosphorous, and chlorophyll were not available. Data were taken every month at a sampling point at station 1 (Fig. 2.1).

Boadella Reservoir data were provided by (Baserba, C. 1999). Meteorological data were taken at the station in Cabanes, except for those relating to atmospheric pressure, which were taken at the Roses meteorological station. Thus, we dispose meteorological data sets accept long wave radiation measurements which was not available. Because of this, cloud cover had to be estimated (section 2.5.2.2). As in the case of the Sau Reservoir, the inflow and outflow volumes of dissolved oxygen, as well as phosphorus and chlorophyll concentration profiles were also unavailable. During certain periods, moreover, there were some missing data sets (Fig. 2 26 and Fig. 2.27).

2.4 Sau Reservoir data

2.4.1 Morphometric data

The Sau Reservoir displayed in (Fig. 2.1). Its maximum width, close to the dam, is 1.3 km. Morphometric characteristics are given in Table 2.1 (Armengol et al., 2003). Sau Reservoir area-elevation and volume-elevation data are represented in Fig. 2.3 and Fig. 2.4 respectively.

Table 2.1 Morphometric characteristics of the Sau Reservoir.

Latitude	$46º46^{''}N4º51'E$
Catchments area	$1.79x10^{9}m^{2}$
Max. volume	$0.1486x10^{9}m^{3}$
Max. area	$5.8x10^{6}m^{2}$
Max. depth	75 m
Max. length	$1.8x10^{4}m$
Bottom elevation	362 m asl
Basin width at crest	260 m
River	Ter

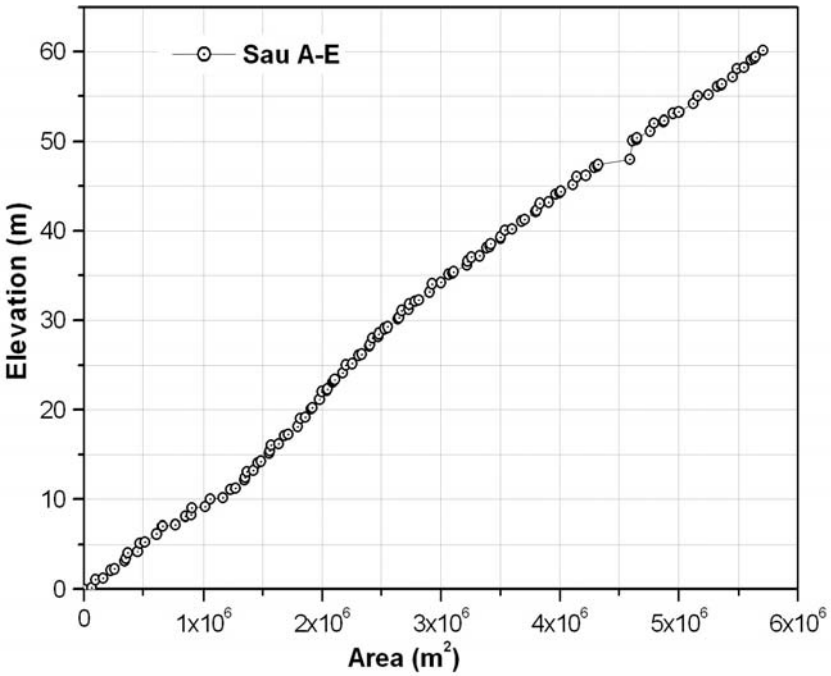

Figure 2.3 Sau Reservoir Area-Elevation

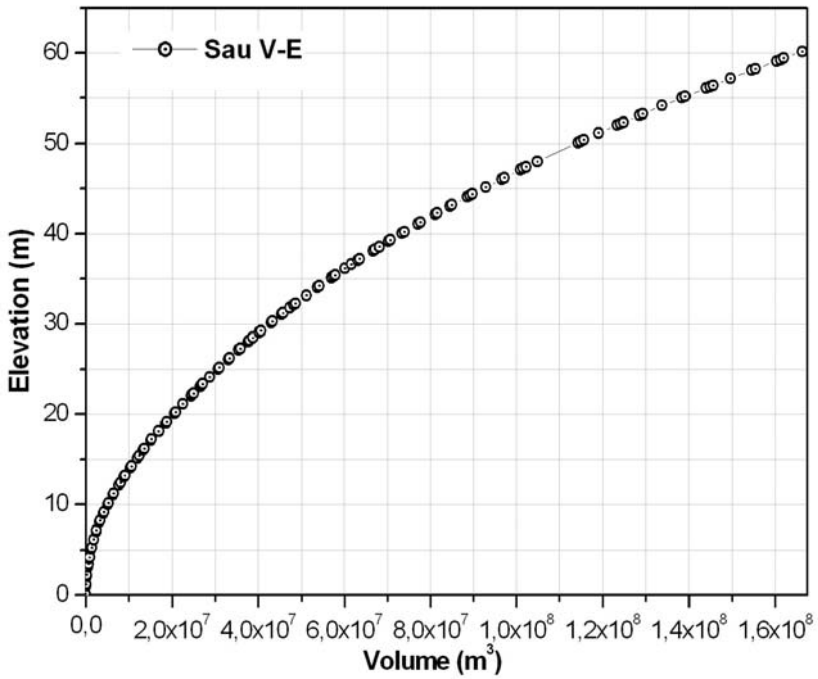

Figure 2.4 Sau Reservoir Volume-Elevation.

2.4.2 Meteorological data

2.4.2.1 Air temperature

Air temperature is an important meteorological variable because any increase has an immediate influence, warming the reservoir and river surface water.

In the Sau Reservoir, the average air temperatures for the years 2000 and 2001 were approximately 14.10ºC and 14.40ºC respectively; the daily averaged minimum and maximum temperatures were 1.58ºC and 25.17ºC respectively for the year 2000 and 2.31ºC and 27.07ºC for the year 2001. The daily averaged air temperature is plotted in Fig. 2.5

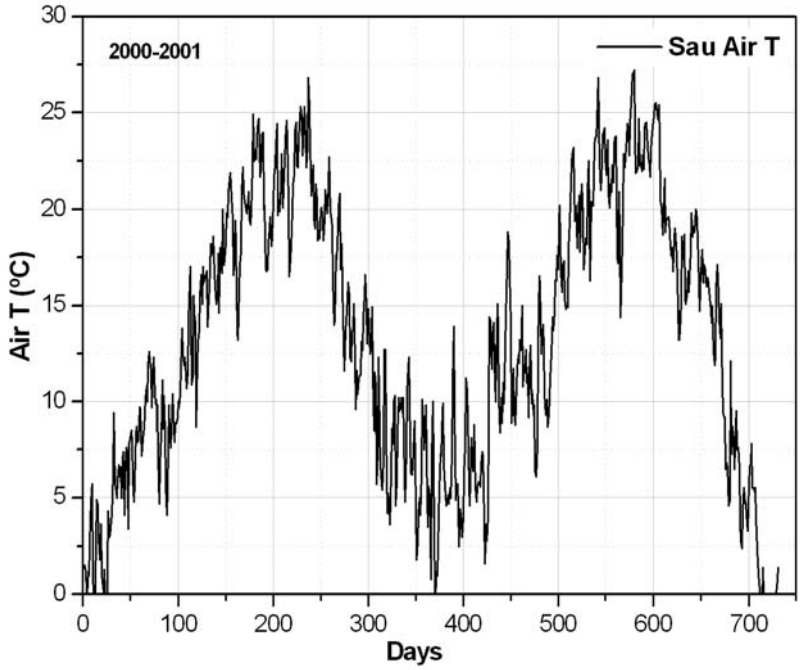

Figure 2.5 Daily air temperatures in the Sau Reservoir.

2.4.2.2 Solar radiation (short wave and long wave radiation)

One of the inputs into the hydrodynamic model is daily short-wave radiation. The model could use, facultatively, either long-wave radiation or cloud cover, but in the Sau Reservoir we use long-wave radiation because it was obtained from a meteorological station. Time series of short-wave and long-wave radiation are presented in Figs. 2.6A and 2.6B.

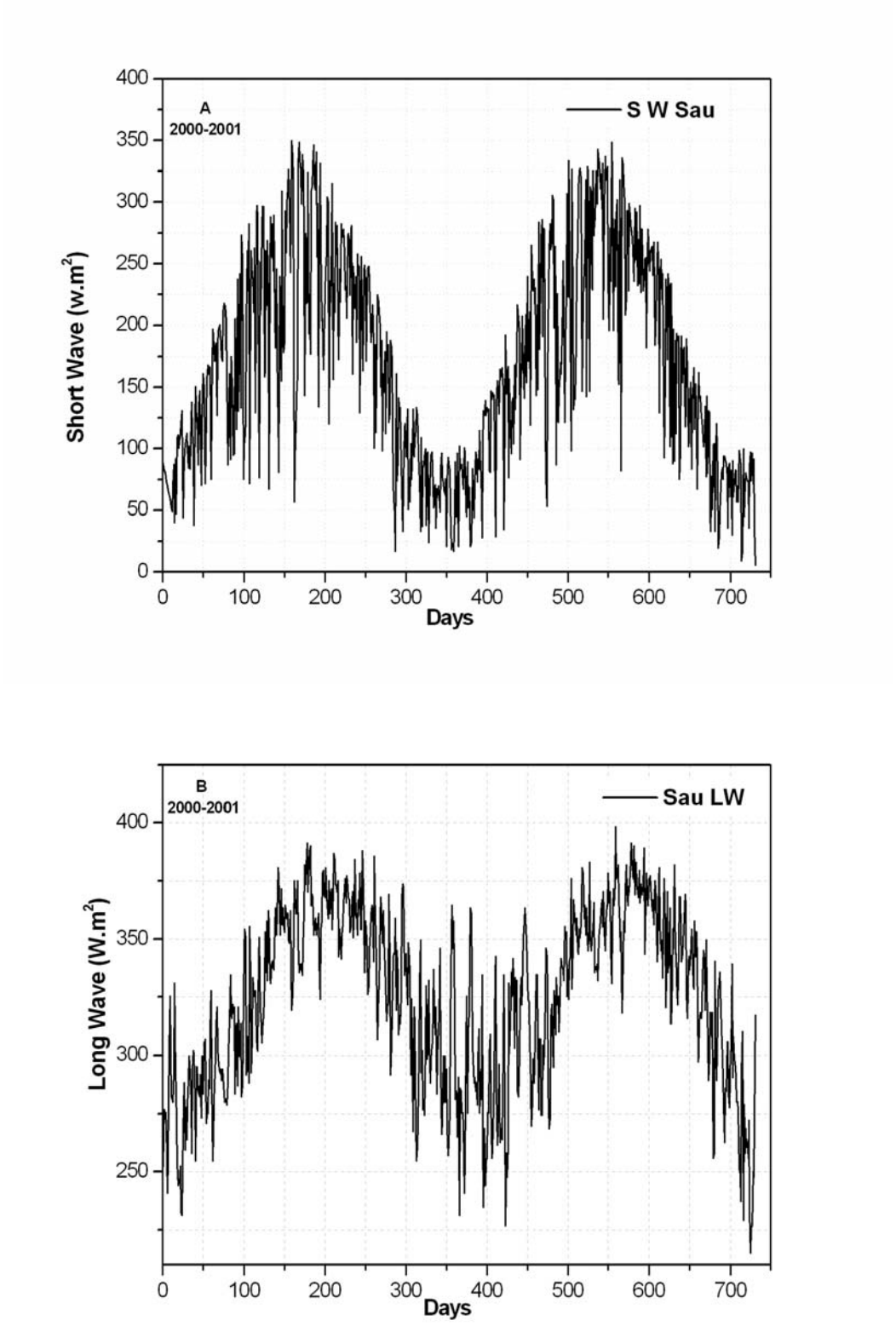

Figure 2.6 Sau Reservoir time series of short wave radiation (A) and long wave radiation (B).

2.4.2.3 Vapour pressure

Average vapour pressure (Fig. 2.7) is estimated by using the Magnus formula (TVA 1979, Eq 2.1) as it was also used in the DYRESM scientific manual

$$e_s(T_S) = \exp\left[2.3026\left(\frac{7.5T_S}{T_S + 273.3} + 0.7858\right)\right] \tag{2.1}$$

where T_S is the dry bulb air temperature in degrees Celsius and $e_s(T_S)$ is the vapour pressure in hectopascals. In the Sau Reservoir, the average vapour pressure is approximately the same, 2.10 mb, for the year 2000 and the year 2001; the minimum vapour pressure for both years was 1.1 mb and the maximum about 2.8 mb.

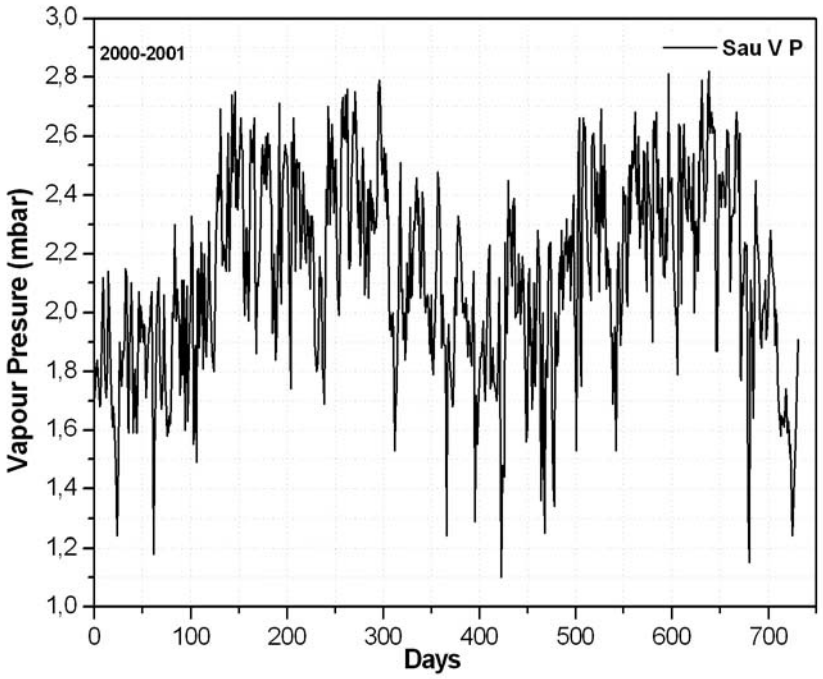

Figure 2.7 Sau Reservoir time series of vapour pressure.

2.4.2.4 Wind velocity

The wind is the main factor principally responsible for turbulent kinetic energy. The Sau Reservoir is characterised by a weak wind speed (Fig. 2.8). Average velocity was about 1.58 m/s for the year 2000 and 1.66 m/s for the year 2001. Minimum velocity was 0.4 m/s for 2000 and 2001, and maximum velocity was 5.6m/s for the year 2000 and 8.7 m/s for 2001.

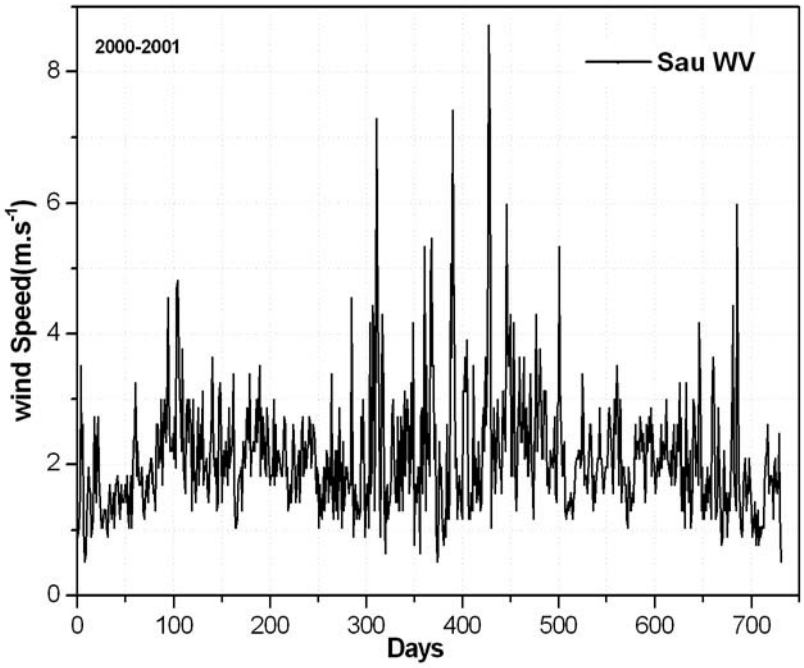

Figure 2.8 Sau Reservoir daily wind velocity.

2.4.2.5 Precipitation

One of the most significant differences between the years studied is that there was less precipitation in 2001 than in 2000. Accumulated precipitation was about 466 mm for the year 2000 while for 2001 it was only 282 mm (Fig. 2.9). Also, precipitation in the year 2000 occurred in spring and summer, although it should be mentioned that there was also heavy rainfall at the end of the year.

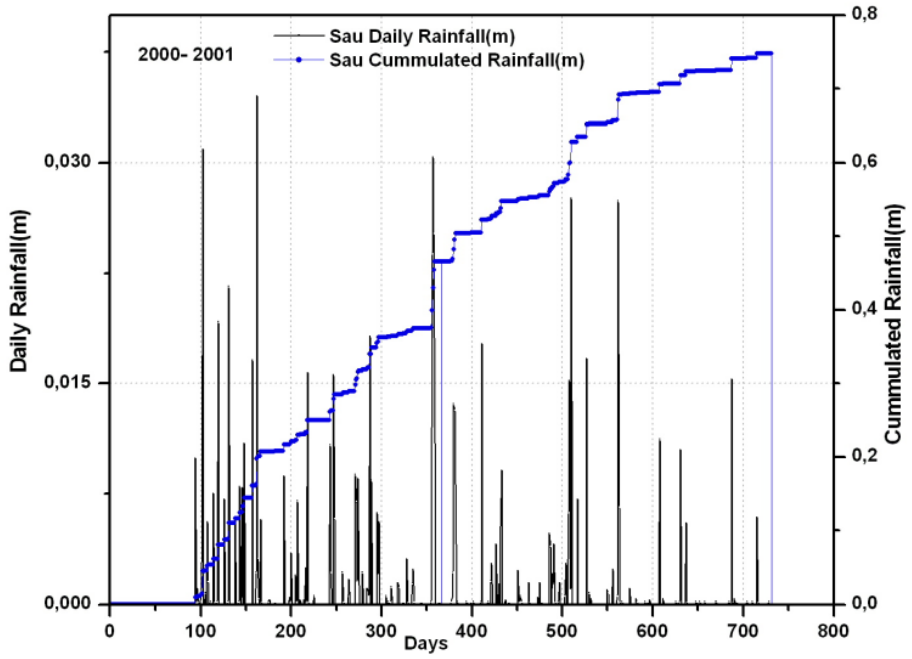

Figure 2.9 Sau Reservoir daily rainfall and accumulated rainfall.

2.4.3 Inflow

The total volume of Ter River inflow entering the Sau Reservoir was approximately 259 hm^3 for the year 2000, and 253 hm^3 for the year 2001, with the main inflow occurring in spring in both years. It should also be mentioned that in 2000 the maximum inflow took place at the end of the year, corresponding to a high precipitation event (Fig. 2.9). High precipitation in the Sau catchment area generated a high runoff (Fig. 2.10B), affecting the water quality in the reservoir by increasing dissolved oxygen, nutrient, and chlorophyll concentrations (Fig. 2.13, 2.14, and 2.15). The inflow temperature {Fig. 2.10A} is estimated using equation (1.2) (see Armengol et al., 2003) in which inflow temperature depends on the average air temperature of the previous 4 days.

$$T_{river} = 1.74 + 0.95.T_{4days} \qquad (2.2)$$

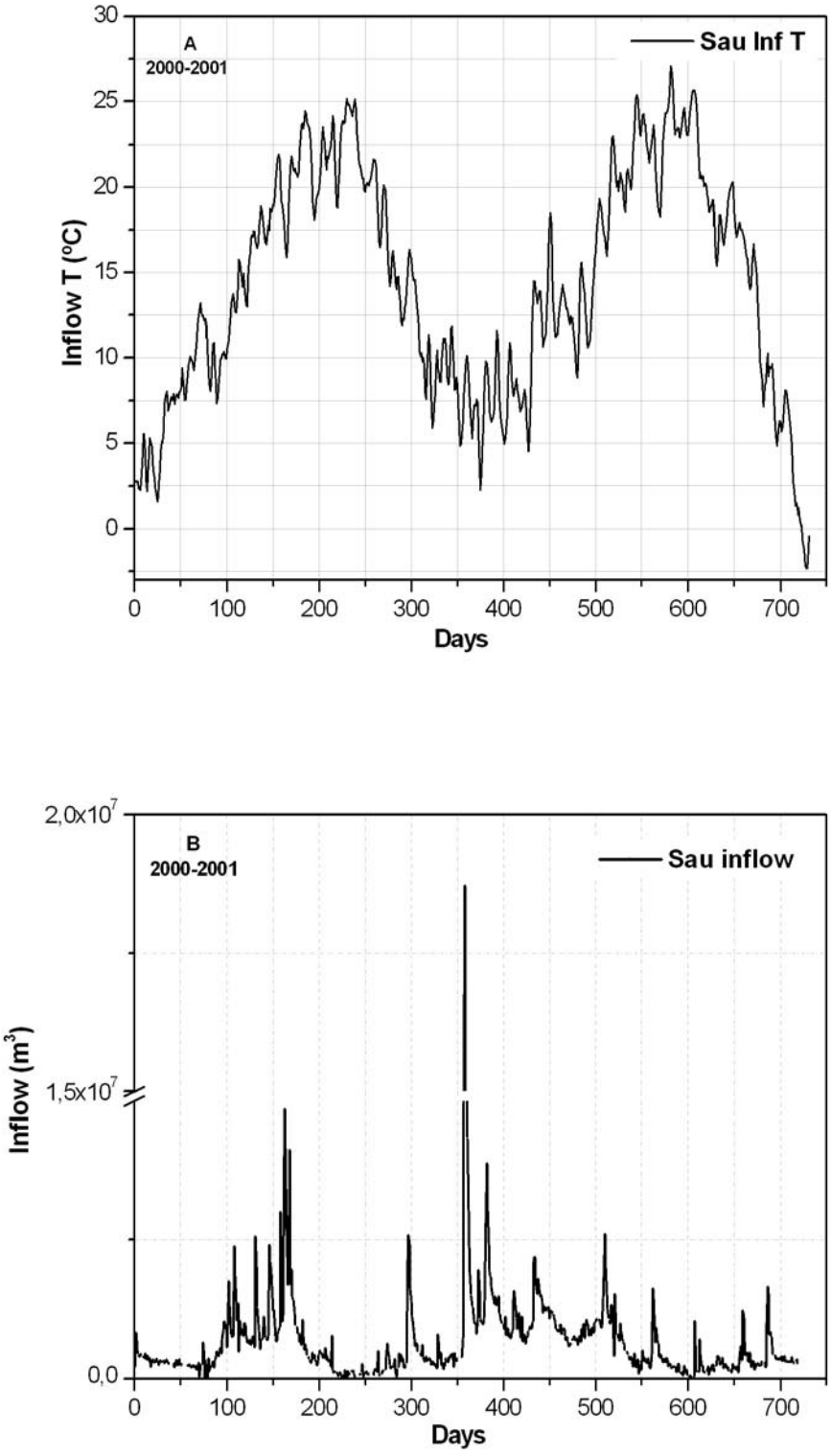

Figure 2.10 Daily inflow temperature (A); Daily inflow volume entering the Sau Reservoir (B).

2.4.4 Outflow

Withdrawal of water from the Sau Reservoir including evaporation (Fig. 2.11) was higher in spring and summer due to the large volume of drinking water supply consumption occurring at those times. Additionally, high temperatures registered though the time series (2000-2001) may have increased water evaporation from the reservoir.

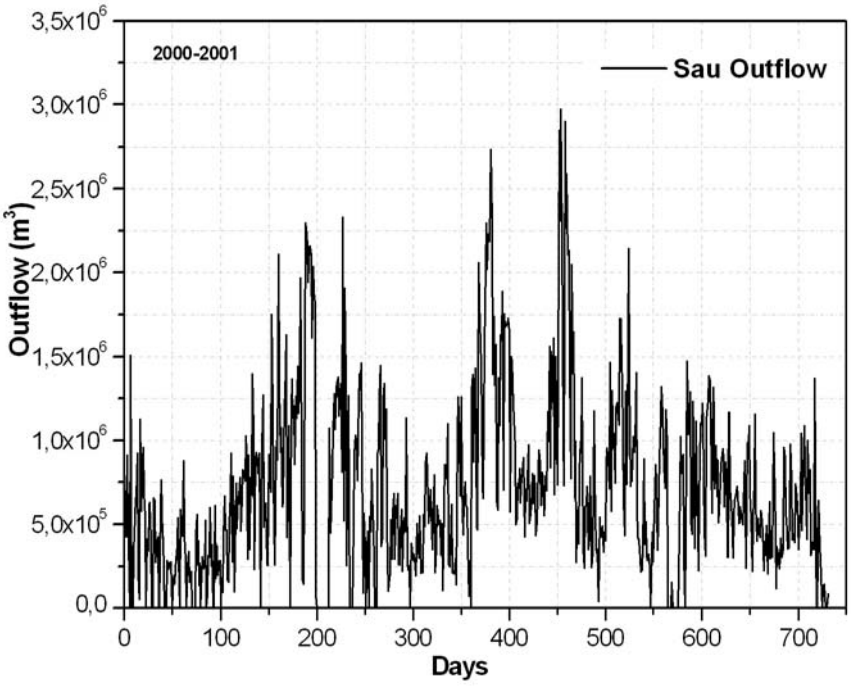

Figure 2.11 Daily outflow volume.

2.4.5 Sau Reservoir profiles

2.4.5.1 Temperature profiles

From Fig. 2.12 one can identify the special and temporal temperature distribution, whereas the stratification starts at the beginning of March and the formation of thermocline expending from March until the end of August. However, mixing occurs at the end December for 2000 and 2001, for the year 2001 mixing is might be due to the strong inflow river caused by the heavy rainfall recorded at the end of year 2000. Additionally, the stratification in 2000 is more or less strong than 2001 this was linked to the small storage water volume relative to the year 2001.

During the stratified period of the year 2000 we can see that the stratification reaches the bottom. This might be due to the highest outflow of the year 2000 occurring at the beginning of June {Fig. 2.10 B}.

The cooling period started after the summer stratification; this period is characterised by a deeper thermocline due to the combination of cooling surface water and wind velocity. Finally, the reservoir mixes completely in winter, producing the thermal overturning characteristic of monomictic reservoirs. The same pattern was evident in the year 2001.

In the year 2000 high precipitation (Fig. 2.9) produced a high inflow (Fig. 2.10B) together with the wind (Fig. 2.8), and surface cooling enhance mixing. In the year 2001 mixing in the Sau Reservoir was similar to 2000 which is due to wind velocity which reached a maximum of approximately 9 m/s (Fig. 2.8) together with river inflow and surface cooling (Fig. 2.5, Fig. 2.8 and Fig. 2.9). Fig. 2.12 illustrates the evolution of temperature in the Sau Reservoir.

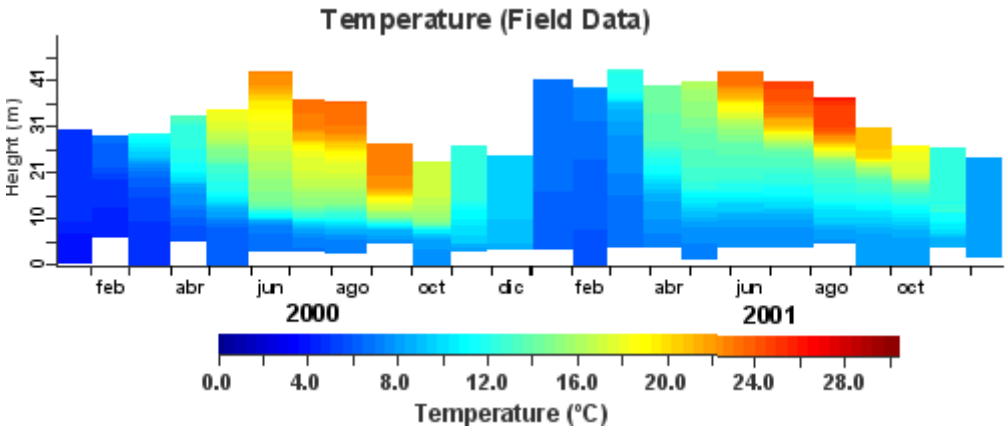

Figure 2.12 Field temperature time series.

2.4.5.2 Dissolved oxygen profiles

The evolution pattern of dissolved oxygen changed considerably from 2000 to 2001. This was due to the hypolimnion anoxic period (Fig. 2.13). The anoxic hypolimnion zone for the year 2000 started at the beginning of spring, continued through summer and lasted until approximately the end of autumn. In 2001, it started at the end of April and lasted till the end of the year. In contrast, the first river inflow at the end of February 2000 may increase dissolved oxygen content which cause the phytoplankton growth. Likewise, the highest inflow in the beginning of 2001 contributes to increase of

dissolved oxygen to 18 mg/l which was the reason of the increase in chlorophyll concentrations. For both years, the measured dissolved oxygen is presented in Fig. 2.13. In this figure the zone which is relatively high of dissolved oxygen was only a few meters from the surface layer and the anoxic zone covered the whole hypolimnion and part of the metalimnion.

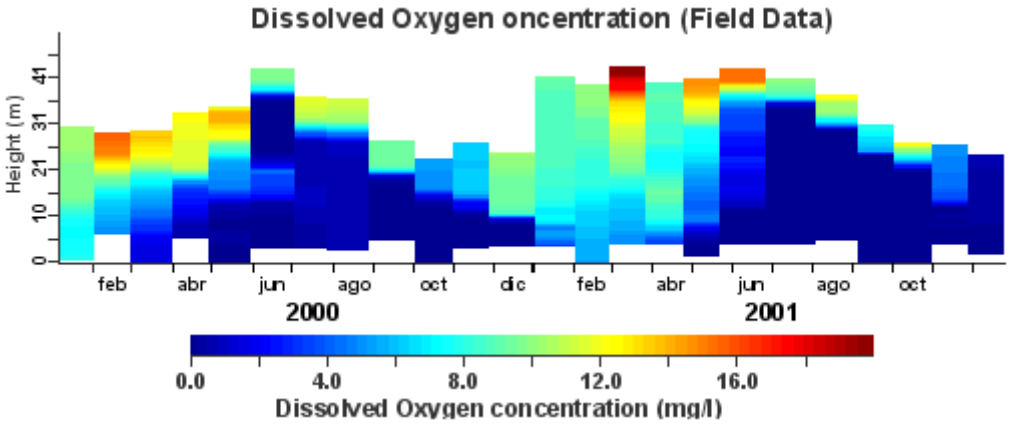

Figure 2.13 Sau Reservoir time series of Observed Dissolved Oxygen.

2.4.5.3 Phosphorus

We focus here on dissolved inorganic phosphorus (Fig. 2.14). After a water treatment plant came into service in 1990 the eutrophication in the Sau Reservoir was improved considerably by diminishing the phosphorus discharge in reservoir, especially in the reservoir's surface water. In winter, mixing occurs. The water from hypolimnion is pushed to the surface, producing a uniform phosphorus concentration, and allowing a reduction in the biologic oxygen demand in the hypolimnion as well as in 2001 the important river inflow which contains sediment load part of them was suspended solid sediment have a great impact on phytoplankton.

In the stratification periods of the years 2000 and 2001, the phosphorus concentration was high on the bottom and low on the surface. In summer, therefore, the chlorophyll concentration was small, as will be seen later on. Phosphorus depletion in the surface layer indicates that this element is probably the main factor limiting the biologic activity in Sau. The other factor to be highlighted is the elevated bottom phosphorus concentration measured in the hypolimnion in the summer period and lasting until the end of the year. This therefore was due to sediment load containing in the river inflow which comes from the Sau catchment area.

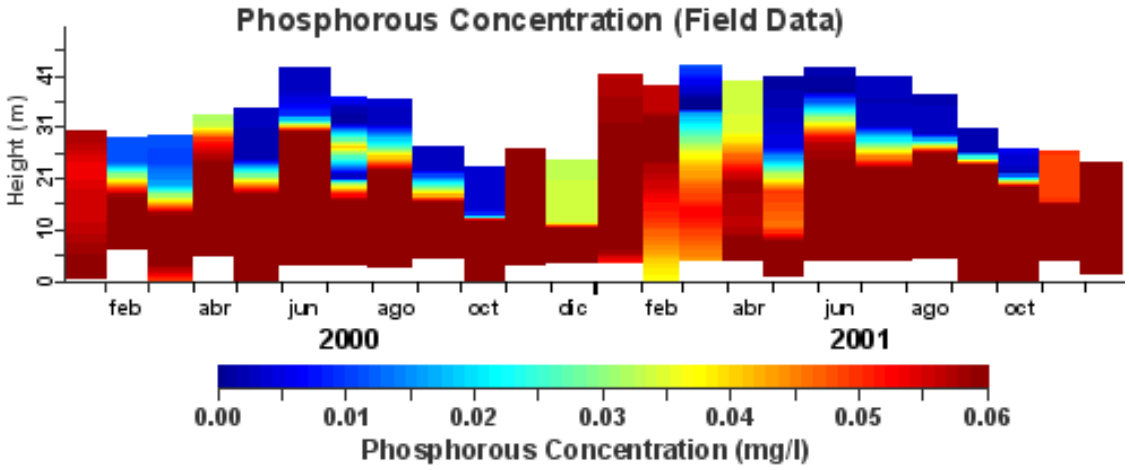

Figure 2.14 Daily Dissolved inorganic phosphorous in the Sau Reservoir.

2.4.5.4 Chlorophyll

In January and February of the year 2000, water discharge entering the reservoir was low, resulting in a lower phosphorous concentration. However, an algal growth peak of concentration appeared in February 2000 where the inflow is negligible which induce development of phytoplankton biomass. There were two other maximum peaks in May and June. This algal growth corresponded to the beginning of the stratification period characterise by an inflow river (Fig. 2.10). The last and the most significant was in September 2000 which as well corresponding to high river inflow. Therefore, in Sau Reservoir a one can estimate in February 2000 limiting factor is light whereas in May, June and September the limiting factor is nutrient. Maximum Algal growth in 2001 was registered in October.

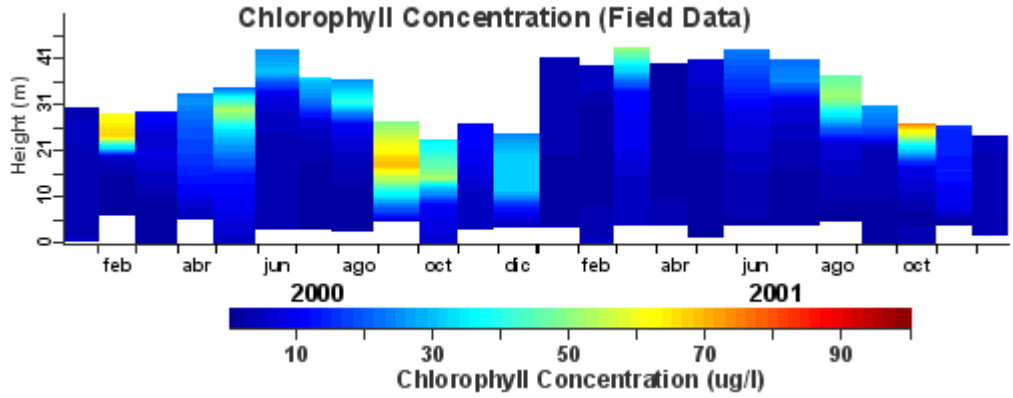

Figure 2.15 Sau Reservoir chlorophyll time series.

2.5 Boadella Reservoir data

2.5.1 Morphometry data

The Boadella Reservoir (Fig.2.2) is located in the north-east of Spain $42º20´´15´´N 2º21´07´´E$. Its primary distinguishing characteristic is its small catchment area $0.182x10^9 m^2$ approximately ten times smaller than that of the Sau Reservoir. The Boadella Reservoir volume is about $0.062x10^9 m^3$, its total surface area is $3.64x10^6 m^2$, its maximum depth is 52 m and its altitude is 160 m above sea level (Serra et al., 2002). In Fig. 2.16 and Fig.2.17 Boadella's area-elevation and volume-elevation data respectively are displayed.

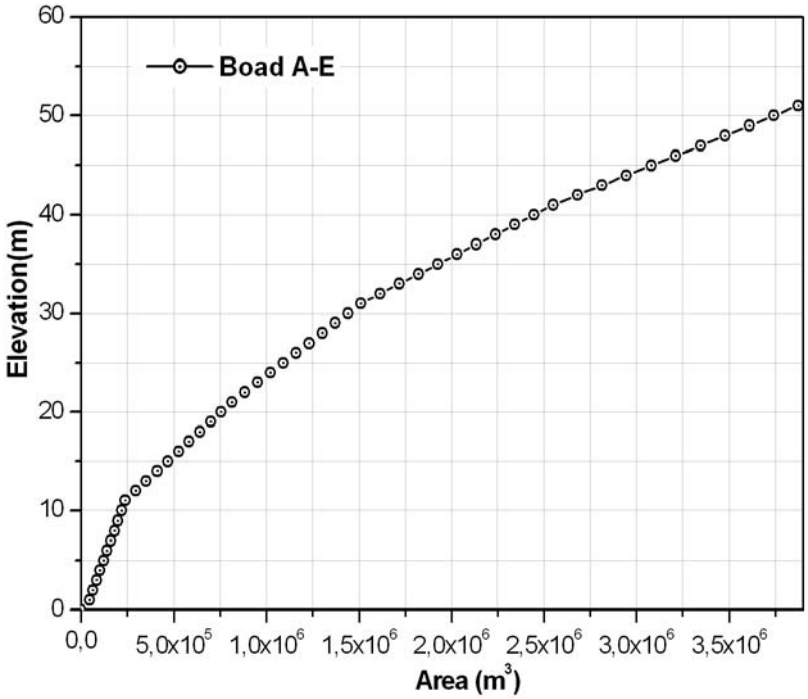

Figure 2.16 Boadella Reservoir Area-Elevation

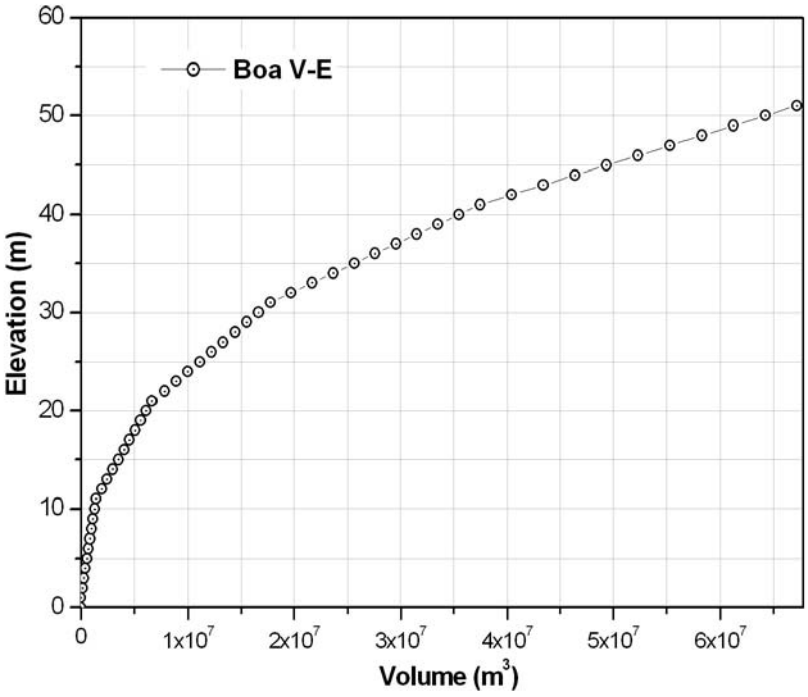

Figure 2.17 Boadella Reservoir Volume-Elevation

2.5.2 Meteorological data

2.5.2.1 Air temperature

The air temperature over the Boadella Reservoir is a little higher than over the Sau Reservoir.

The average is about 15.22ºC for 2000 and 15.42ºC for 2001. Minimum and maximum are 2.3ºC and 28.2ºC respectively for 2000 and -0.5ºC and 27.8ºC respectively for 2001. The average air temperature is plotted in Fig. 2.18.

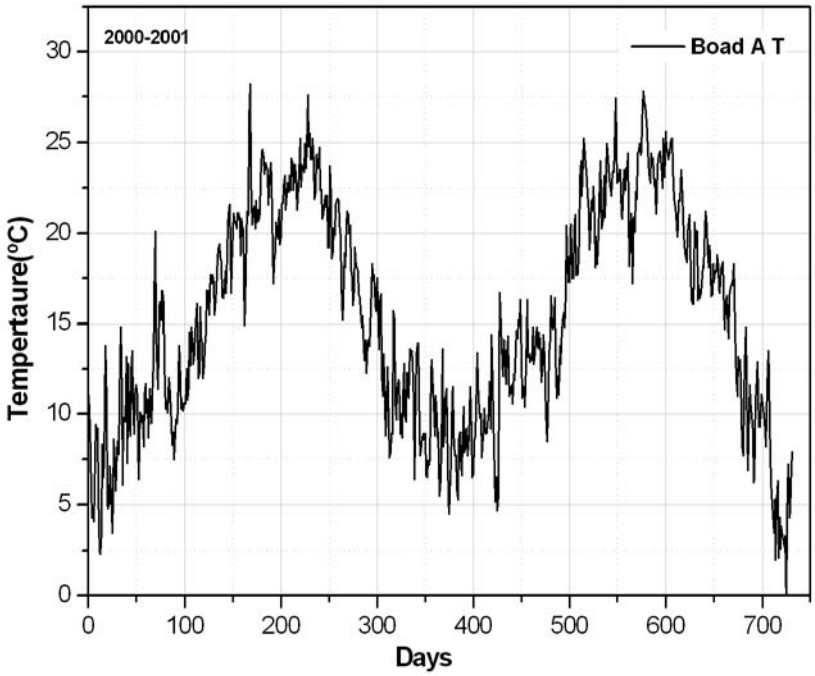

Figure 2.18 Boadella Reservoir a*ir temperature time series*

2.5.2.2 Solar radiation

Long-wave radiation data is not available for the Boadella Reservoir. As the hydrodynamic model requires either long-wave radiation or cloud cover, in this case we have used measured short-wave radiation (Fig. 2.19A) to estimate cloud cover (Fig. 2.19B) by interpolation between cloudy and clear sky using the following equations (Colomer, et al., 1996):

$$K_0 = 231 - 123\sin(\pi(D+85)/183) \quad (2.3)$$

$$K_1 = 56 - 39\sin(\pi(D+75)/183) \quad (2.4)$$

where D is the day, ranging from 1 to 365; K_0 corresponds to clear sky in which the cloud cover C=0; and K_1 corresponds to the cloudy sky where cloud cover is C=1.

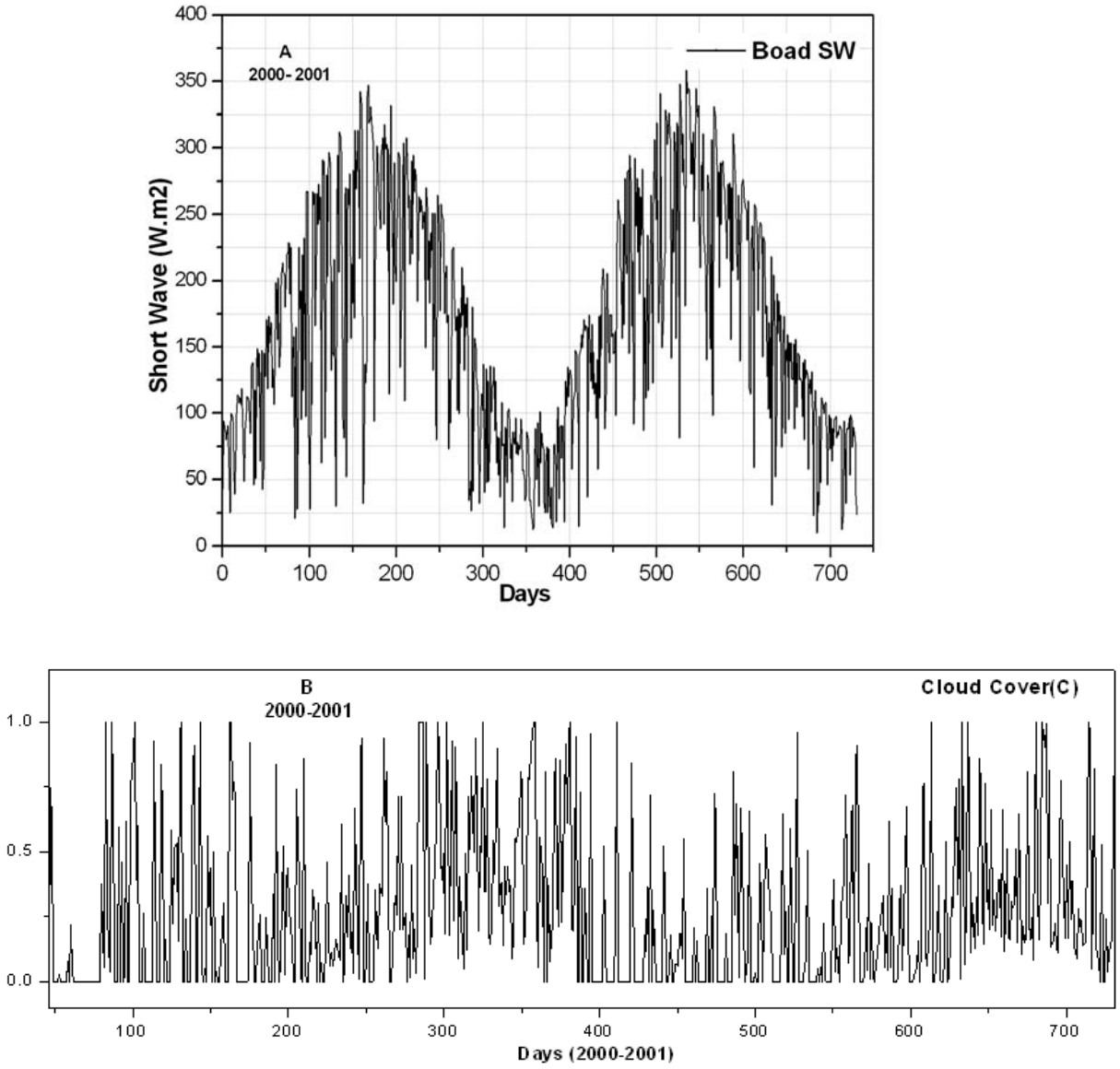

Figure 2.19 Short-wave radiation (A) and cloud cover (B) time series.

2.5.2.3 Vapour pressure

As with the case for the Sau Reservoir, the average vapour pressure in the Boadella Reservoir (Fig. 2.20) was estimated using the formula (2.1) described in section 2.4.2.3. Vapour pressure in the Boadella Reservoir is higher than in Sau. Average vapour pressure was approximately the same (13 mbar) for the year 2000 and 2001. The minimum pressure was 2.4 mbar and the maximum about 26 mbar for both years.

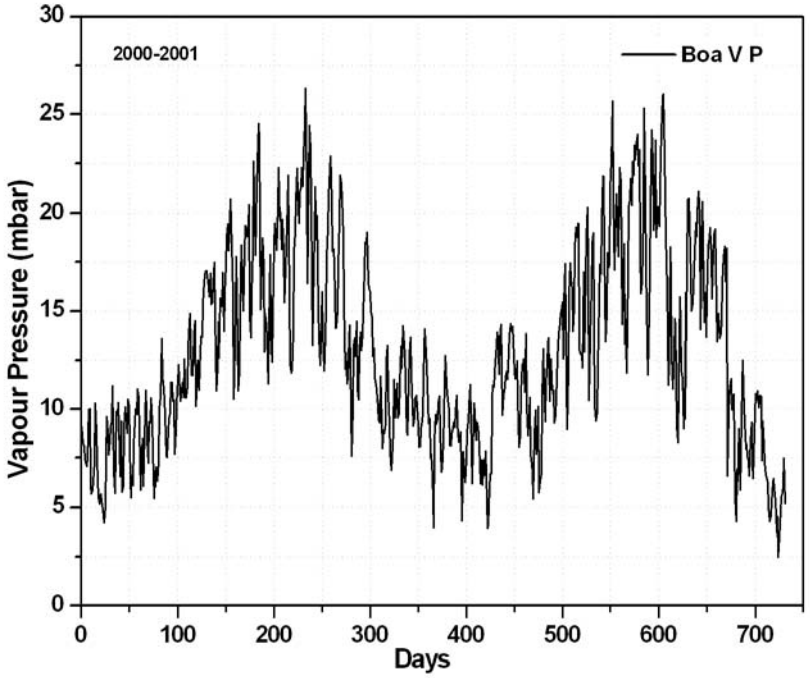

Figure 2.20 Boadella Reservoir vapour pressure time series

2.5.2.4 Wind velocity

The Boadella Reservoir's wind velocity (Fig. 2.21) is higher than Sau's; the average is 1.86 m/s, with a maximum of 9.4 m/s.

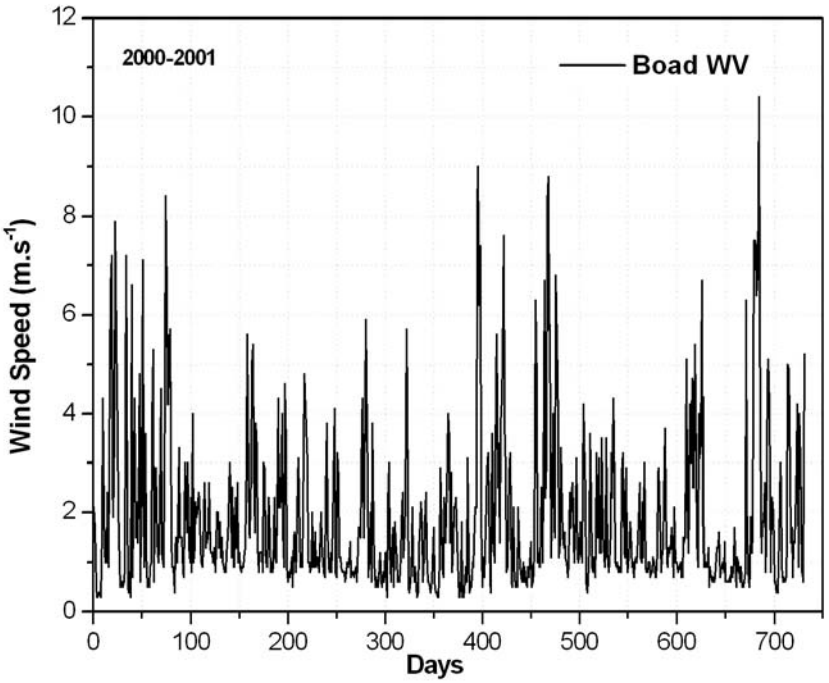

Figure 2.21 Boadella Reservoir wind speed time series

2.5.2.5 Precipitation

Accumulated precipitation is higher in the Boadella Reservoir than in Sau. It was 914mm for the year 2000 and 712mm for the year 2001 (Fig. 2.22). For both years precipitation occurred in the spring and autumn.

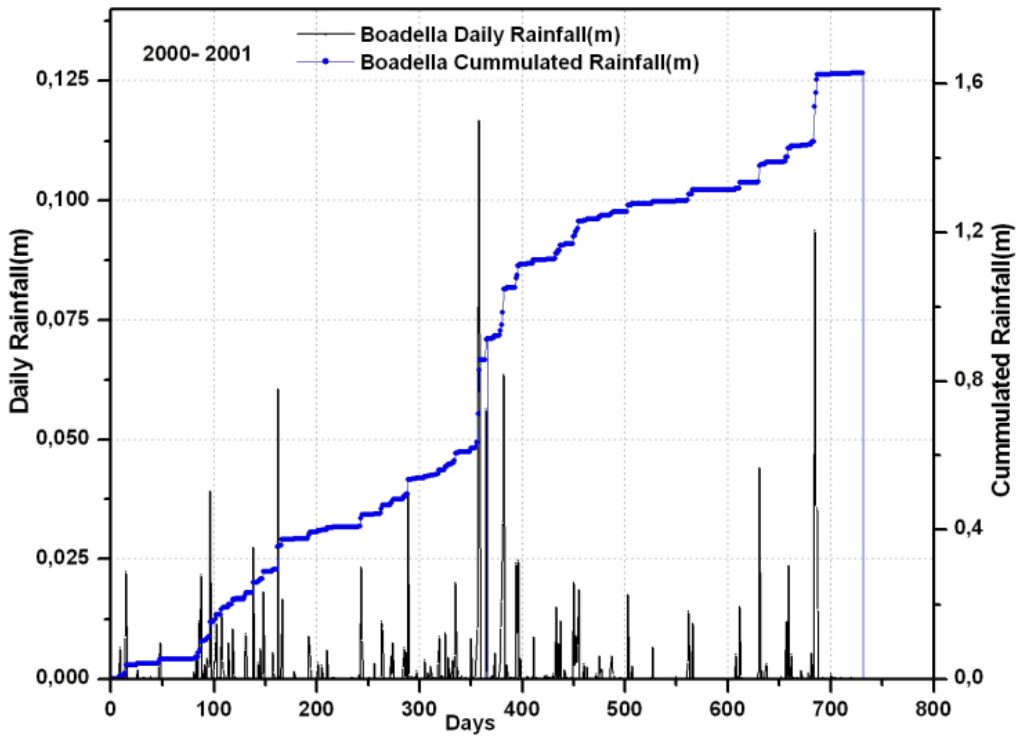

Figure 2.22 Daily and accumulated rainfall for the Boadella Reservoir

2.5.3 Inflow

As Boadella's catchment area is small (section 2.5.1) and the variation of precipitation is not as high as is the case of Sau, the inflow volume (Fig. 2.23B) that goes into Boadella is also small: 40 hm^3 for the year 2000 and 30 hm^3 for the year 2001. The main inflow entering Boadella occurred in spring 2000 and 2001. The maximum inflow was observed at the end of 2000, corresponding to a high precipitation event (Fig. 2.22 and Fig. 2.23B).

As previously mentioned, inflow temperature was estimated using equation (2.2) (see section 2.4.3) in which river temperature depends on the average air temperature of the previous 4 days (Fig. 2.23A).

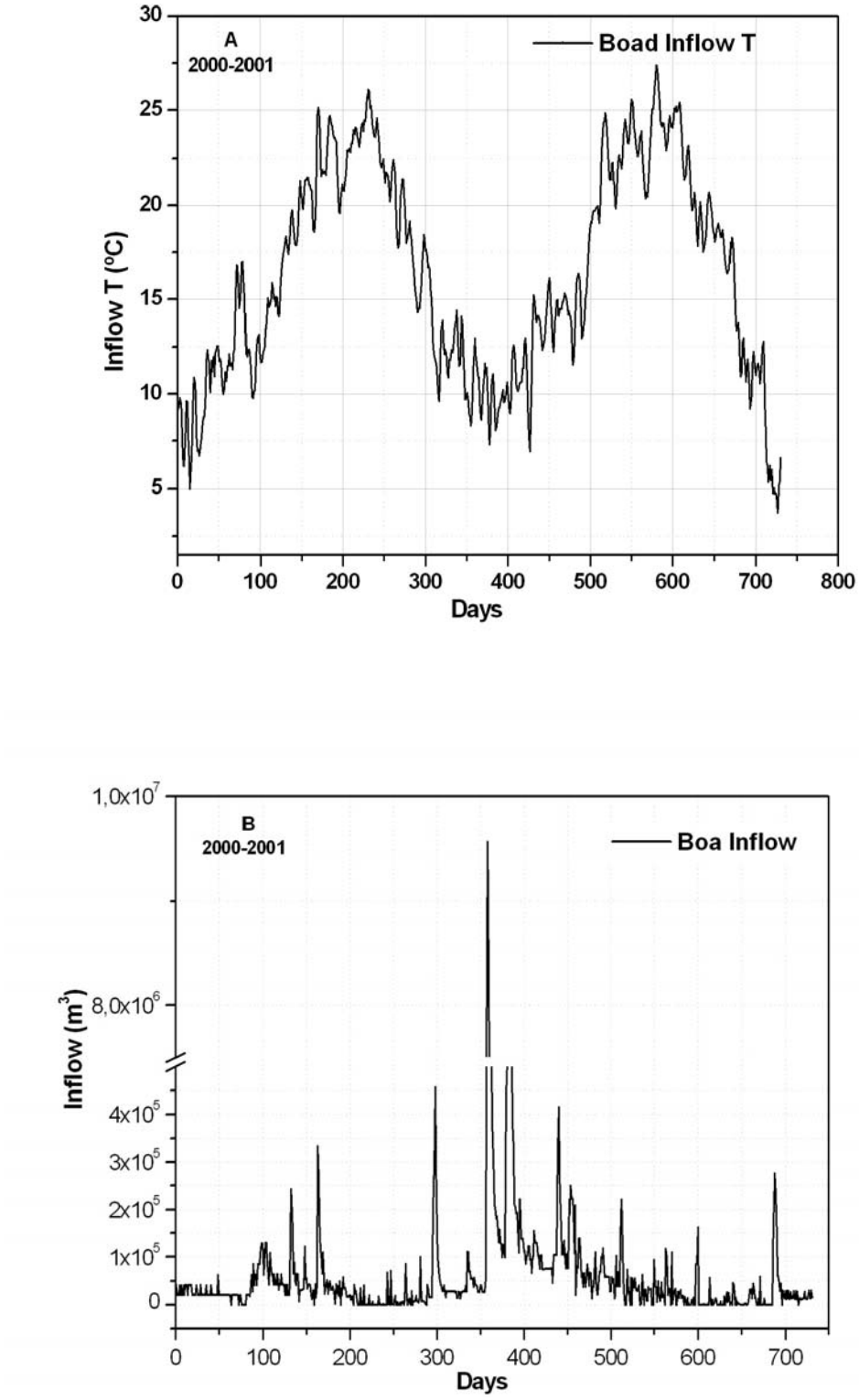

Figure 2.23 Boadella Reservoir daily inflow temperatures (A) and daily inflow volume (B)

2.5.4 Outflow

Water withdrawal from the Boadella Reservoir including evaporation (Fig. 2.24) increases in spring and summer, mostly due to agricultural irrigation. One maximum peak outflow at the beginning of 2001 is due to the large volume of precipitation occurring at that time.

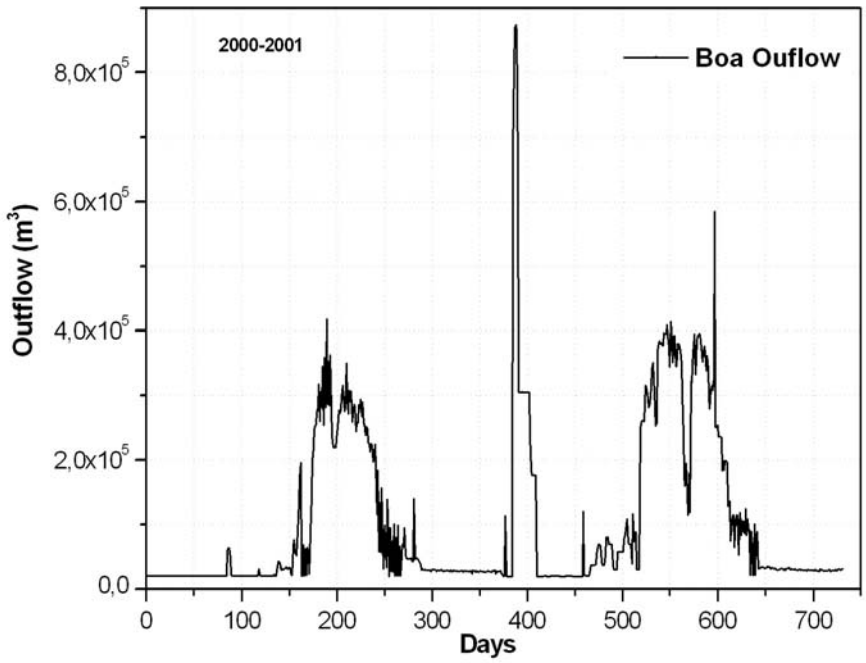

Figure 2.24 Boadella Reservoir outflow time series

2.5.5 Boadella Reservoir profiles

2.5.5.1 Temperature profiles

The Boadella temperature profiles presented in Fig. 2.25 show special and temporal evolution of temperature across the water column. Stratification starts later at the end of April 2000 and the formation of thermocline expending from April until the end of August 2000, the same pattern at 2001. Mixing occurs at the end October for 2000 where the height of storage water volume was (17m) another mixing period starting from the middle of January until the beginning of Mai 2000 this was due the high precipitation that produced high inflow into the reservoir which, together with the wind and surface cooling, contributed to mixing (see Fig. 2.9 and Fig. 2.10B). Additionally,

the stratification in 2000 is more or less strong than 2001 this was linked to the small storage water volume relative to the year 2001 as it was described in Sau Reservoir.

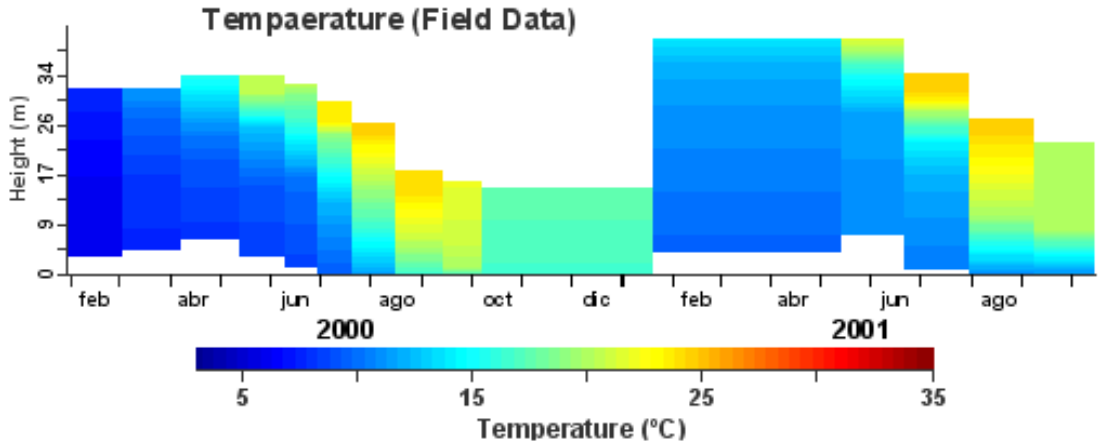

Figure 2.25 Boadella Reservoir time series of observed temperature

2.5.5.2 Dissolved oxygen

Dissolved oxygen profiles (Fig. 2.26) indicate the spatial and temporal variability of the dissolved oxygen concentration. In the stratification period of year 2000, the anoxic hypolimnion zone went from the end of spring to the end of the summer, but in 2001 it started at the end of April and lasted till the end of summer unfortunately we don't dispose dissolved oxygen concentration profile in Mai. Mixing in 2000 correspond to high dissolved oxygen this could be the reason of small river inflow and wind velocity which is relatively high that might be enhance mixing. However, after the beginning of Mai water storage level is decreasing due to the outflow which stabilise the thermal structure and diminish the dissolved oxygen at the bottom. Whereas, in 2001 data was not enough to compare them with 2000. In contrast, heavy precipitation at the end of 2000 (Figs. 2.22, 2.23B) may increase dissolved oxygen content causing phytoplankton growth. See (Fig 2.28).

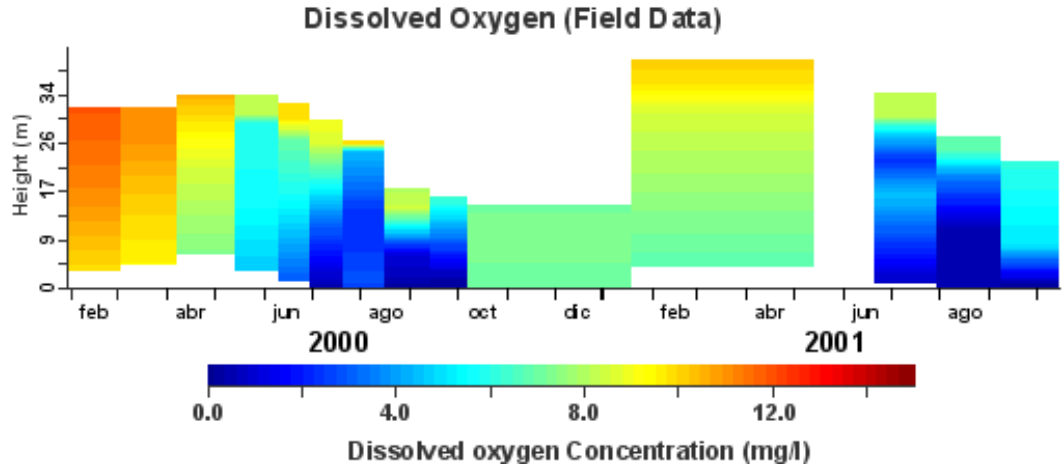

Figure 2.26 Boadella Reservoir time series of measured dissolved oxygen

2.5.5.3 Phosphorus

In the Boadella Reservoir, unfortunately, there were only two vertical profiles. Also there are cases where the phosphorus concentrations are below the detection limit of the measuring system. In Fig. 2.27 we can see these two phosphorus profiles.

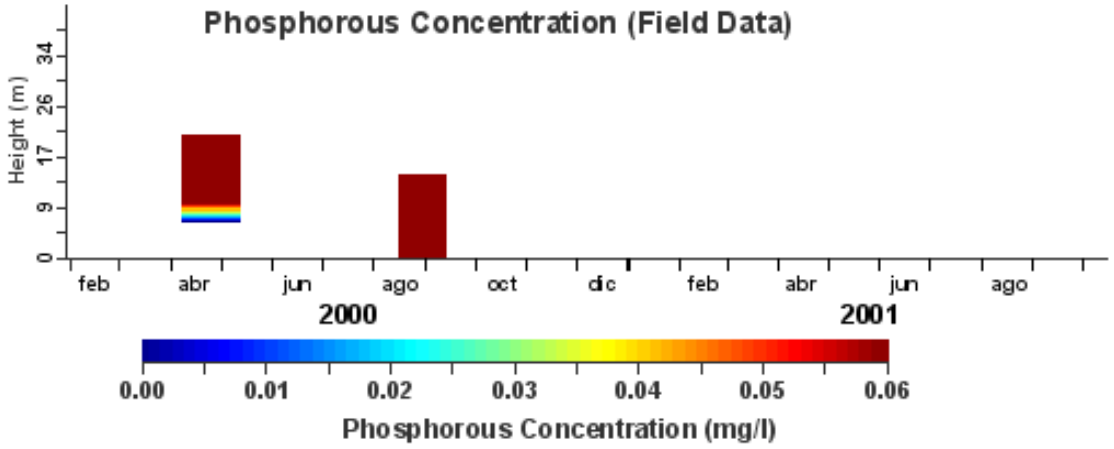

Figure 2.27 Boadella Reservoir time series of field dissolved inorganic phosphorus

2.5.5.4 Chlorophyll

Through time series of chlorophyll profiles (Fig. 2.28) there are two peaks of algal growth corresponding to the summer of 2000 and another at the beginning of the stratified period of the year 2001. Therefore, observed chlorophyll concentration at the beginning of spring, probably due to the inflow peak (Fig 2.23) coming from the catchment area and reaching the reservoir carrying considerable nutrient concentrations.

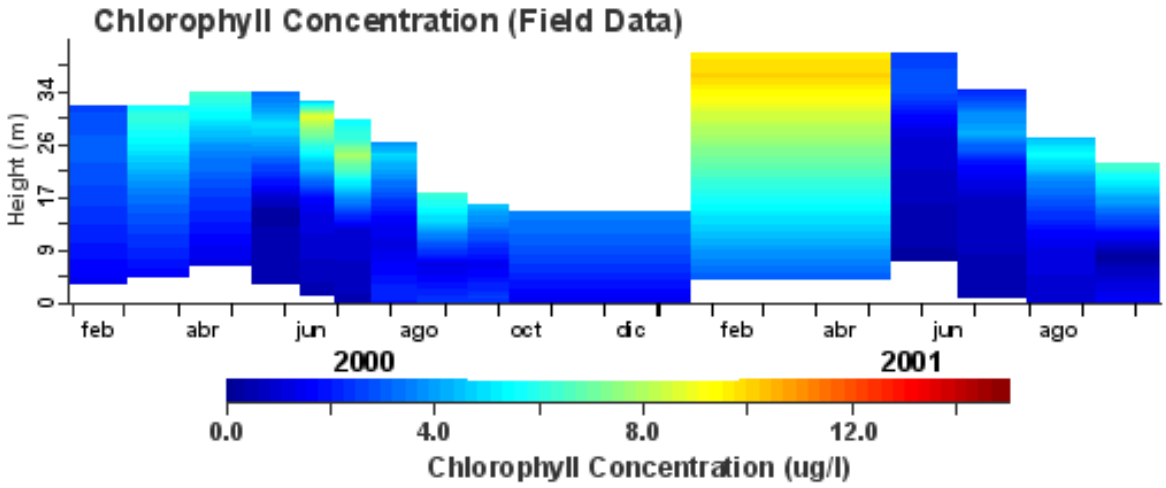

Figure 2.28 Boadella Reservoir chlorophyll time series

CHAPTER 3

Criteria for using a one-dimensional DYRESM model in the Sau and Boadella reservoirs

3.1 Introduction

The understanding of lake hydrodynamics has made much progress in the last twenty years. However, it is still difficult for the general limnological practitioner to gain a quantitative description of the hydrodynamical regimes in a particular lake at a particular time (Imberger, J. (1994))

In general hydraulics characterisation of flow is based essentially on the Reynolds and Froude numbers. So flows are subdivided into laminar or turbulent and super or sub-critical. Therefore, an analogy methodology may be established to permit the limnologist to classify hydrodynamic regime in lakes. Such hydrodynamical regime is important because the mixing and transport process operating in a lake determine, to a large degree, the ecological response of the lake to meteorological forcing, inflows and outflows. Thus, one-dimensional model like the DYRESM is applied to a Mediterranean reservoir such as the Sau or Boadella, it is important to check the validity of assumptions on which its application is based. Accordingly, in this study we have estimated a set of numbers comprising the Lake number, the Wedderburn and Burger numbers, and inflow and outflow Froude numbers. For both reservoirs, we have used two years worth of time series data (2000-2001) consisting of temperature profiles, morphometry data, meteorological data, and inflow and withdrawal data. The temperature profiles have been converted to density profiles using the UNESCO (1981) state formula equation. Later, we have used these density profiles to calculate the non-dimensional numbers.

3.2 Lake Number

The Lake number L_N is a dimensionless parameter defined as the ratio of the moments of the stabilizing force of gravity associated with density stratification to the destabilizing forces caused by wind and considered to be the dominating force. This assumes that the inflow, outflow, and any artificial destratification devices have a minimal destabilizing force. L_N describes the water upwelling from the hypolimnion to the surface layer, expressed by the equation:

$$L_N = \frac{\left(Z_g - Z_o\right) Mg \left(1 - \frac{Z_T}{Z_H}\right)}{A^{3/2}\left(1 - \frac{Z_g}{Z_H}\right)\rho_0 . u_*^2} \tag{3.1}$$

where Z_0 is the centre of gravity of the water mass and Z_g is the centre of volume for the entire lake body; Z_T is the height to the centre of the metalimnion; Z_H is the depth from the bottom of the reservoir; M is the total mass of water [Kg]; g is acceleration due to gravity [$m.s^{-2}$]; ρ_0 is the average water density [$kg.m^{-3}$]; A is the surface area of the reservoir $A(Z)$; and u_* is the water friction velocity [$m.s^{-1}$].

Z_0 and Z_g are defined respectively as follows:

$$Z_0 = \frac{\sum_{i=0}^{Z_H} \rho_i(Z_i) . Z_i . A(Z_i)}{\sum_{i=0}^{Z_m} \rho_i(Z_i) . A(Z_i)} \tag{3.2}$$

$$Z_g = \frac{\sum_{i=0}^{Z_m} . Z_i . A(Z_i)}{\sum_{i=0}^{Z_m} . A(Z_i)} \tag{3.3}$$

The friction velocity u_* was approximated by the bulk aerodynamic formula:

$$u_*^2 = \frac{\rho_a}{\rho_o} C_D . U_{10}^2 \tag{3.4}$$

where U_{10} is the wind velocity at 10 m above the water surface [$m.s^{-1}$]; C_D is the drag coefficient $=1.3.10^{-3}$ [dimensionless]; and $\frac{\rho_a}{\rho_0}$ is the ratio between air and water densities = $1.2.10^{-3}$ [dimensionless].

The value of $L_N = 1$ indicates that the wind is just sufficient to force the seasonal thermocline to be deflected to the surface at the upwind end of the lake. For $L_N >> 1$ stratification is strong and dominates the forces produced by surface wind energy. Under these circumstances, the isopycnals are expected to be primarily horizontal and little seiching of the seasonal thermocline or turbulent mixing in the hypolimnion are expected. For $L_N << 1$, stratification is weak with respect to wind stress. Under these circumstances, the seasonal thermocline is expected to experience strong seiching and the hypolimnion is expected to experience extensive turbulent mixing due to internal shear (Imberger 1989). Thus the hypolimnion water, very rich in nutrients, will reach the surface layer during the wind episode (Imberger 2001).

3.3 Wedderburn Number

The Wedderburn number represents the ratio of the baroclinic restoring force to the wind disturbance force, or the ratio of the restoring moment about the centre of the volume of the lake to the disturbance moment. W describes the upwelling of water from the metalimnion into the water surface, expressed by:

where g' is the modified acceleration due to gravity across the uppermost thermocline.

$$W = \frac{g' h^2}{u_*^2 . L} \tag{3.5}$$

This is represented by $g' = \frac{\Delta\rho}{\rho_o} g$, where $\Delta\rho$ is the density difference between the surface layer and the mean water density, and h is the depth of the diurnal thermocline; u_* is the water shear velocity due to wind stress and approximated by the bulk aerodynamic formula as previously defined in the Lake number calculation; and L is the length of the lake.

$W = 1$ represents the threshold for upwelling of the upper region of the thermocline. For $W >> 1$, tilting of the isotherms due to applied wind stress will be small and horizontal variations negligible. This coincides with strong stratification, light winds, and slow deepening of the mixed layer. For $W << 1$, deepening is dominated by internal shear production and will occur over a much shorter time scale than horizontal convection in the surface layer (Imberger & Patterson 1990). Where W is small and L_N large, only the upper region of the thermocline will respond to wind forcing. Where W and L_N are small, the lake as a whole should respond, and vertical mixing should occur throughout it (Imberger and Patterson 1990).

3.4 Burger Number

The Burger number S_i is an indicator of the influence of the earth's rotation on water motion in reservoirs; that is to say, it characterises the influence of the earth's rotation influence on the water internal waves. S_i is expressed by:

$$S_i = \frac{c_i}{L_{.w} f} \tag{3.6}$$

where L_w is the width of the reservoir and $\frac{c_i}{f}$ is the Rossby radius; c_i is the wave velocity expressed by:

$$c_i = \sqrt{g' H} \tag{3.7}$$

$g' = g.\frac{\Delta\rho}{\rho_0}$ is the reduced gravity; $\Delta\rho$ is the difference between surface water and mean reservoir water density; ρ_0 is the mean water density, and H is the mean reservoir water depth, which depends on the inflow entering the reservoir and water withdrawal from the reservoir. f is the Coriolis parameter equal to the double rate of rotation of the earth at the latitude of the lake, expressed by $f = 2\Omega \sin\varphi$. $\Omega = 7.292.10^{-5} rad^{-1}$ is the earth's angular velocity and $\varphi = 42.3°$ is the latitude of the reservoir.

$S_i = 1$ is the critical value indicating that the rotation is of the same magnitude as gravity. When $S_i >> 1$, the internal oscillations increasingly take on the characteristics of simple gravitational seiches (Antenucci & Imberger 2001).

When $S_i << 1$, the dynamics of the lake are dominated by the earth's rotation. The waves have characteristics similar to those of an inertial oscillation, with the majority of the energy in the wave being in the form of kinetic energy.

3.5 Inflow Froude number

The regime behaviour of the river inflow entering the reservoir is described by the inflow Froude number, F_{ri}

$$\frac{h_i}{H} = \left[\frac{Q_i}{g_i^{'1/2} H^{3/2} . L_w} \right]^{2/3} = F_{ri}^{2/3} \qquad (3.8)$$

where Q_i is the peak inflow discharge; H is the total depth of the reservoir; $g_i^{'} = \frac{\Delta\rho}{\rho 0}$ is the reduced gravity; $\Delta\rho$ is the difference between inflowing water density and the mean reservoir water density; ρ_0 is the mean water density; and $Fri = 1$ is the critical value of the plunge or rise. Where $F_{r_i} >> 1$, the inflow is too large to separate as an underflow or an overflow. When $F_{r_i} << 1$, the inflow separates as an underflow or an overflow. Once it has been established that the river water underflows ($\Delta\rho_i > 1$ and hi/H<1), it is necessary to carry out a more detailed analysis to estimate its entrainment into the downflow and thus the depth of the inflow intrusion.

3.6 Outflow Froude number

The outflow Froude number characterises the type of water withdrawal, expressed by the equation:

$$F_{r_0} = \left[\frac{Q_0}{g'^{1/2} H^{5/2}.} \right] \tag{3.9}$$

where Q_0 is the outflow discharge; $g' = \frac{\Delta\rho}{\rho 0}$ is the reduced gravity; $\Delta\rho$ is the difference between outflow water density and the mean reservoir water density; ρ_0 is the mean water density; H is the total depth of the reservoir. Where $F_{r_0} << 1$, then the outflow is selective from a depth corresponding to the outflow level.

3.7 Methods

Lake numbers were computed for each recorded temperature profile using equation 3.1. We used twenty four temperature profiles measured over two years (2000-2001) for the Sau Reservoir and fifteen for the Boadella Reservoir. For each two available monthly water temperatures profiles we estimate daily water temperature profile in between by linear interpolation. Thus, every profile was converted to density stratification profiles $\rho(Z)$ at every height Z above the reservoir bottoms, using the UNESCO (1981) equation of state formula (Chen and Millero 1986). As water depth decreases and increases with water inflow and outflow, the water surface and the reservoir volume change. To calculate both, interpolation from the bathymetric data was necessary. To determine the daily velocity friction we used equation 2.4, with a drag coefficient of $1.3.10^{-3}$, and a ratio between air and water densities of $1.2.10^{-3}$. Wind velocity is given in meteorological data in Fig. 2.8 for the Sau Reservoir and in Fig. 2.21 Chapter 2 for the Boadella Reservoir. The total mass of water was determined by multiplying each layer's density by its corresponding volume. The centre of gravity and the centre of volume were estimated using equations 3.2 and 3.3. The height to the centre of the metalimnion Z_t was estimated by using temperature profiles. The mean water density was taken as $1000\, kg.m^{-3}$. The depth of the reservoir Z_H and its area were estimated using morphometry data (Sections 2.4.1 and 2.5.1, Chapter 2). The estimated lake numbers are 712 in Sau reservoir and 636 in Boadella Reservoir

As described above for lake number, Wedderburn number values were estimated by linear interpolation between existing profiles. For each temperature profile using equation 3.5 daily friction velocity u_* had been previously defined in the calculation of the Lake number. The depth of the diurnal thermocline h was approximated for each temperature profile.

Modified acceleration due to gravity g' is the ratio of the difference in diurnal thermocline density from the mean water density, divided by the mean water density multiplied by gravity g. L is the average length of the reservoir: $L = 3000m$ for Sau and $L = 1500m$ for Boadella.

The Burger number was obtained using equation 3.6 in which the Rossby radius was calculated as the ratio between longwave phase velocity and inertial frequency.

Longwave phase speed is a function of reduced gravity g', which depends on the difference between surface water density and mean water density divided by the mean reservoir water density. Inertial frequency depends on the latitude of a reservoir; the Sau and Boadella reservoirs are located in the same region and have approximately the same altitude. The earth's angular velocity is about $7.292.10^{-5} rad^{-1}$ □□

The inflow Froude number was calculated using equation 3.8. The discharge or inflow rate Q_i is the peak inflow discharge entering the reservoir and was estimated from the inflow file: approximately $217m^3.s^{-1}$ for the Sau Reservoir and $111.m^3.s^{-1}$ for Boadella (Figs. 2.10B and 2.23B in Chapter 2.) The reduced gravity g_i' is the difference between inflow density and mean reservoir density divided by the mean density. The average width of the reservoir is $B = 700m$ for Sau and $600m$ for Boadella. The total depth of the reservoir H is variable, depending on the volume entering and leaving it.

The outflow Froude number was computed using equation 3.9. The outflow Q_0 was deduced from the withdrawal data (see Figs. 2.11 and 2.24 in Chapter 2). The reduced gravity for outflow is the ratio of the outflow density minus the mean water density to the mean water density. H is the reservoir water depth.

3.8 Results and discussions

3.8.1 Lake number

The L_N values obtained for the Sau Reservoir are always above 1.0 and are relatively high in magnitude. The maximum value is approximately 1874 in the middle of June 2000 (stratification period) corresponding to lowest wind velocity 0.8m/s and the minimum is around 2 approximately in the middle of December 2001. Thus, $L_N \succ 1$ indicating that stratification is the dominant force when compared to wind stress. Minimum and maximum wind velocities are 0.8 and 2.9(m/s) respectively. There is low turbulence and no mixing in deeper water, due to the isolation of the bottom waters from the surface. Consequently, upwelling of the hypolimnion induced by wind stress is unlikely. However at the end of 2001 the Lake number was equal 2, indicating that the hypolimnion was relatively mixed.

The L_N of the Boadella Reservoir fluctuated from a minimum value of 5 in the beginning of June 2000 corresponding relatively to high wind velocity 5.6m/s (see section 2.5.2.4 Chapter 2) to a maximum of 2226 in the end of Mars 2000 corresponding to the lowest wind velocity 0.4 m/s. Compared to Sau the stratification is strong in the first year (2000) and during the second (2001). This is linked to low wind velocity, for which minimum value and maximum values are 0.8 and 2.9 for Sau and 0.7 and 2.1 for Boadella (see Figs. 2.8 and 2.21, Chapter 2.) It should also be noted that morphometry plays an important role in the determination of Lake number, and that determination of the thermocline is difficult. In both reservoirs, water upwelling from the hypolimnetic occurs at the winter end autumn in 2000 and 2001. Fig 3.1 shows the differences in Sau and Boadella‘s Lake numbers. In this figure we see that lake number diminished corresponding to the peak inflow (see Fig. 2.10B, Chapter 2) in the end of the year 2000 means that may inflow also contribute in hypolimnion mixing.

However, in Boadella Reservoir the lack of profiles from the end of August until the end of April influence the estimation of lake number for comparison purposes versus inflow. Also, withdrawal being selective may enhance stratification. For both reservoirs through the period 2000 to 2001 Lake numbers are bigger than the critical value. This indicates that stratification is relatively strong and that although the water of the upper hypolimnion is reaching the surface, the deepest part of the hypolimnion remains unmixed if not influenced by inflow/outflow and cooling forces. Unfortunately, there are fewer profiles for Boadella than there are for Sau. However, the variation in its Lake

number is small, as is the case for Sau. Also, it should be noted that the wind velocity in Boadella, on the days when profiles were taken, was relatively low. We can therefore conclude that both reservoirs were not completely mixed, at least at the time the profiles were taken. It has should also be noted, however, that the profiles were taken during the day. In winter, at daily time $Z_g - Z_0$ is very low but still positive during the day, and the mean velocity of the wind is in general not high enough to overcome stratification. For example, on 09/02/2000:

$Z_g - Z_0 = 1.6.10^{-3} m$, $u^* = 0.0017.m.s^{-1}$ and $L_N = 60$. However, it is very likely that at night time $Z_g - Z_0$ was close to 0 and L_N went to 0. In these circumstances hypolimnetic mixing could be expected.

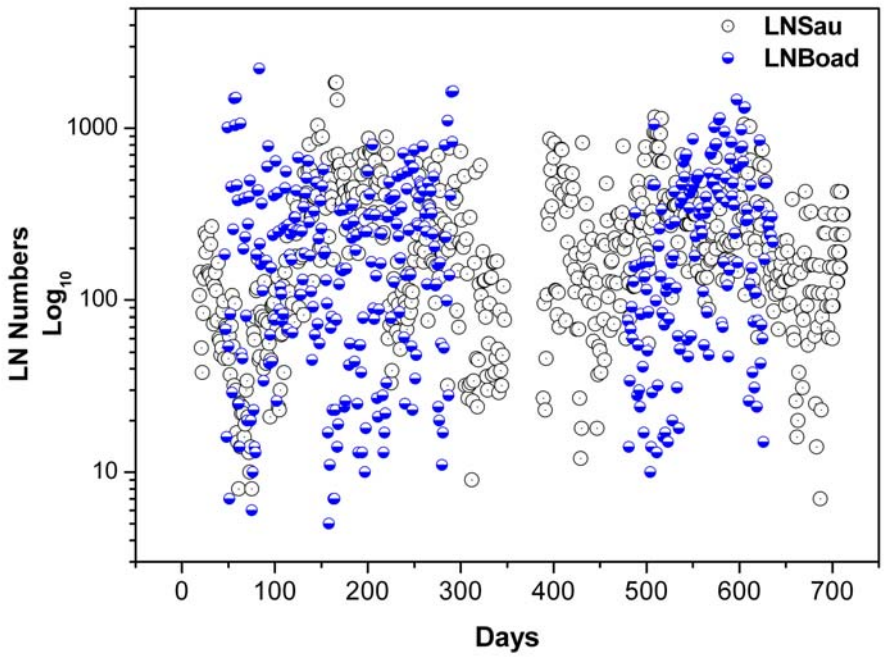

Fig 3.1 The differences in the Sau and Boadella Lake numbers

3.8.2 Wedderburn number

The Wedderburn numbers in the Sau Reservoir do change substantially, tending to oscillate over the two years between 0 and 750. 0nly one value is below 1 corresponding to the value in the beginning of November 2000 corresponding to the high wind velocity 5.6 m/s. Most Wedderburn numbers are above the critical value 1.0, indicating that wind stress on the surface of the lake is able to overcome the stratification in the water column and metalimnetic water can be expected to be vented into the surface layer if we neglect other disturbing forces such as inflow/outflow and cooling.

Wedderburn numbers in the Boadella Reservoir range from approximately 0 to 454 at the end of May and are smaller than those of Sau, indicating that in Sau Reservoir, the diurnal mixed layer is easily mixed. See Fig. 3.2 for Sau and Boadella Wedderburn number differences.

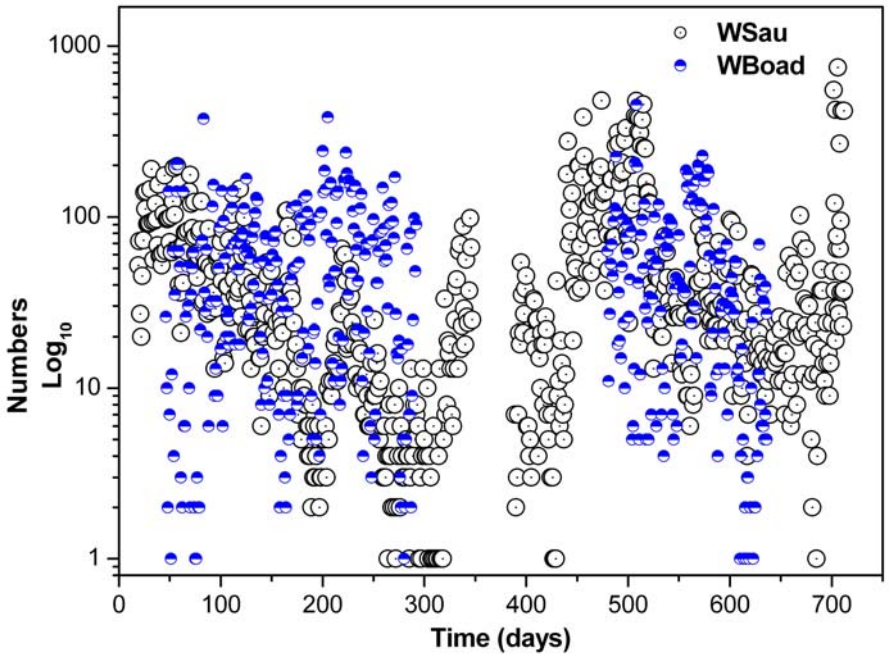

Figure 3.2 Sau and Boadella Wedderburn numbers

3.8.3 Burger number

The Sau Reservoir experiences substantial fluctuation in Si values throughout the two years, with all the values above 1. Burger numbers range from 1.20 to 2.3, with a mean value of approximately 1.75. Variation in the Si can be attributed solely to changes in the phase speed of the wave, since the inertial frequency at the corresponding latitude f and characteristic length scale L_w are both constant. The Burger number is high than the critical value 1.0 and therefore the rotational effects are insignificant. However, given that Si is close to 1, rotation would be discarded. The Sau and Boadella Burger numbers are shown in Fig.3.3

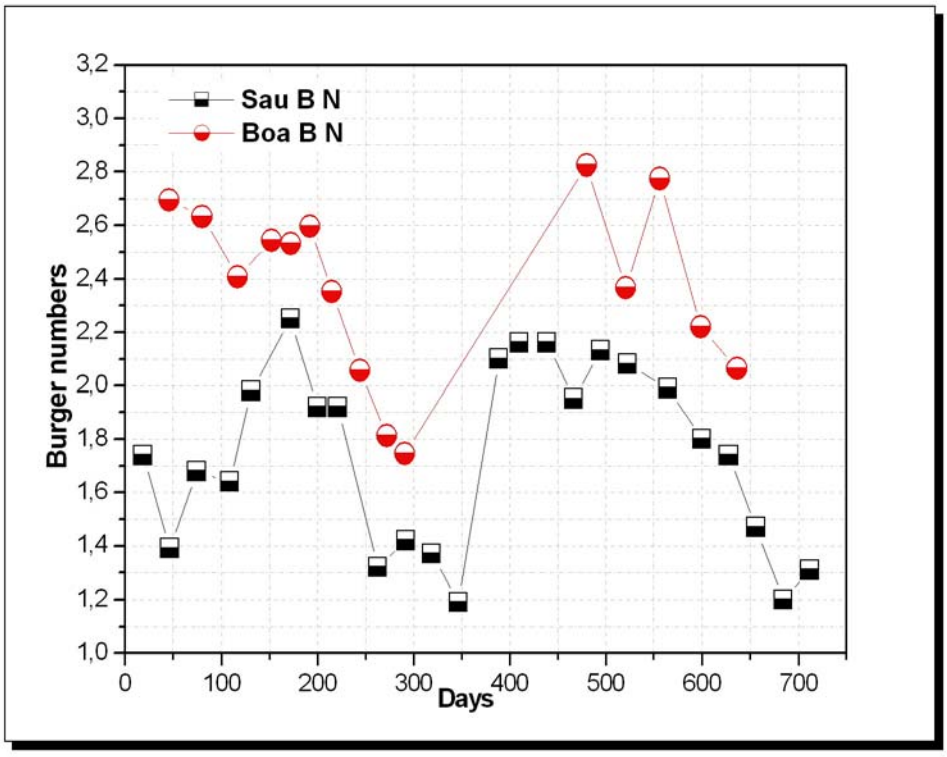

Figure 3.3 Comparison between the Sau and Boadella Burger numbers. Sau is represented by squares, and Boadella by circles.

3.8.4 Inflow Froude number

The average Sau inflow Froude number is 0.01. This is smaller than the critical value 1.0 which means that the inflow inertial force is weaker than the inflow gravity force, and flow separation occurs as the river enters the reservoir. It is important to note that it would be necessary to carry out a more detailed analysis to estimate the entrainment into the inflow and the depth of the downflow insertion.

The inflow Froude number for Boadella is smaller for Sau. This is due to the fact that the velocity of the River Ter which flows into Sau is higher than the velocity of the Muga and Arnera rivers which flow into Boadella. Fig.3.4 shows the inflow Froude numbers for Sau and Boadella.

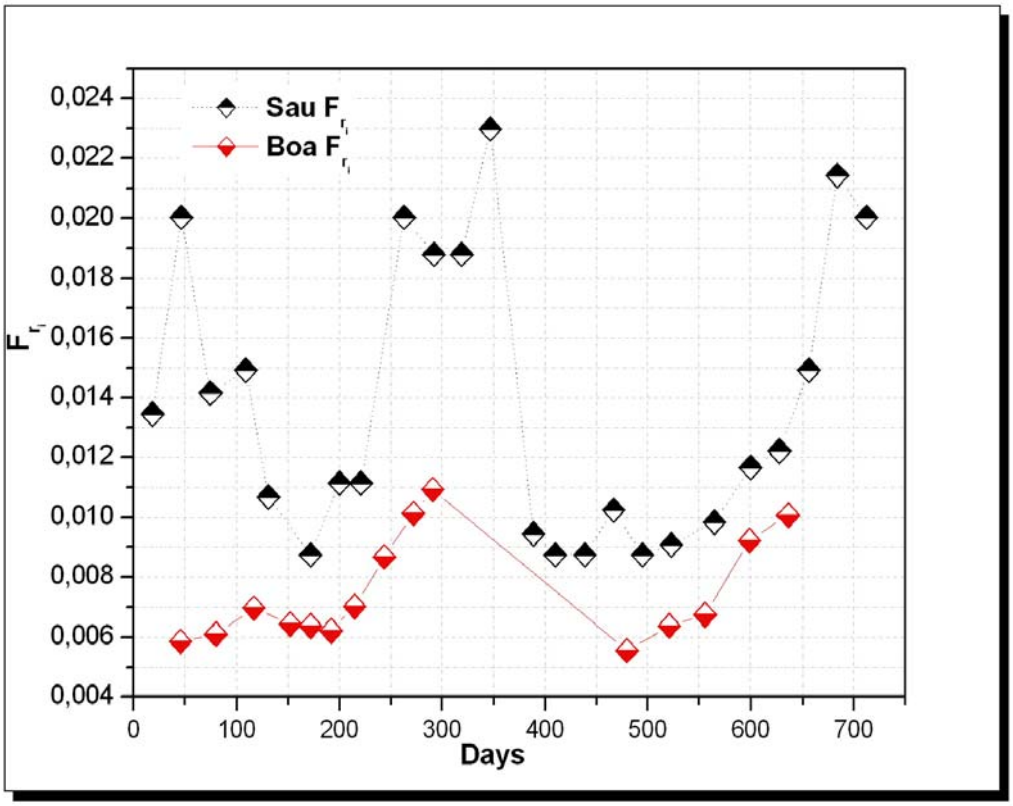

Figure 3.4 Sau and Boadella inflow Froude numbers

3.8.5 Outflow Froude number

Sau's average outflow Froude number is about 0.01, which is lower than the critical value of 1.0. Boadella's average outflow Froude number is 0.001, ten times smaller than Sau's one. This indicates that in both reservoirs the outflow is selective. Fig. 3.5 shows the Sau and Boadella outflow Froude numbers.

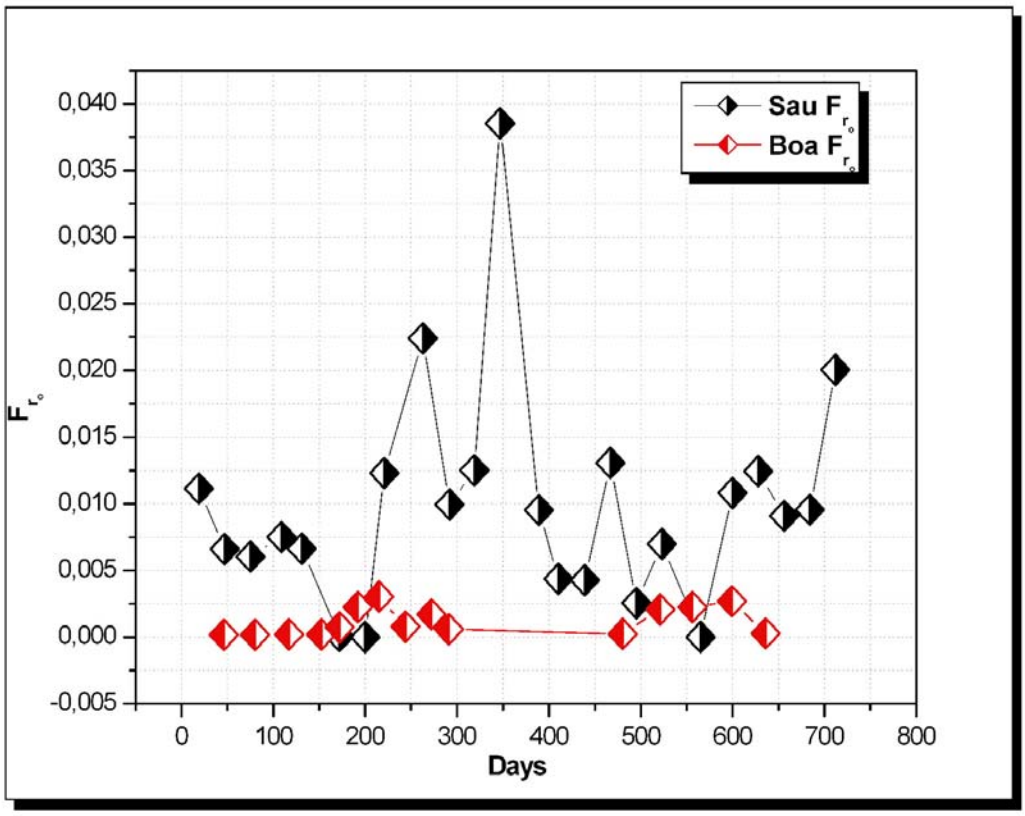

Figure 3.5 Sau and Boadella outflow Froude numbers

3.9 Conclusions

The Lake number L_N is an indicator of dynamic stability and of the extent of deep turbulent mixing, while the Wedderburn number W is an indicator of surface layer mixing. In both reservoirs, L_N is large and W is small for the profiles under study. This means that the wind will induce higher vertical mode oscillations (Imbeger, J. 2001). Where $L_N \prec 1$, the one-dimensional DYRESM model can be used. It should be pointed out, however, that to calculate the L_N we have used daily mean wind velocity and temperature profiles taken during the daytime. It is likely that there are times during the night and/or when there are very high winds that $L_N \prec 0$, and hypolimnetic upwelling takes place. Our available data of two years monthly temperature profiles for estimation of lake number and Wedderburn number are not enough because it leads to an overestimation of these numbers especially when the days when profiles were taken are calm therefore daily temperature profiles and daily inflow are needed to judge perfectly whether the one dimensional hydrodynamic may be applied or not. For this reason, daily lake numbers, which were obtained by interpolation of daily temperature from monthly observed water temperature profiles, lake numbers (L_N) are greater than one means that the buoyancy force is greater than wind force and the deflection of the centre of the water masse is small. Thus, density structure is approximately horizontal and the one dimensional assumption is valid. Also we have estimate the daily wedderburn number as we did for lake numbers. Wedderburn numbers, are mostly greater than one indicating that tilting of the isotherms is small; this is due to the weakness of the wind stress.

The Burger number S_i is slightly larger than one, indicating that rotation might be discarded.

$F_{r_i} << 1$ and $F_{r_o} << 1$ indicate that in both reservoirs flow separation occurs, and that outflow is selective.

CHAPTER 4

Application of the DYRESM-CAEDYM model to the Sau Reservoir

Abstract

The aim of this chapter is to describe the application to the Sau Reservoir of the one dimensional hydrodynamic DYRESM model linked to the water quality CAEDYM model. Simulation was undertaken for two years between 2000 and 2001 with the aim of predicting thermal structure and water quality variables such as dissolved oxygen, dissolved inorganic phosphorus and chlorophyll in the reservoir. Inputs were meteorological data, river inflow and outflow data, morphometry parameters, an initial profile and file configuration data. The CAEDYM model also requires a configuration file and initial profiles for all the water quality data, as well as the calibration of different parameters such as sediment-dissolved oxygen, the sediment flux release rate of phosphorus and the maximum potential growth rate of phytoplankton.

4.1 Introduction

Most temperate lakes develop strong thermal stratification every summer. This stratification of the water column means that there are water density differences. In classical limnology the water column can be divided into three layers: epilimnion, metalimnion and hypolimnion, although many Mediterranean lakes present a continuously stratified profile (Casamitjana et al. 1993). Chemical and biological gradients reflect the thermal stratification (Reynolds 1992; Watanabe 1992), which is mainly affected by external forces such as heat input, wind velocity and Lake Morphometry.

The stratification magnitude also depends on the river inflow temperature (Straškraba 1973; Riera et al. 1992; Straškraba et al. 1993; Armengol et al. 1994; Hocking and Straškraba 1994). The River Ter, the Sau's main tributary, is polluted and contains a high concentration of nutrients, mainly ammonia and soluble reactive phosphorus (Vidal & Om 1993; Armengol et al. 1994), but also particulate and dissolved organic matter (Simek et al. 1998). The inflow temperature is usually lower than the reservoir's surface layer and therefore the water sinks to the depth at which its density is equal to that of the reservoir water at that level. The inflow water is characterised by a higher flow velocity, and consequently causes thermocline erosion. Additionally, inflow is one of the main sources of nutrients and other chemical material entering a reservoir, and its intrusion can influence the vertical gradient of nutrients (Armengol et al. 1986; Vidal and Om Tubau 1993; Komárková and Hejzlar 1996).

The DYRESM-CAEDYM (Imberger and Patterson 1981) combines a one dimensional hydrodynamic model with a water quality model to predict thermal structure and water quality variables such as dissolved oxygen, dissolved inorganic phosphorus and chlorophyll. The validity of this model was checked in the previous chapter and its suitability for application to the Sau Reservoir in north-eastern Spain established. We will calibrate it for the dry year 2001, and validate it for the year 2000.

4.2 Materials and methods

The Sau Reservoir is the first of a cascade of reservoirs situated in the central part of the River Ter, which was first filled in 1964. The River Ter is 200 km long and has its source in the Pyrenees in the NE of Spain. One of the most characteristic of Sau, a river valley reservoir 18.225 km long, is its canyon-shaped morphology (Fig. 4.1). The length of the lacustrine part of the reservoir is 3600 m and its maximum width is 1300 m (Armengol et al. 1999). The use of the Sau Reservoir water as a drinking water supply to the Barcelona metropolitan area explains why it has been studied ever since it was first used for this purpose. As Vidal & Om (1993) and (Armengol et al. 1994) have shown, the Sau's trophic condition has evolved in response to human activity in the watershed over time, in particular in terms of the presence of soluble reactive phosphorus and inorganic dissolved nitrogen. Following the construction of sewage treatment plants the phosphorus has decreased but the dissolved inorganic nitrogen has increased. We are attempting to study the hydrodynamics and water quality of the Sau

Reservoir for 2000-2001. The available data was supplied by a team led by Professor Armengol. Temperature calibration has been done by varying minimum maximum layer thickness as (Andrew et al. 2007) has found. Additionally, in our study we fined out that also vertical mixing coefficients and effective surface area are very important calibration parameters.

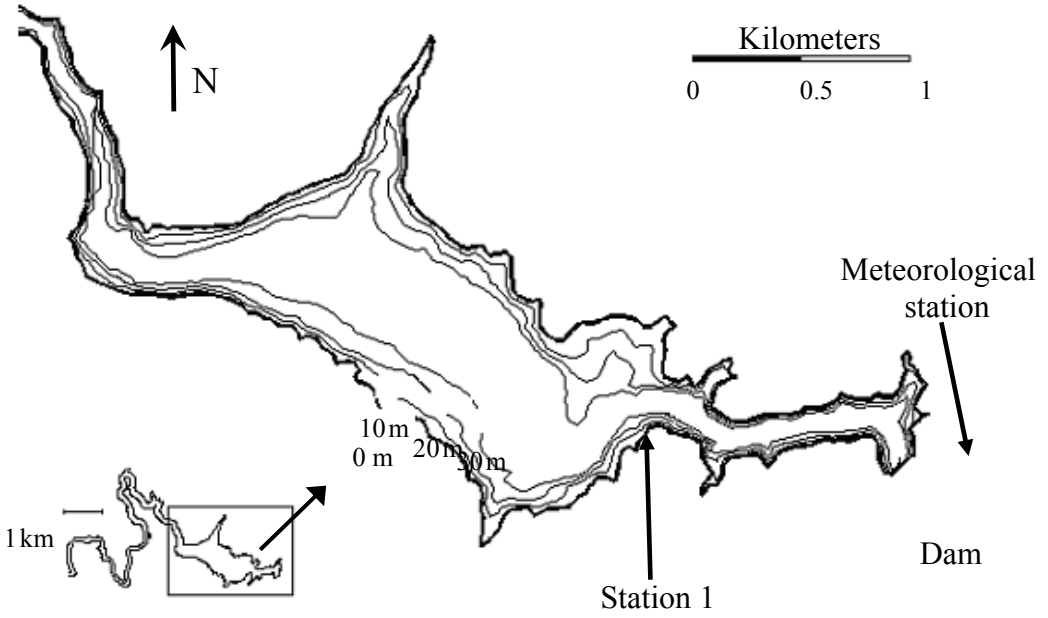

Figure 4.1 Bathymetric map of the Sau Reservoir showing the location of measuring stations and the meteorological station.

4.3 DYRESM-CAEDYM model

The DYRESM (Dynamic Reservoir Simulation Model) was developed in the Water Research Centre of the University of Western Australia. It is a one dimensional hydrodynamic model that simulates temperature, salinity and density in lakes and reservoirs. DYRESM model driver to the CAEDYM water quality model is a process model, based on a Lagrangian layer scheme in which the lake is modeled by a series of horizontal layers of uniform property but variable thickness. The layer positions change as inflow, outflow, evaporation and rainfall affect the stored volume, and layer thicknesses change as the layers are moved vertically to accommodate volume changes. The input data are necessary daily meteorological data for DYRESM include total solar

radiation, average air temperature, average vapor pressure, average wind speed, and total rainfall. Daily total inflow volumes and average daily concentrations of temperature and salinity along with water quality parameters must be given with the inflow data. Daily total outflow volumes from specified heights above the lake bottom must also be given. Reservoir bathymetry is input as a table of height from the lake bottom versus the surface area, and cumulative volume. Initial conditions in the form of vertical profiles for temperature and salinity along with all water quality parameters in the water column must also be provided.

An extensive description of the model has been given in Imberger and Patterson (1981), Hocking et al. (1988), Hocking and Patterson (1991) and Casamitjana and Schladow (1993). The model is based on layers of uniform properties. The layers move vertically, expanding and contracting in response to mass fluxes. Physical processes of heat exchange across water surfaces, heat distribution by mixing based on a turbulent energy budget formulation which includes the effects of convective overturn, stirring by wind, and shear production at the interface between the epilimnion and hypolimnion can all be modelled by it. Turbulent diffusion is modelled by the solution of the diffusion equation with a variable coefficient determined from energy released by the plunging of streams, and wind induced seiching. The criteria for the application of the DYRESM model to the Sau Reservoir were presented in the previous chapter.

The CAEDYM (Computational Aquatic Ecosystem Dynamics Model) is a water quality model also developed in the Water Research Center of the University of Western Australia. It is designed to be coupled with a hydrodynamic driver 1D model such as the DYRESM for the simulation of lakes and reservoirs. The CAEDYM contains process description for nutrient cycling, phytoplankton, zooplankton and dissolved oxygen dynamics (Griffin et al. 2001; Romero and Imberger 2003). State variables and an ecological parameterization description have been given by (Hamilton and Schladow 1997). The CAEDYM model used in this study was configured to simulate the dynamics of phosphorus, nitrogen, dissolved oxygen and algae.

The assumption of the DYRESM-CAEDYM model's applicability to the Sau Reservoir was explained in chapter 3. As a first step, we will calibrate the model for the year 2001 which was a dry year. After that we will validate the model for the year 2000. It should

be noted that the inflow file in the ecological model must include daily water quality concentration data as well as daily temperature and salinity. The lack of daily river water quality data such as dissolved oxygen dissolved inorganic phosphorus and chlorophyll makes the simulation impossible unless hypothetical data is used. Then, estimation of inexistent observed river inflow daily water quality concentration of nutrient is difficult. Our hypothesis based on using those available water quality concentration of nutrient in reservoir to derive from them river inflow daily water quality concentration of nutrient. Thus, daily river inflow data of nutrient concentrations were taken as the long-term average nutrient concentrations in the reservoir constant over the whole simulation length. In our study the CAEDYM model was configured to simulate the dynamics of dissolved oxygen, dissolved inorganic phosphorus and one phytoplankton group.

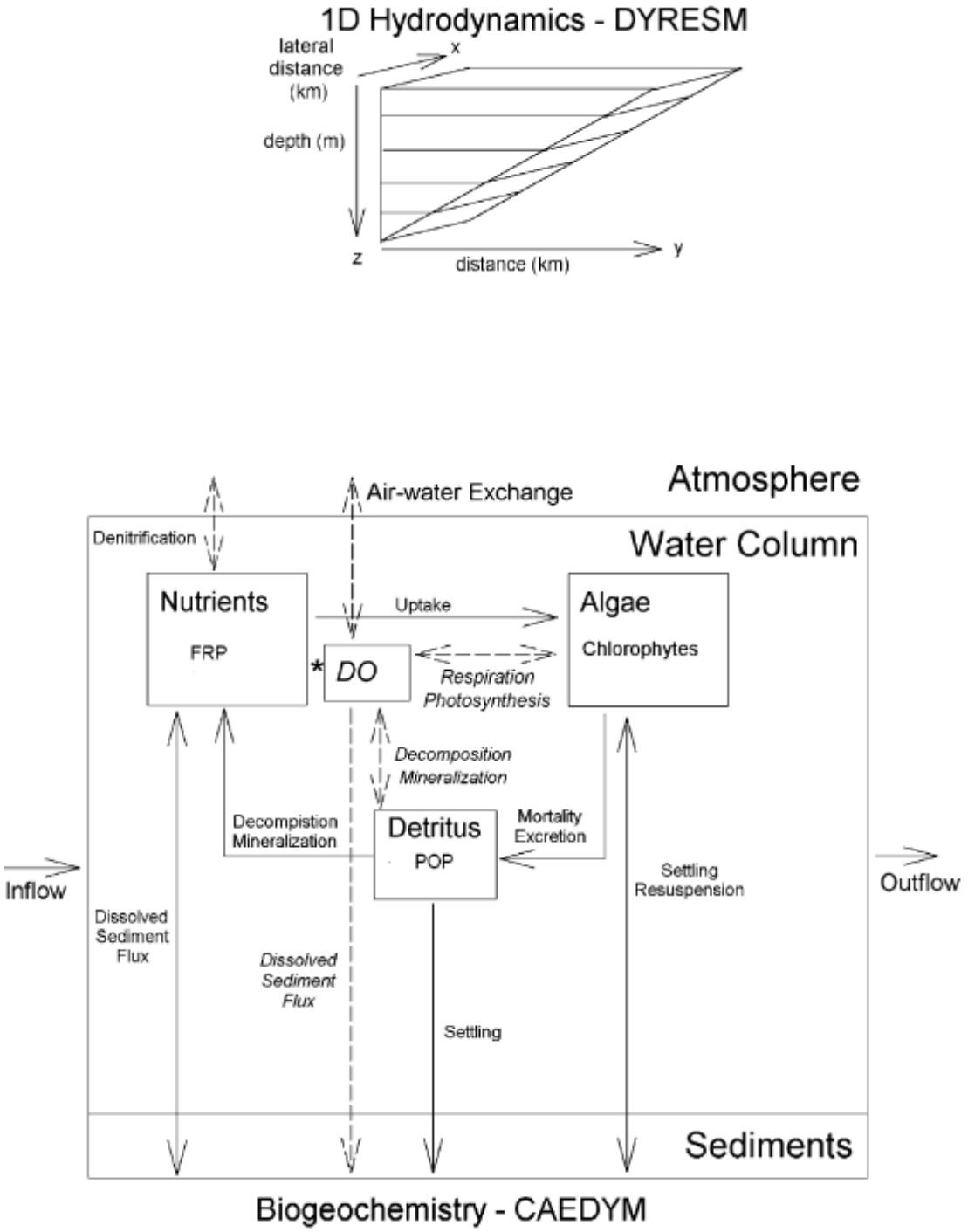

Figure 4.2 The coupled DYRESM-CAEDYM model simulates temperature, dissolved oxygen, phosphorus and chlorophyll in the Sau Reservoir.

4.4 DYERESM-CAEDYM Calibration and Validation

DYRESM-CAEDYM was configured to simulate temperature, water quality parameters as dissolved oxygen, nutrients and chlorophyll for Sau Reservoir during two years period 2000–2001. Simulation start dates were chosen as the nineteen in January 2000 for which first temperature profiles were recorded.

The Calibration Process of the model is required because biologically systems are inherently different. However, in hydrodynamic model DYRESM several input parameters implicated in thermal processes were tested for their influence on heating and mixing in the DYRESM model. So varying wind speed by using a wind factor multiplier of 1.3 and 1.5 does not give a substantial variation in the predicted thermal structure, probably due to the weak wind velocity registered in 2000 and 2001 (Fig. 2.8, Chapter 2). Only changes in benthic boundary layer thickness from zero to 0.02 resulted in slight difference in surface water temperatures. However, tested parameters, such as minimum and maximum layer thickness, vertical mixing coefficient, effective surface area, wind stirring coefficient potential energy mixing and base extinction coefficient produced acceptable changes in predicted water temperature profiles. So minimum and maximum layer thickness, diffusive fluxes constant and effective surface area were designated as highly sensitive parameters. Thus, six separate calibrations were performed, the first for layer thickness and the second for the wind stirring efficiency parameter, to identify the values of these parameters in calibration process which would result in the least amount of error between observed and predicted temperature profiles. Minimum layer thickness was varied from 0.5, 0.6, 0.75 and 1.0 m and maximum layer thickness from 1, 1.5, 2.0 and 2.5. For the calibration of layer thickness, all simulations involved maximum layer thickness set to equal or less than twice the minimum layer thickness. The second calibration tested values of 0.8, 0.4, 0.07, and 0.02 for the wind stirring efficiency ,the third setting is the vertical mixing coefficient which has testing values of 200, 1000, 5200, and 7200 with the reference of the adequate values of minimum layer thickness, maximum layer thickness and wind stirring efficiency values identified in the preceding calibration.

Fourth setting is effective area coefficient, the tested values area are 5000, 30000, 500000 and 10000000, fifth is the base extinction coefficient with value varying from

0.25, 0.6, 1.5 and 3.0 and finally setting values of potential energy mixing coefficient at 0.001, 0.07, 0.2 and 0.5 at albedo values of 0.08 and 0.12 respectively.

A maximum layer thickness of 1.5 m and minimum layer thickness of 0.5 m were the best settings to predict water temperature at all depths (Fig. 4.3A) as was described by (Andrew J et al 2007). Simulation also, demonstrated that wind stirring efficiency parameter of 0.07 performed well as predictors of water temperature, bottom temperature T_B and thermocline depth Z_T (Fig. 4.3B). However, we admit a value of 0.06 to remain consistent with the recommendation in the DYRESM operating literature (Antenucci and Imerito 2003) where wind stirring efficiency was estimated to 0.06.

Increasing in vertical mixing coefficient tend to decrease in differences between predicted and observed temperature $W_{T,}$ predicted and observed bottom temperature T_B , and predicted and observed thermocline depth Z_T (Fig. 4.3C). Thus, the best value was 7200. Effective surface area giving the best thermocline depth Z_T was value of 1.10^7 but corresponding at high difference between predicted and observed water temperature and bottom temperature W_T and T_B (Fig. 4.3D).

Base light extinction coefficient only decreases the difference between predicted and observed thermocline temperature and have no influence to the water temperature and bottom temperature (Fig.4.3F). Finally, simulations demonstrated that thermocline depth was less accurately predicted than at lower albedo. Whereas an increase solely in albedo increased differences between predicted and observed temperatures as well as differences between predicted and observed bottom temperature (Fig. 4.3E). Table 4.1 summarizes sensitive and insensitive parameters in the model.

Parameter Set Value albedo	0.08
Benthic boundary layer thickness (m)	0.00
bulk aerodynamic momentum transport coefficient	0.0013
critical wind speed (m s–1)	3.0
effective surface area coefficient	1.0×10^7
emissivity of a water surface	0.96
non-neutral atmospheric stability correction switch	No
potential energy mixing efficiency	0.20
shear production efficiency	0.08
vertical mixing coefficient	200
wind stirring efficiency	0.06
Following calibrations	
minimum layer thickness	0.5 m
maximum layer thickness	1.5 m
effective surface area coefficient	1×10^7
vertical mixing coefficient	7200

Tab le 4.1. Values of coupled model parameters and model simulation specifications.

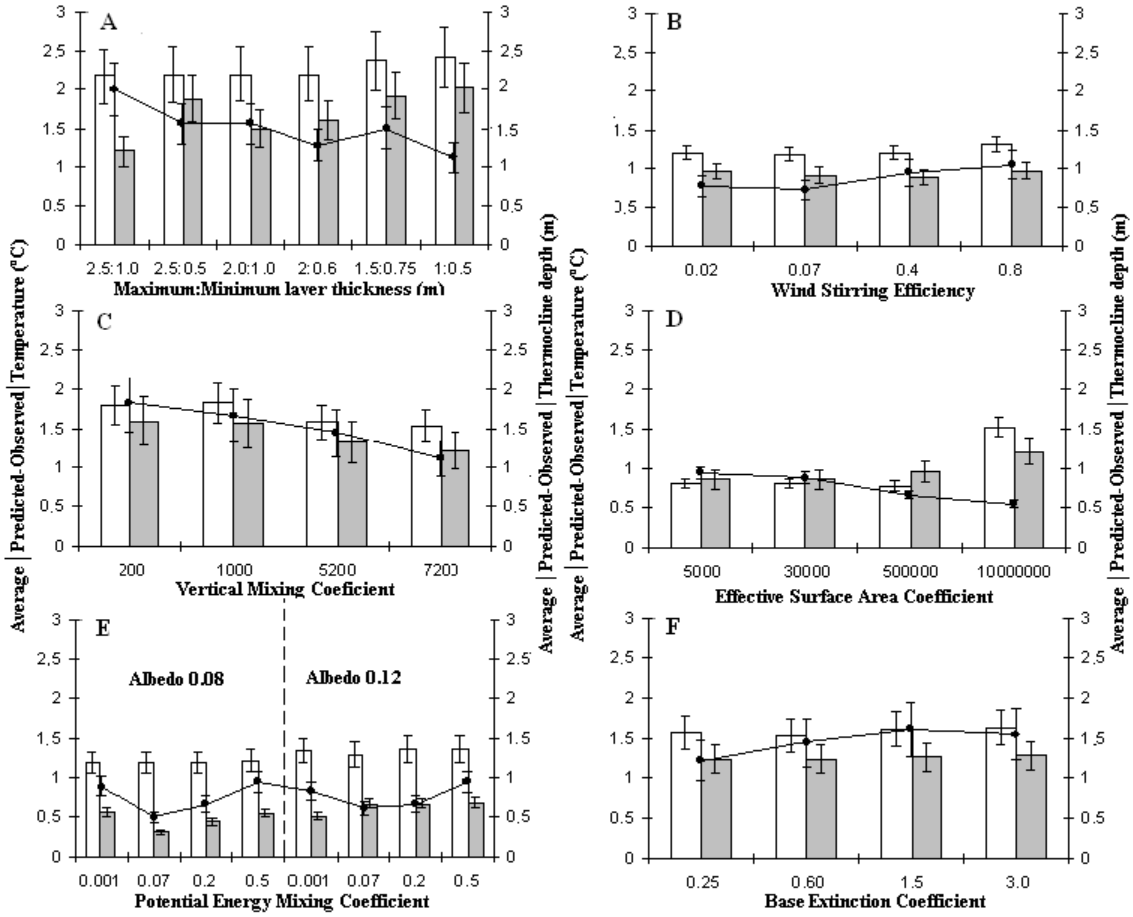

Figure 4.3 *Average absolute difference ± standard error of the mean between DYRESM-CAEDYM predicted and observed water temperature (white), bottom water temperature (gray) and thermocline depth (line) at various layer thickness setting (A), wind stirring efficiency values (B), Vertical mixing coefficient (C), effective surface area coefficient (D), albedo and potential energy mixing coefficient values (E), and base extinction coefficient(F).*

The ecological model was calibrated by trial-and-error adjustment of the most sensitive water quality parameters to give the best match with trends in the field, meaning that the calibration process has to start with temperature, dissolved oxygen, phosphorus and finally with the chlorophyll. After temperature calibration the mean sensitive parameters in dissolved oxygen are static dissolved consumption by sediments and half saturation constant for sediment oxygen demand, the principal parameters in phosphorus calibration are maximum rate of phytoplankton phosphorus uptake, sediment flux release rate of phosphorus, the parameters that affect chlorophyll are growth rate, phosphorus and light utilisation. The water quality calibration parameters are grouped in table 4.2.

As previously stated, the calibration period was assigned to the dry year from 23 January to 13 November 2001.

Calibration of dissolved oxygen requires checking of the sediment oxygen demand, the organic contribution and the inflow concentration. The calibration of dissolved inorganic phosphorus depends on the inflow concentration, the sediment release rate, inorganic particulates, phytoplankton, and, finally, chlorophyll, which is the most difficult parameter to calibrate because it depends on the information that is available about modelled species such as growth rate, nutrients, light utilization and settling or vertical migration characteristics. The overall calibrated parameters are grouped in Table 4.2.

After calibration, the DYRESM-CAEDYM model is used to simulate reservoir behaviour over 705 days, from 19 January 2000 to 31 November 2001, a two year period that includes the one year calibration period. It will be seen later that there is strong density stratification during the warmer months of the year. Simulated dissolved oxygen concentrations will demonstrate the existence of an anoxic zone in the deeper hypolimnion during the stratification period. Phosphorus simulation will also show an important load of this nutrient at the bottom of the hypolimnion. For chlorophyll the simulation will show the existence of algal blooms at the surface. The two year series of simulated temperature, dissolved oxygen, phosphorus and chlorophyll compared to field series are shown in Figs 4.10, 4.11, 4.12, and 4.13.

Parameter	Description	Units	Assigned range	Assigned value
Dissolved Oxygen				
ϑ_{op}	Temperature multiplier for SOD	-	1.02-1.14	1.07
F_{SOD}	Static sediment exchange rate	$g/m^2/day$	0.02-15	3.2
K_{SOD}	½ sat constant for static DO sediment	$mgDO.l^{-1}$	-	0.2
ϑ_{ON}	Temperature multiplier for nitrification	-	1.001-1.10	1.08
k_n	Nitrification rate coefficient	day^{-1}	0.01-0.1	0.02
K_N	Half saturation constant for nitrification	$mgDO.l^{-1}$	-	2.0
k_r	Phytoplankton respiration mortality/excretion	day^{-1}	0.01-0.10	0.08
K_{DOB}	Half sat const for DO dependence of POM/DOM decomposition	$mgDO.l^{-1}$	-	3.0
Dissolved Inorganic Phosphorus				
$IP_{\min}$	Minimum phytoplankton internal Phosphorus	$mg\ P(mg\ ChIa^{-1})$	0.1-1.0	0.6
$IP_{\max}$	Maximum phytoplankton internal Phosphorus	$mg\ P(mg\ ChIa^{-1})$	1.0-5.0	2.2
$Up_{\max}$	Maximum rate of phytoplankton phosphorus uptake	$mg\ P(mg\ ChIa^{-1})day^{-1}$	0.05-1.0	0.2
K_{ep}	Specific attenuation coefficient (phytoplankton)	$\mu g.Chlal^{-1}.m^{-1}$	-	0.016
K_{ePOC}	Specific attenuation coefficient of POC (particles)	$mg.m.l^{-1}$	-	0.001
$POP_{1\max}$	Max transfer of POPL->DOPL [Decomposition]	day^{-1}	-	0.03
$DOP_{1\max}$	Max mineralization of DOPL->PO4 [Mineralization]	day^{-1}	0.01-1.0	0.075
$DOP_{2\max}$	Max mineralization of DOPR->PO4 [Mineralization]	day^{-1}	0.002-0.018	0.003
S_p	Sediment flux release rate of phosphorus	$g.m^{-2}.day^{-1}$	3.10^5-8.10^5	5.10^5
K_P	Half saturation constant for phosphorus	$mg.L^{-1}$	0.001-0.025	0.005
ϑ_S	Temperature multiplier of sediment fluxes	-	1.001-1.10	1.05
Chlorophyll				
$P_{\max}$	Maximum potential growth rate of phytoplankton	day^{-1}	1.3-3.5	1.3
ϑ_p	Phytoplankton temperature multiplier	-	1.02-1.14	1.06
I_K I	Parameter for initial slope of P_I curve	$\mu Em^{-2}s^{-1}$	100-500	100

Table 4.2 The major calibrated water quality parameters used in the DYRESM-CAEDYM model.

4.5 Simulation and results

Daily averaged short wave radiation, long wave radiation, wind speed, inflow/inflow temperature and withdrawal from 2000 to 2001 are represented in Figs. 2.6, 2. 8, 2.10 and 2.11 in Chapter 2.

Good agreement was found between the simulated and the observed temperatures measured at the Nàutic station. (Station 1). For the year 2001 (Fig. 4.4) the agreement is specially good for the period ranging from January to July, and during the autumn the maximum difference observed was 1ºC. However, during the stratification period running from July to the end of September, the simulated temperature in July and August was higher than the observed, may be metalimnion position is not completely well captured. The maximum observed difference was 4.5ºC. In the surface layer (Fig. 4.13A) simulated temperatures fit well with observed ones.

For comparison purposes we chose four profiles on Julian days 44, 101, 199, and 290 because they represent four seasons in the year 2001. In Fig. 4.5 the difference between simulated and observed profiles is presented. On Julian day 44, the simulated bottom temperature is about 0.5 ºC lower than the observed and on Julian day 101 the simulated hypolimnetic temperature is approximately 1ºC higher than the observed. However, the epilimnion temperatures taken during the same days show an inverse tendency. For

Julian day 199 there is a small difference between simulated and observed temperatures in the surface mixed layer and for Julian day 290 simulated and observed temperatures are very similar. The simulated metalimnetic temperature is higher than the observed one for Julian days 44 and 101. The opposite is the case for Julian day 199, but the simulated temperature is approximately the same as the observed one for Julian day 290.

In Fig. 4.4, the temperature isolines are more separated in the observed than in the simulated data (see also Fig. 4.9) meaning that the predicted metalimnion temperature is high than the observed temperature.. This may be due to two dimensional effects such as higher internal mode waves not taken into account in a 1D model (Vidal et al. 2005), or to the fact that metalimnetic mixing in the DFYRESM model is stronger than in reality. Despite of this, the comparison between simulated and observed temperatures shows that the DYRESM-CAEDYM model can be accepted as a good tool for predicting the evolution of the thermal cycle in the Sau Reservoir.

The simulated dissolved oxygen concentrations in Fig. 4.6A are in reasonable agreement with the field measurements. Simulated dissolved oxygen concentrations in Figs 4.6A and 4.10A give a good prediction of dissolved oxygen represented in the depletion of the reservoir's hypolimnion. The concentration of dissolved oxygen is in the range of 0 to 4 $mg.l^{-1}$. This lower DO concentration promotes anaerobic processes, and produces gases such as methane, hydrogen sulphide and ammonia. These gases impart a bad taste to drinking water and in large concentrations can be toxic. Therefore it is therefore necessary to intervene quickly using a destratification system to maintain water quality standards. The high amount of dissolved oxygen measured in the surface layer's March profile (18mg/l) (see Fig. 4.13B) is probably due to a peak in the level of bloom algae, most likely other type of phytoplankton, in early spring, which the model cannot reproduce. From January to March 2001, there is a deficit (5mg/l) (see Fig. 4.13B) of dissolved oxygen in the bottom layer, despite the mixing in this period. The reason is that the deeper hypolimnion is not totally mixed, which is in agreement with the high Lake numbers found in Chapter 3. However, from the end of October 2001 until the end of the same year the opposite occurs: simulated dissolved oxygen is a little higher than that in the field; the difference is estimated at (5mg/l). In general, though, it

can be said that the DYERSM-CAEDYM model is a good predictor of dissolved oxygen in the Sau Reservoir in spite of the anomalies described above.

The simulated dissolved inorganic phosphorus concentration displayed in Figs. 4.7A and 4.11A exhibit the same trend as the concentration that was measured. A high phosphorus concentration at the bottom and depletion in the surface layer were observed during the stratification period, which indicates that this element is probably the main factor of limiting the biological activity in the Sau Reservoir. Also, mixing occurred in winter and autumn. So we can say the model gives a good prediction of the phosphorus for half of the year 2001. Nevertheless, from time to time we observe a simulated phosphorus concentration that is high compared to that observed in the field, which is perhaps due to the river inflow phosphorus concentration. On the other hand, for the second half of the same year there is a big deficit between simulated and observed phosphorus concentrations, especially in the hypolimnion (see Figs 4.7C and 4.11C). The reason is still unclear but the excess of phosphorus on the bottom layer in the field may be due to an extra source of phosphorus that has not been taken into account, such as ground water flow, or to illegal seepage of agricultural sewage water, infiltrating directly from the catchment area to the reservoir and bypassing treatment plants. It appears that the DYRESM-CADYM model simulates dissolved inorganic phosphorus in the surface layer well (Fig. 4.13C) and accurately represents trends elsewhere in the field. However, the big difference between the field and simulations in the bottom layer may depend on the accuracy of data. The neglect of lateral and longitudinal phosphorus concentrations may also impact on the simulation.

With regard to chlorophyll, the DYRESM-CAEDYM model's simulation correctly indicates the existence of phytoplankton blooms at the surface level from early spring, as shown in Figs 4.8A and 4.12A. However, in the simulation theses blooms extend to July with a high order of magnitude compared to what was observed (Fig. 4.13D). The probable cause is the existence of one or more different phytoplankton species as diatoms which we have not been considered. As it was described by Serra et al. (2007); green algae, diatoms, and cryptophyceae were the dominant phytoplankton community in the summer period. Therefore, inclusion of S_i dynamics into CAEDYM may reduce the algal biomass peak via limitation by this third macronutrient , as well as the limitations of the one dimensional model may be the cause of this deference. In March and August the simulated and observed levels are far apart. Chlorophyll is therefore seen to be very difficult to calibrate because it depends on all the variables described above, and any changes in their calibration factors affect its concentration.

Finally, one can conclude that combine model DYRESM-CAEDYM offers a general tool that is capable to produce best result for temperature, dissolved oxygen, good tendency for phosphorus, and small divergence in reproducing the seasonal variation of biomass of the phytoplankton this could be due to daily river inflow data. As it was mention by (Vidal et Om 1993), (Armengol et al. 1994), (Hmilton et al.1995).and (Armengol et al. 2003). Therefore, input data of river inflow should be primordial. Or, suggesting substantial extensions of the model that require using in lake water quality as inflow daily concentration.

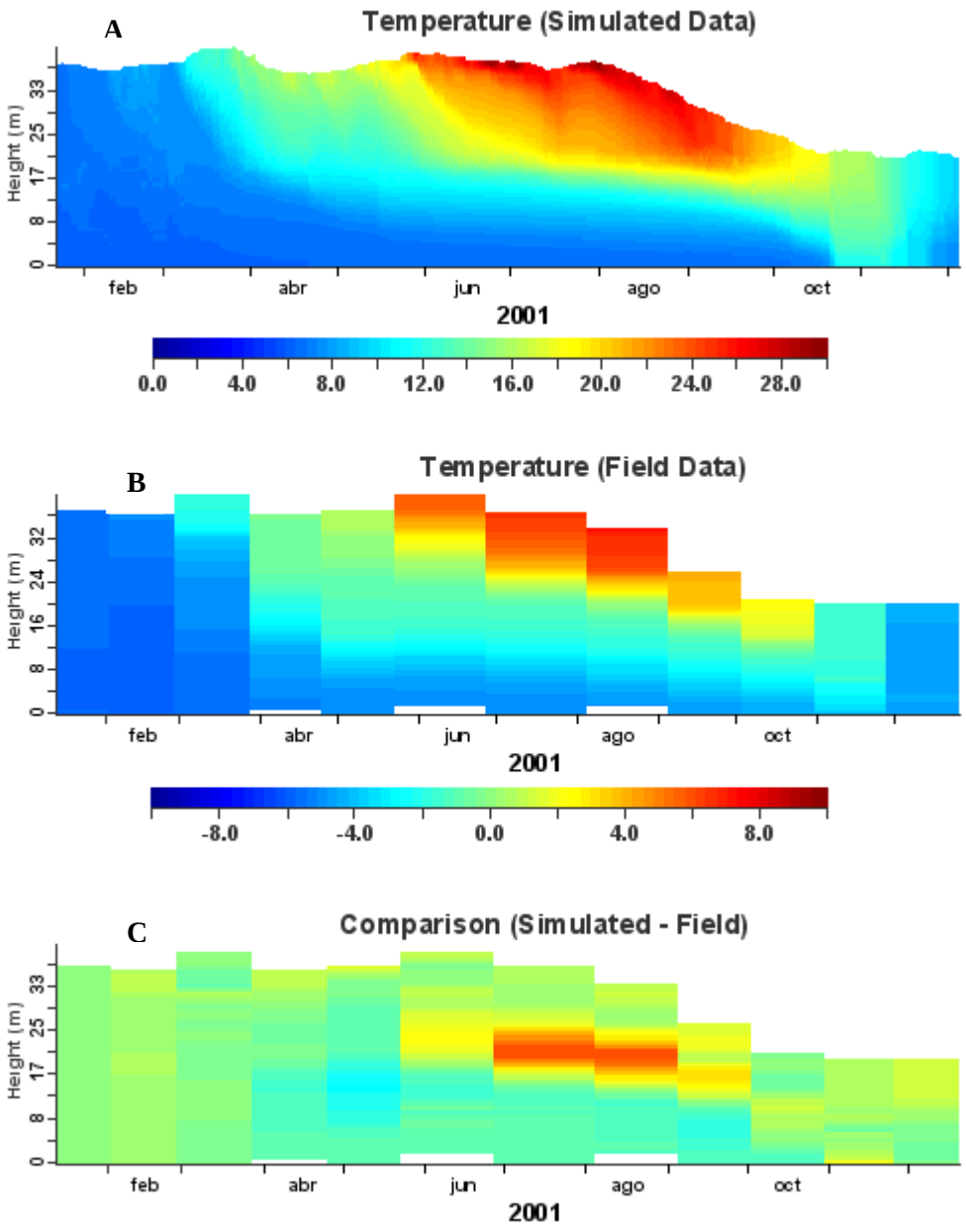

Figure 4.4 One year (2001): Simulated temperature (A), Measured temperature (B) and difference between simulated and measured(C).

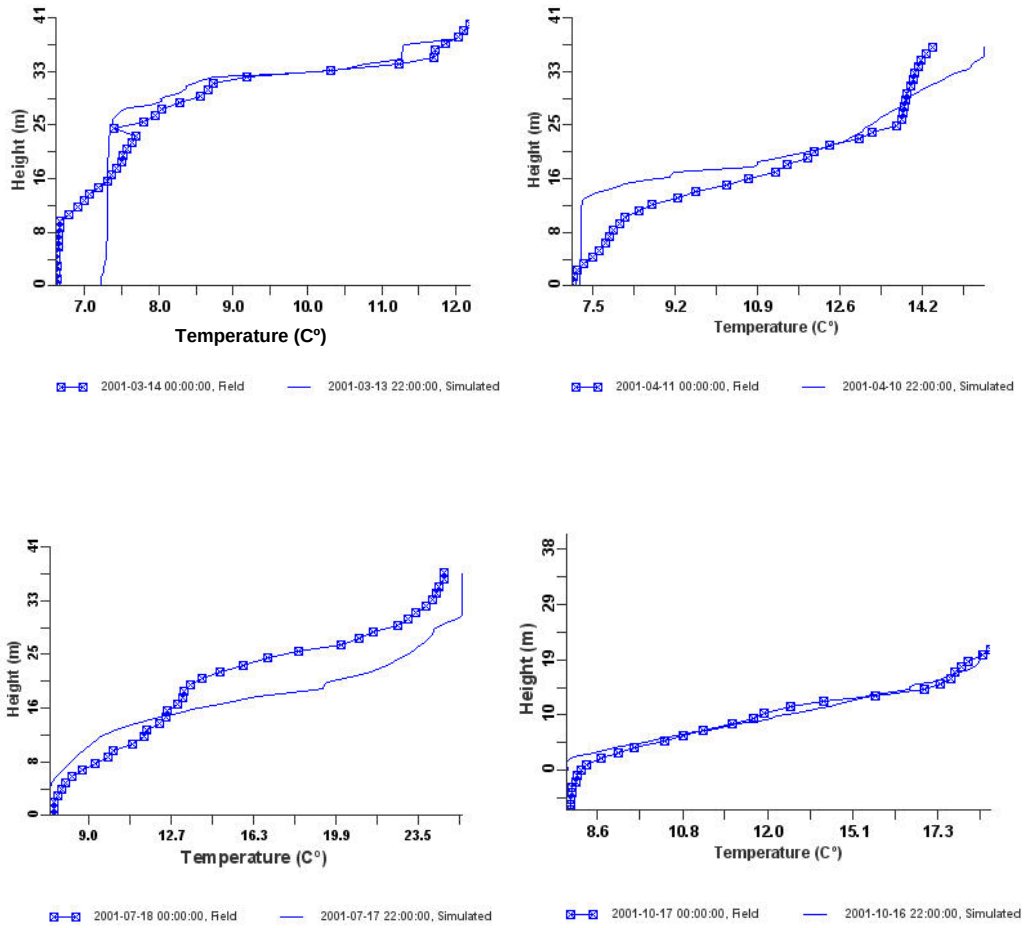

Figure 4.5 Comparison of temperature profiles between observed and simulated results on four Julian days: 44, 101,199 and 290 of the year2001. Squares represent the observed results and the lines represent the simulations.

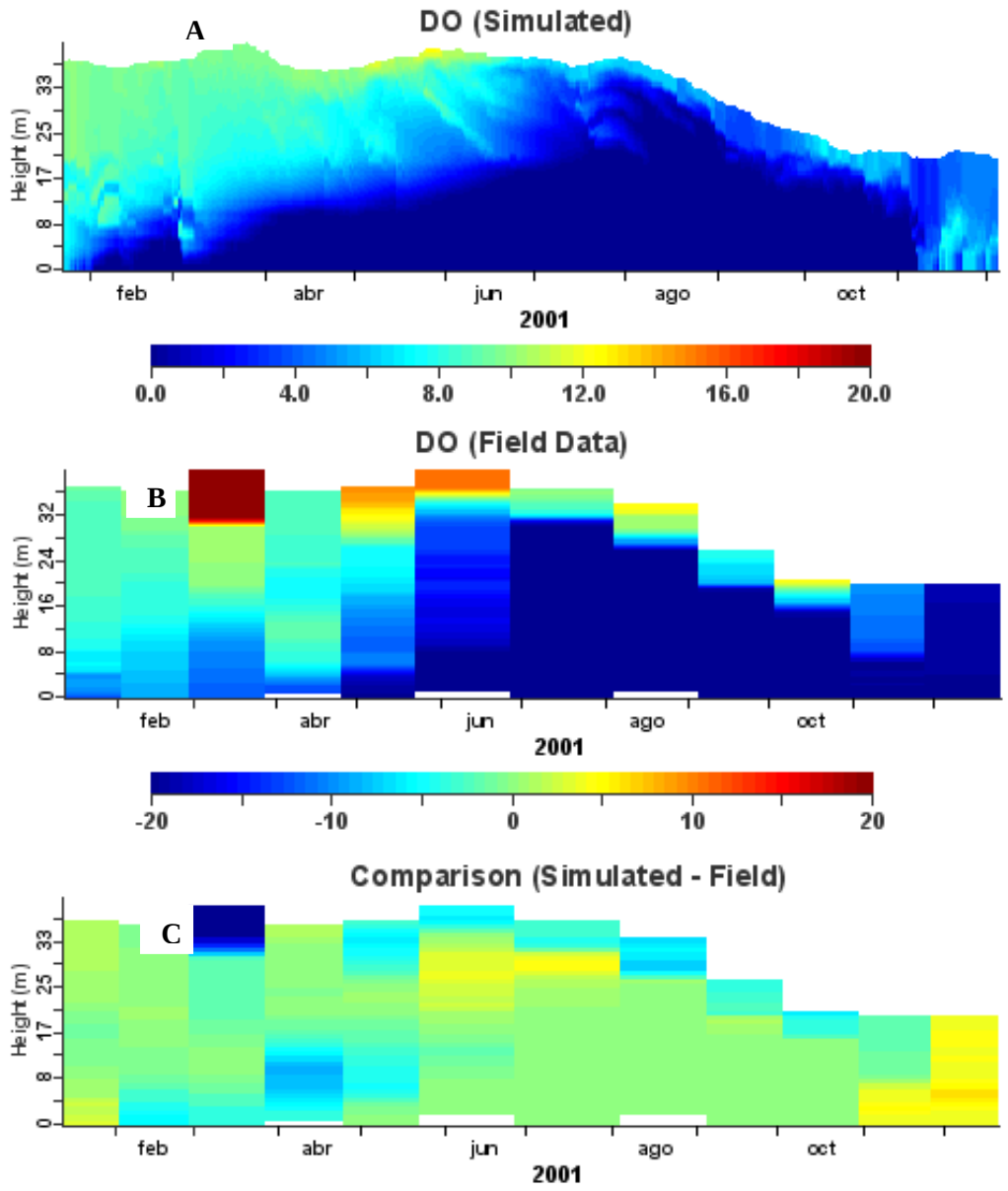

Figure 4. 6 One year (2001): Simulated dissolved oxygen (A), Observed dissolved oxygen (B) and Comparison (C).

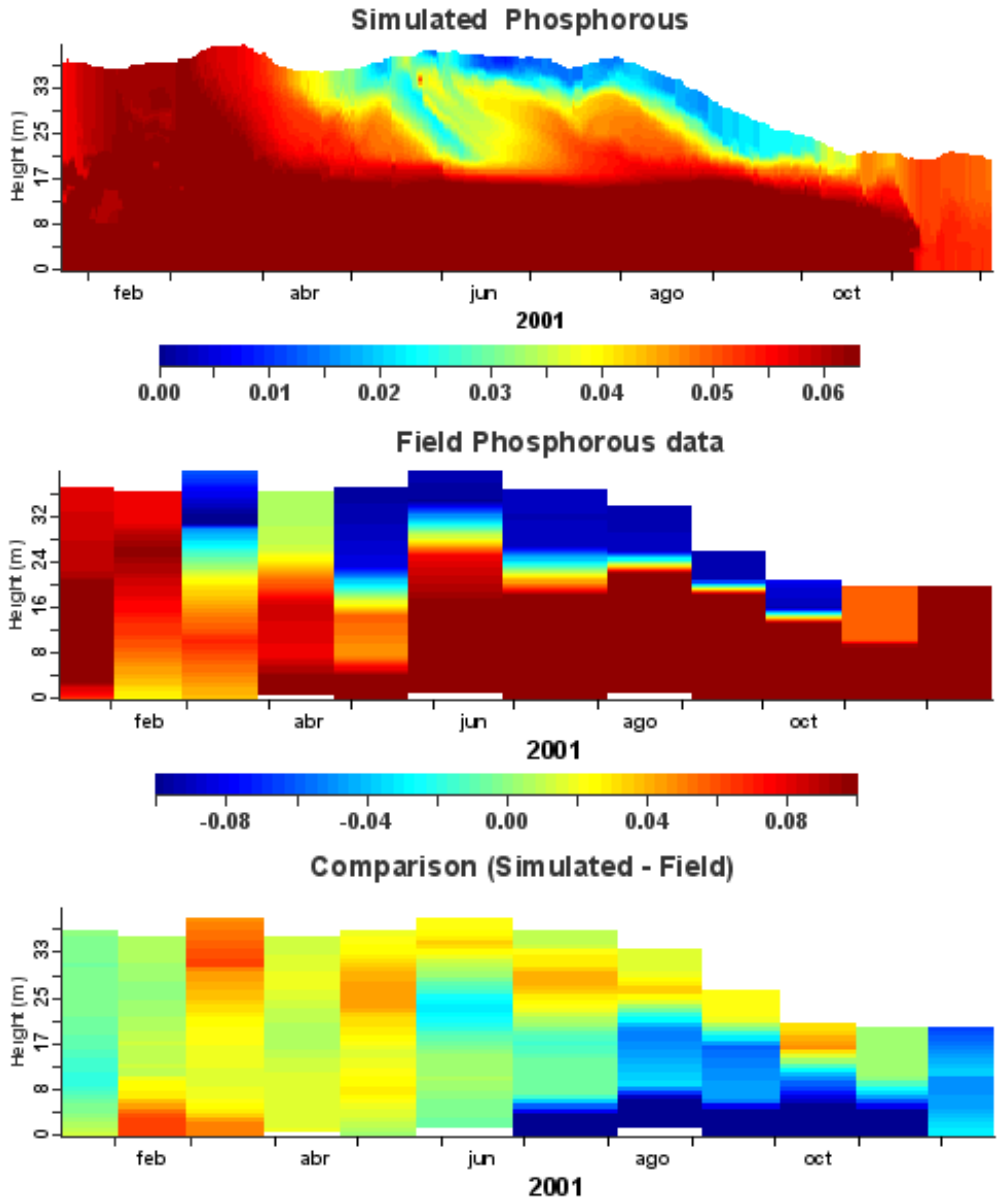

Figure 4.7 One year (2001): Simulated dissolved inorganic phosphorus (A), Measured dissolved inorganic phosphorus (B) and Comparison (C).

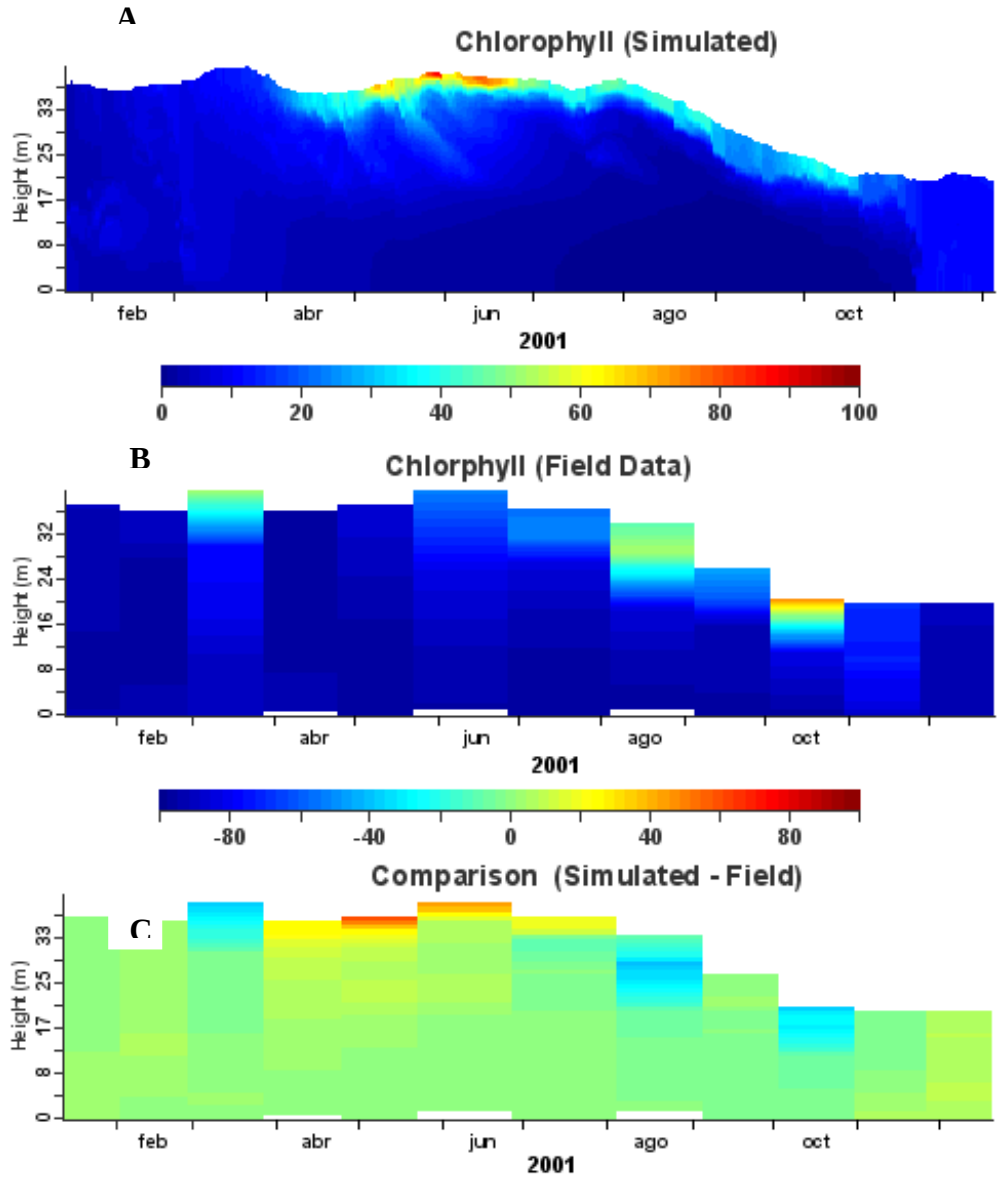

Figure 4.8 One year (2001): Simulated chlorophyll (A), Field chlorophyll (B) and Comparison (C).

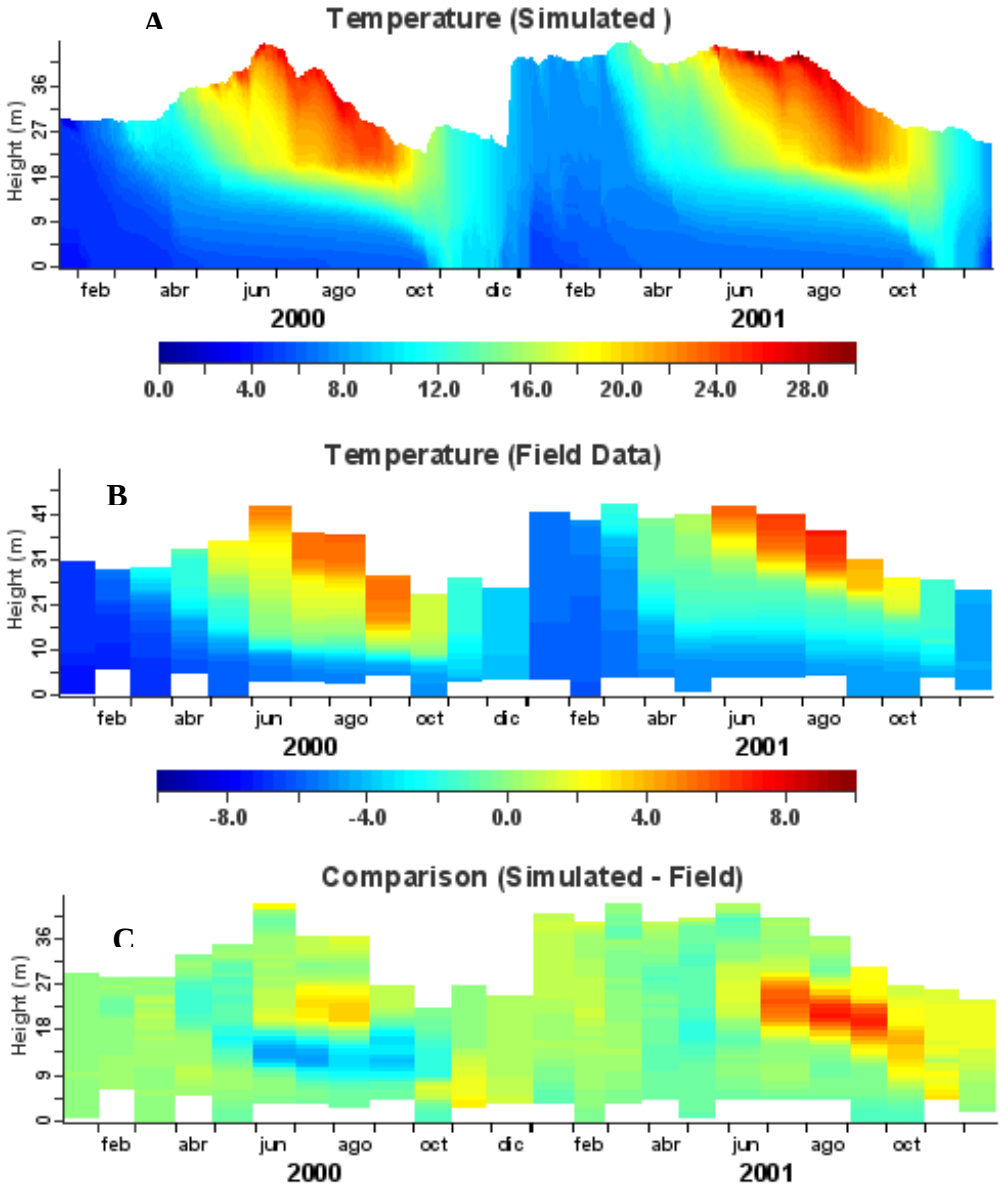

Figure 4.9 Two years (2000-2001): Simulated temperature (A), Measured temperature (B) and Comparison (C).

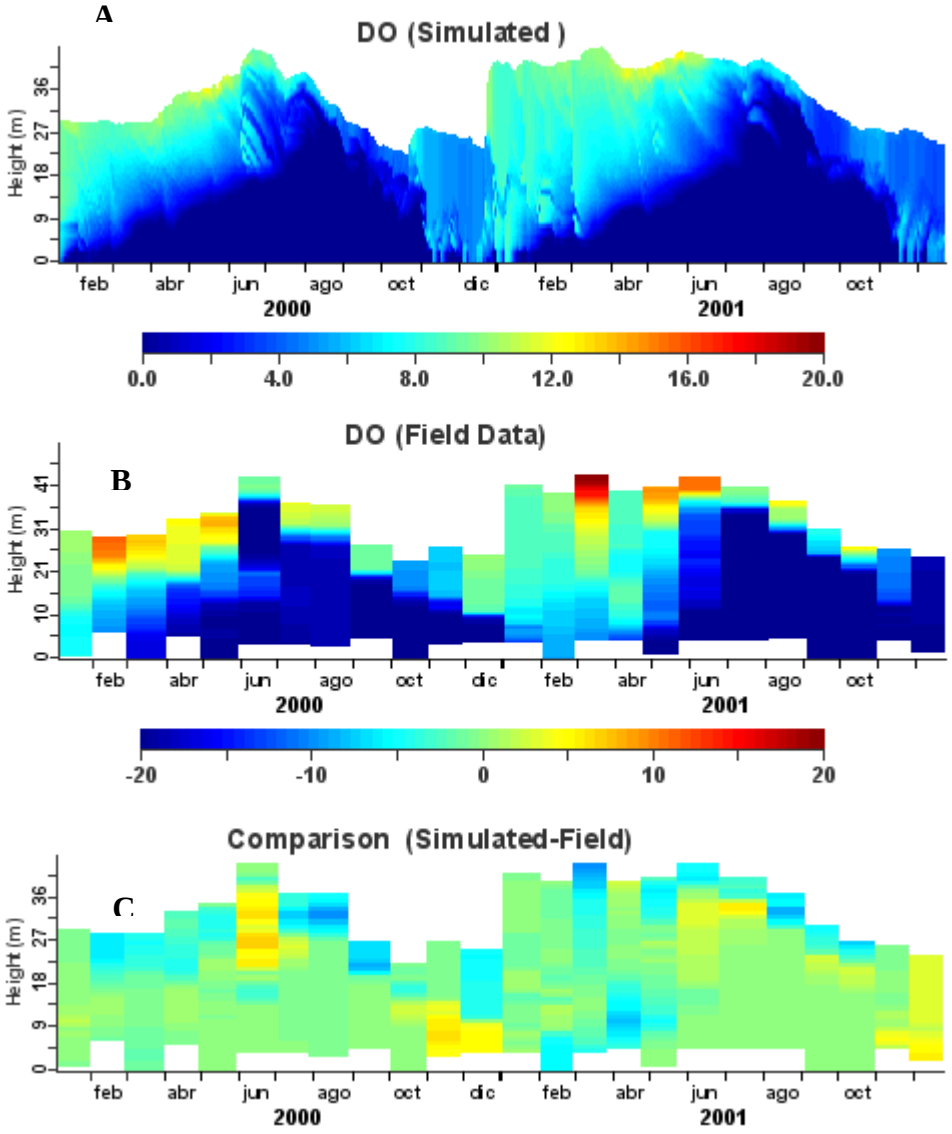

Figure 4.10 Two years (2000-2001): Simulated dissolved oxygen (A), Measured dissolved oxygen (B) and Comparison (C).

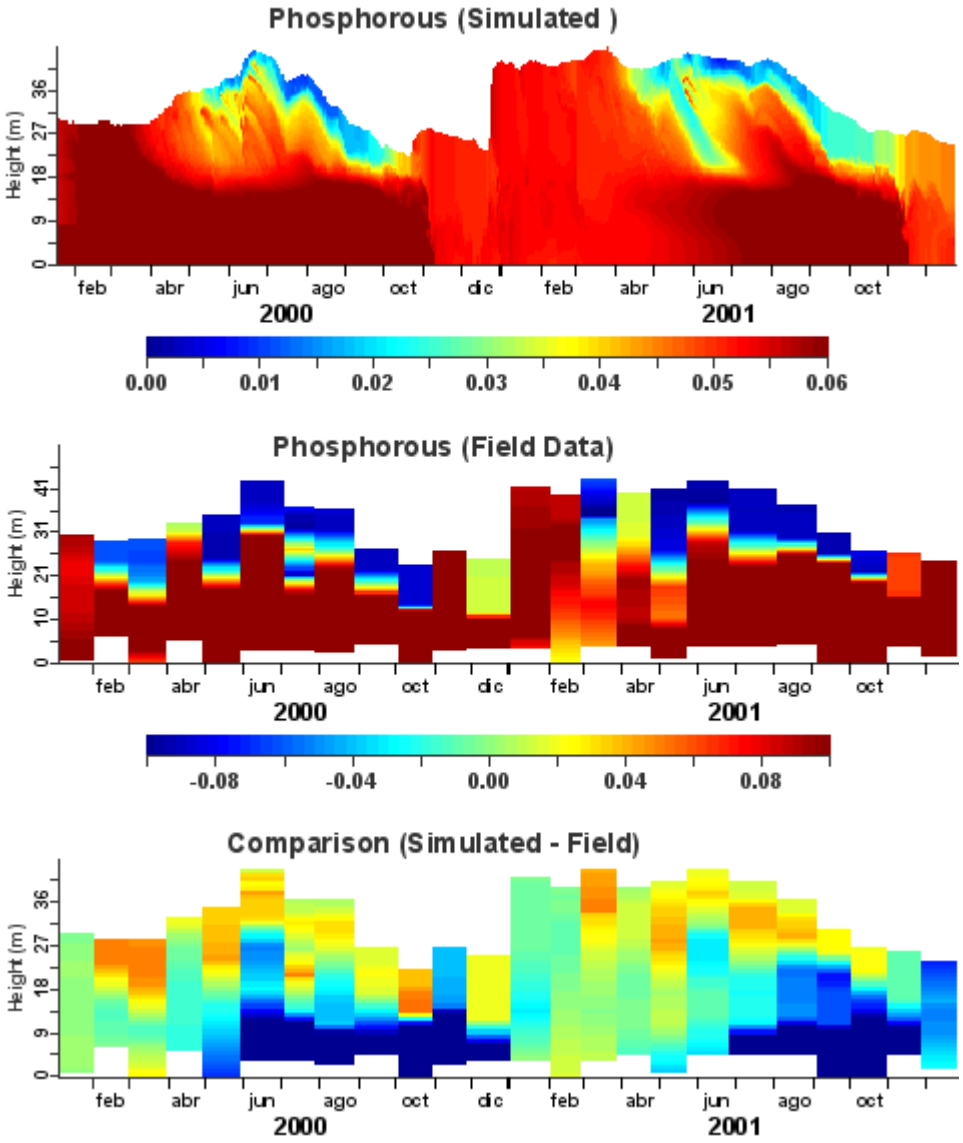

Figure 4.11 Two years (2000-2001) Simulated dissolved inorganic phosphorus (A), Field dissolved inorganic phosphorus (B) and Comparison (C).

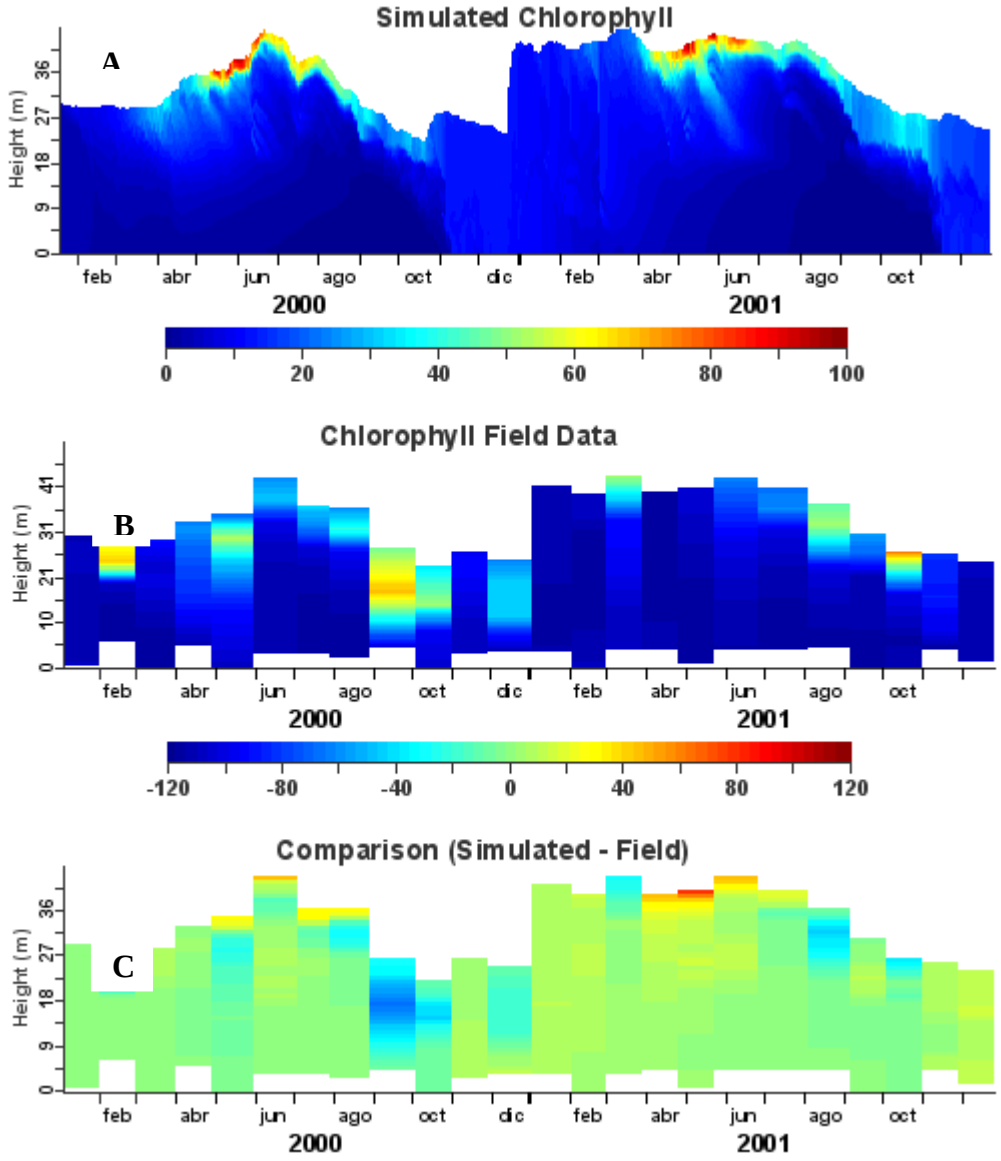

Figure 4.12 Two years (2000-2001): Simulated Chlorophyll (A), Field Chlorophyll (B) and Difference (C).

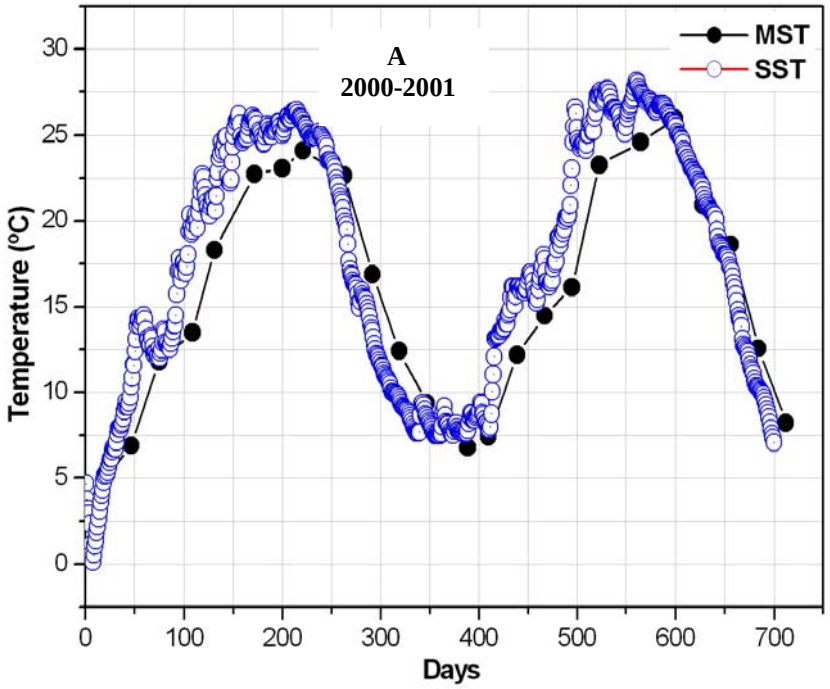
A
2000-2001
MST
SST
Temperature (ºC)
Days
0
5
10
15
20
25
30
0
100
200
300
400
500
600
700

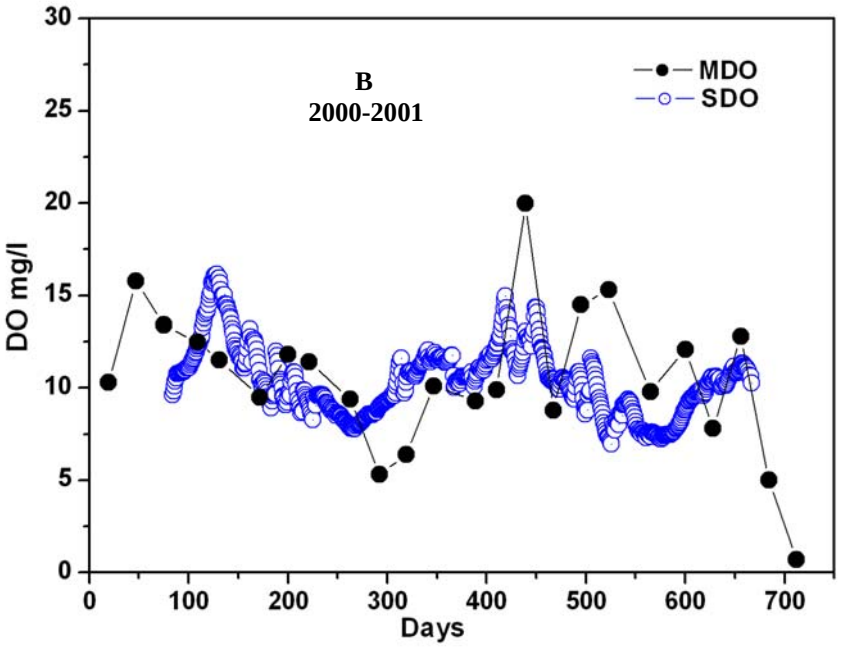
B
2000-2001
MDO
SDO
DO mg/l
Days
0
5
10
15
20
25
30
0
100
200
300
400
500
600
700

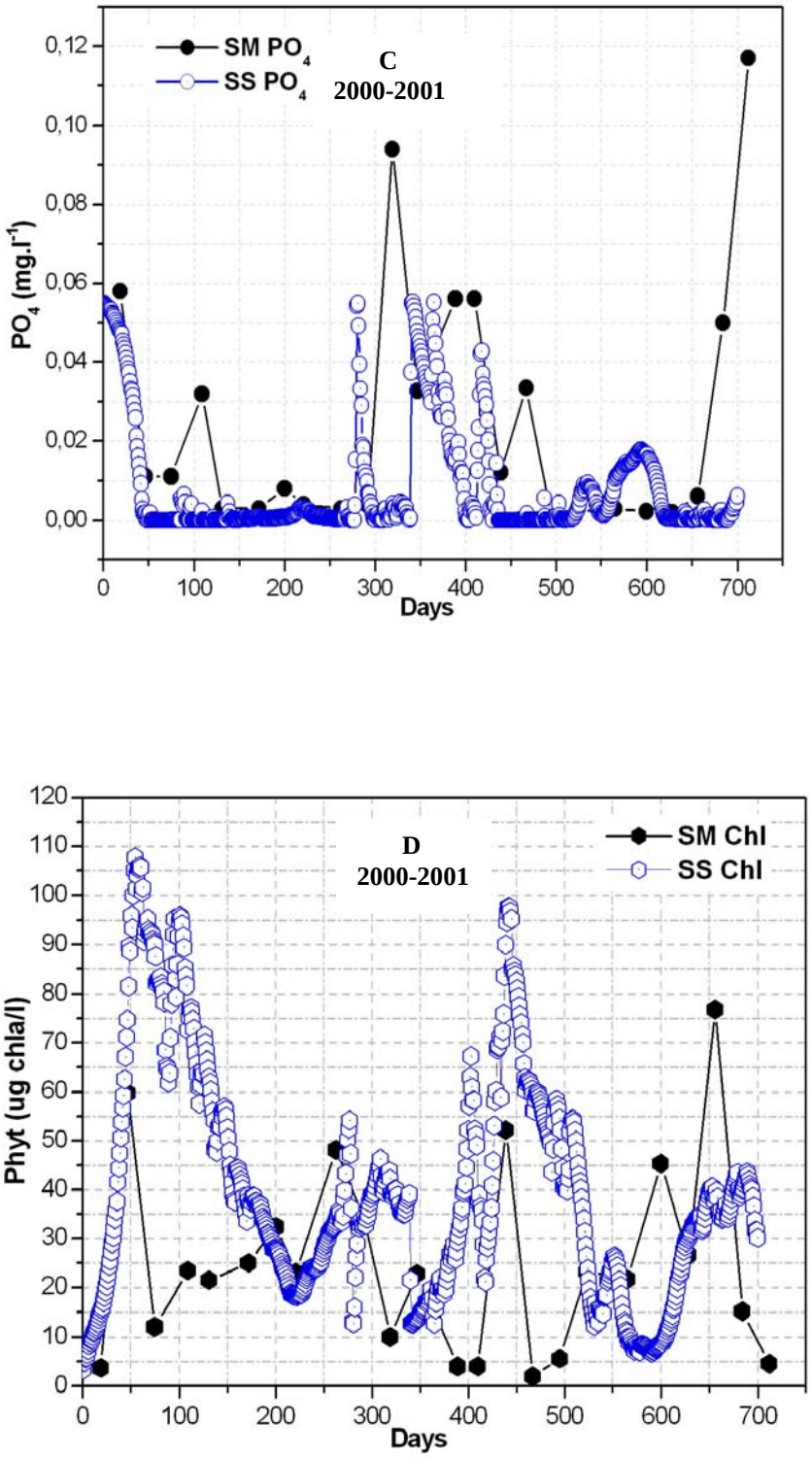

Figure 4.13 Comparison between water surface simulation (open circles) and observation (filled circles) of Temperature (A), Dissolved oxygen (B), Phosphorus (C) and Chlorophyll (D).

4.6 Conclusion

The DYRESM-CAEDYM model requires daily inflow data concerning temperature and dissolved oxygen, nutrient and chlorophyll concentrations. However, where there is a lack of real measurements of these concentrations, it is acceptable to allow hypothetical data. Our hypothesis is based on the idea of using variable reservoir profiles to deduce daily inflow concentrations constant throughout the simulation period. So, daily phosphorus and chlorophyll concentrations were considered as the long-term mean of the in-lake concentrations. Following a long calibration and validation process we can say that the DYRESM-CAEDYM model is a useful tool to aid the understanding of hydrodynamic, nutrient and phytoplankton dynamics. In general, the model reflects reality in terms of temperature and dissolved oxygen measurements, and gives a general view of trends in phosphorus and chlorophyll concentrations. Obviously, it would not be realistic to expect a perfect fit with the observed data, so we have to accept some uncertainty. Unfortunately, the differences between the simulated and observed measurements especially for phosphorus and chlorophyll can be linked to many different factors, such as data accuracy, inflow water nutrient and chlorophyll concentrations data, the neglect of certain parameters such as groundwater, and the limits of the one dimensional assumption. Some types of phytoplankton not taken into account in our modelling that could interfere and have a negative effect on the simulation, especially when modelling chlorophyll, could also be responsible. But in the end, the DYRESM-CAEDYM model is adequate for predicting the hydrodynamic and water quality of Mediterranean reservoirs, especially if the river is as well controlled as the reservoir. In (chapter 5) we will see what happens with another reservoir, the Boadella Reservoir which is smaller in size than Sau when we apply the same model.

CHAPTER 5

Application of the Dyresm-Caedym model to the Boadella Reservoir

Abstract

For reasons of comparison, the aim of this chapter is to apply the DYRESM-CAEDYM model to another reservoir, the Boadella Reservoir, located in the same region as the Sau Reservoir mentioned in Chapter 4. The simulation length is two years (2000-2001). The model is used to predict temperature, DO, dissolved inorganic phosphorus and chlorophyll. The DYRESM-CAEDYM input data are explained for the Sau Reservoir, but these data are not complete. Thus, the simulation may not be reliable or well analysed because of a lack of field nutrient data, so we will focus on the simulation temperature, dissolved oxygen and chlorophyll. After simulation and calibration, we attempt to find the difference between them in terms of water quality behaviour.

5.1 Introduction

Most reservoirs are conceived in response to the growth in demand for drinking water, irrigation water and/or water for recreational purposes. The major temperate reservoirs are stratified in summer when the water demand is very high, and to supply that demand water is withdrawn, generally at different levels of water column stratification.

The stratification of such a reservoir is the result of various physical processes that distribute heat from the lake surface to its deeper layers. These processes depend not only on meteorological variables such as wind velocity, rainfall, and short and long

wave radiation, but also on the biochemical characteristics of the water body. For example, the penetration of short wave radiation depends on the particulate matter in the water. Particulate matter may be subdivided into biological and physical matter. Inorganic particles include sand, minerals or metals. Organic particles take many forms: viruses, colloids, bacteria, phytoplankton or large particles such as zooplankton (Mobbley 1990).

Temperature distribution is fundamental and crucial to understanding the performance and functioning of reservoir ecosystems (Kimmel et al. 1990). From a management point of view, it is usually preferable to practice selective withdrawal. The effects of water withdrawal have been found to be important in determining thermal stratification in reservoirs (Martin & Arneson 1978; Ford 1990). Surface withdrawal generally dissipates heat because the heated water layer is directly removed, and cooler, denser hypolimnetic water remains. In contrast, bottom withdrawal tends to store heat because removing cool hypolimnetic water results in an expansion of the epilimnion layer heated by solar radiation (Kennedy 1999). In addition, selectively releasing hypolimnetic water can lead to warming of the hypolimnion, and a decrease in the thermal stability of the water column. Decreased stability can promote vertical entrainment of nutrients in the epilimnion (Effler et al. 1986). From a water quality point of view, selective withdrawal of hypolimnetic water is better because it can increase the net export of phosphorus from anoxic reservoirs (Martin & Arneson 1978). A shortened hypolimnetic residence time could also reduce the potential for the development of anaerobic conditions, thereby reducing phosphorus release even further (Cooke et al. 1993). Indicator factors such as nutrient availability are important for determining phytoplankton distribution (Cottingham et al. 1998; Vrede et al. 1999).

Consequently, hydrodynamics plays a major role in determining phytoplankton and zooplankton dynamics and changes in water quality (Straškraba et al. 1993; Hamilton & Schladow 1997; Berman & Shteinman 1998).

5.2 Materials and methods

The Boadella Reservoir (Fig. 5.1) was built in response to urban growth, tourist development, intensive agriculture and the demand for drinking water. The Boadella catchment area is located in the north-east of Spain in the eastern pre-Pyrenees. The total catchment area consists of $364\ Ha$. It has a maximum capacity of $62.10^6\ m^3$. The yearly average total net inflow in the reservoir is $69.10^6\ Hm^3$ and occurs through two main tributaries, the Muga and the Arnera. It has been estimated that the Muga contributes 65% and the Arnera 35% to the total inflow (Casamitjana et al. 2003). The Boadella Reservoir is used mainly to supply drinking water to Figueres and other small towns downstream as well for irrigation purposes. It has also been used to sustain hydroelectric power plant. A percentage of the outflow water is released to the river as 'ecological flow'. One of the main characteristics of the Mediterranean climate is its variability: dry and wet years combine with hot or cool ones to produce many different types of seasonal patterns. Because of this, the reservoir's hydrological regime depends mainly on the seasonal nature of rainfall events, which commonly occur in the form of concentrated storm fronts in spring and fall and relatively low rainfall in summer and winter (Serra et al. 2002 and Casamitjana et al. 2003). The nutrient input in the reservoir is not very high, with average values of 3.2 $\mu g.Nl^{-1}$ for nitrates and 0.2 $\mu g.Pl^{-1}$ for total phosphorus (APHA 1989). Although the small ration N:P causes the appearance of cyanobacteria (Baserba, 1999). The chlorophyll a concentration values (Jeffrey & Humphrey 1975) can be as high as 27.8 $\mu g.Chl^{-1}$ with a mean value of 5 $\mu g.Chl^{-1}$ and because of this the reservoir can be considered eutrophic. During the stratification period, the hypolimnion of the reservoir is anoxic, with ammonium, sulphides and other fermentation products that contribute to the reduction of the redox potential and to the re-dissolution of the phosphorus from the sediments (Baserba 1999).

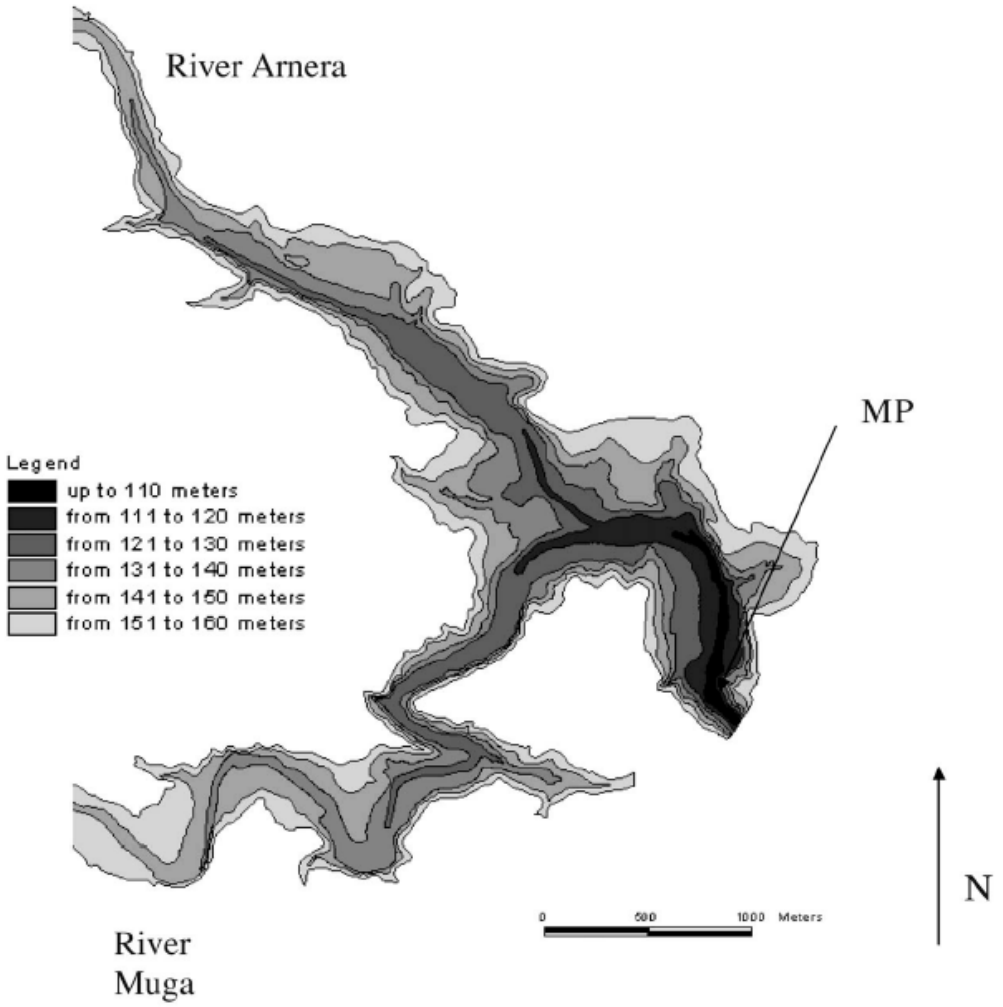

Figure 5.1 Boadella Reservoir bathymetry.

5.3 DYRESM-CAEDYM model

In this chapter, I will not focus on descriptions of the DYRESM hydrodynamic model and the CAEDYM water quality model because they have already been described in Chapter 4.

Rather, this research is primarily an attempt to understand the hydrodynamics of the Boadella Reservoir and its effect on water quality for the period between January 2000 and December 2001. Thus, we have used the combined DYRESM-CAEDYM model (Fig. 4.2 in chapter 4) to simulate the same variables as had been done for the Sau Reservoir during the same time series. The data used as input data for the model are morphometric data (Chapter 2, Section 2.4.1) and meteorological data (Chapter 2, Section 2.4.2), which consist of air temperature (Fig. 2.18), short wave radiation (Fig. 2.19A), wind speed (Fig. 2.21), vapour pressure (Fig. 2.20), rainfall (Fig. 2.22) and cloud cover (Fig. 2.19B), which is estimated by interpolation between clear and cloudy skies. Inflow temperature data (Fig. 2.23A) obtained by averaging the air temperature for the previous four days, daily inflow data (Fig. 2.23B) and outflow data (Fig. 2.24). It should be mentioned that all the above input data and figures can be found in greater detail in Chapter 2. Unfortunately, what are missing again are the unavailable values for daily inflow water quality data, such as daily dissolved oxygen concentration, daily nutrient concentration and chlorophyll concentration.

5.4 DYERESM-CAEDYM Calibration and Validation

The DYRESM hydrodynamic model was calibrated by adjusting certain parameters such as minimum and maximum layer thickness, wind stirring coefficient, diffusive flux constant, effective surface area, potential energy mixing coefficient with different albedo values and base extinction coefficient. As stated in previous chapter, tested parameters, such as meteorological parameters such as (air temperature, radiation, rainfall, vapour pressure and wind speed), inflow temperature does not produce adequate variation in the predicted thermal structure compared to observed temperature profiles. As we have done for Sau Reservoir we will use an identical calibration process for Boadella Reservoir which will not be described here and we will give only the differences between them. Thus, obtained results for Boadella Reservoir were similar to one of the Sau except the maximum layer thickness which was equal to 1.0 m and was the best setting (Fig. 5.2A) as it was described by (Andrew J et al 2007). It is worth mentioning that the differences between predicted and observed temperatures, bottom temperatures and thermocline depth (Fig. 5.2, A, B, C, D, E and F) are high in magnitude compared to those values of Sau Reservoir (Fig. 4.3, A, B, C, D, E and F chapter 4). Table 5.1 summarizes sensitive and insensitive parameters in the model.

Parameter Set Value albedo	0.08
Benthic boundary layer thickness (m)	0.00
bulk aerodynamic momentum transport coefficient	0.0013
critical wind speed (m s–1)	3.0
effective surface area coefficient	1.0×10^7
emissivity of a water surface	0.96
non-neutral atmospheric stability correction switch	No
potential energy mixing efficiency	0.20
shear production efficiency	0.08
vertical mixing coefficient	200
wind stirring efficiency	0.06
Following calibrations	
minimum layer thickness	0.5 m
maximum layer thickness	1.0 m
effective surface area coefficient	1×10^7
vertical mixing coefficient	7200

Table 5.1 Values of coupled model parameters and model simulation specifications.

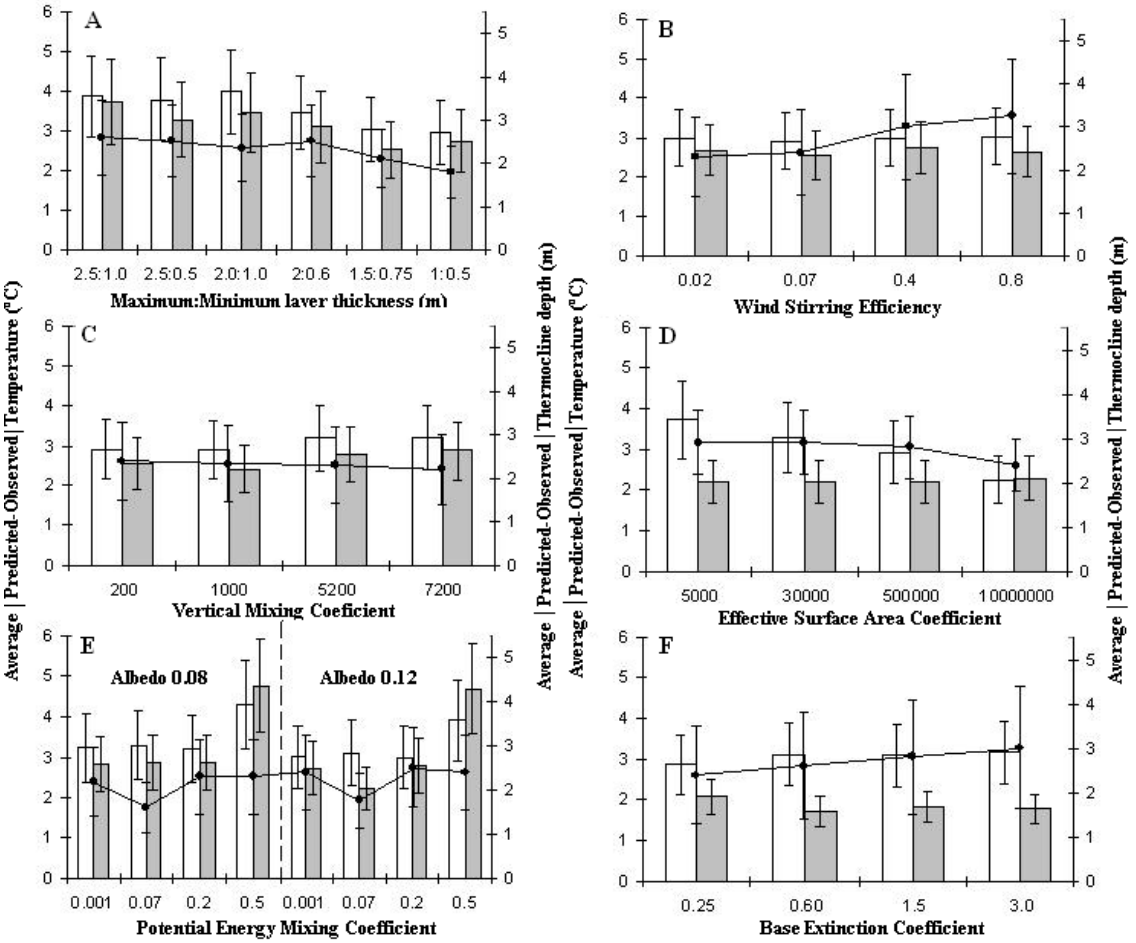

Figure 5.2 *Average absolute difference ± standard error of the mean between DYRESM-CAEDYM predicted and observed water temperature (white), bottom water temperature (gray) and thermocline depth (line) at various layer thickness setting (A), wind stirring efficiency values (B), Vertical mixing coefficient (C), effective surface area coefficient (D), albedo and potential energy mixing coefficient values (E), and base extinction coefficient(F).*

The ecological model was calibrated by trial-and-error adjustment, just like the Sau Reservoir. The difference between calibration processes for the two reservoirs is that for Boadella the calibration period is the year 2000 while the year 2001 was used for Sau. The calibration sequence in the CAEDYM model is temperature first and then, in this order, dissolved oxygen, dissolved inorganic phosphorus and chlorophyll.

After temperature calibration the mean sensitive parameters in dissolved oxygen is sediment oxygen demand, by varying static dissolved consumption by sediments and half saturation constant for sediment oxygen demand. Thus were the mean sensitive parameters. The calibration of dissolved inorganic phosphorous has not been done

because due to lack of field data. Finally, chlorophyll is the most difficult parameter to calibrate because it depends on the information available on modeled species such as growth rate, phosphorus and light utilisation. The overall calibrated water quality parameters are grouped in Table 5.2.

Model validation is used to simulate the observed reservoir behaviour over a simulation length of approximately two years (674 days) including a calibration period of a dry year (2000) and a wet year (2001). Hence, the simulation started on 15 February 2000 and ended on 5 November 2001. Later on it will be observed that there is strong density stratification during warmer months of the years for the temperature simulation. Simulated dissolved oxygen concentrations will demonstrate the existence of an anoxic area in the deeper hypolimnion during the stratification period. For chlorophyll the simulation will show the existence of algal blooms at the surface. The two year series of simulated temperature, dissolved oxygen and chlorophyll compared to field series are shown in (Figs. 5.8, 5.9 and 5.10).

Parameter	Description	Units	Assigned range	Assigned value
Dissolved Oxygen				
ϑ_{op}	Temperature multiplier for SOD	-	1.02-1.14	1.08
F_{SOD}	Static sediment exchange rate	$g/m^2/day$	0.02-15	0.95
K_{SOD}	½ sat constant for static DO sediment	$mgDO.l^{-1}$	-	0.5
ϑ_{ON}	Temperature multiplier for nitrification	-	1.001-1.10	1.08
k_n	Nitrification rate coefficient	day^{-1}	0.01-0.1	0.08
K_N	Half saturation constant for nitrification	$mgDO.l^{-1}$	-	0.5
k_r	Phytoplankton respiration mortality/excretion	day^{-1}	0.01-0.10	0.10
K_{DOB}	Half sat const for DO dependence of POM/DOM decomposition	$mgDO.l^{-1}$	-	2.5
Dissolved Inorganic Phosphorus				
$IP_{\min}$	Minimum phytoplankton internal Phosphorus	$mg\ P(mg\ ChIa^{-1})$	0.1-1.0	0.3
$IP_{\max}$	Maximum phytoplankton internal Phosphorus	$mg\ P(mg\ ChIa^{-1})$	1.0-5.0	2.2
$Up_{\max}$	Maximum rate of phytoplankton phosphorus uptake	$mg\ P(mg\ ChIa^{-1})day^{-1}$	0.05-1.0	0.3
K_{ep}	Specific attenuation coefficient (phytoplankton)	$\mu g.Chlal^{-1}.m^{-1}$	-	0.02
K_{ePOC}	Specific attenuation coefficient of POC (particles)	$mg.m.l^{-1}$	-	0.001
$POP_{1\max}$	Max transfer of POPL->DOPL [Decomposition]	day^{-1}	-	0.055
$DOP_{1\max}$	Max mineralization of DOPL->PO4 [Mineralization]	day^{-1}	0.01-1.0	0.055
$DOP_{2\max}$	Max mineralization of DOPR->PO4 [Mineralization]	day^{-1}	0.002-0.018	0.0025
S_p	Sediment flux release rate of phosphorus	$g.m^{-2}.day^{-1}$	3.10^5-8.10^5	5.10^5
K_P	Half saturation constant for phosphorus	$mg.L^{-1}$	0.001-0.025	0.005
ϑ_S	Temperature multiplier of sediment fluxes	-	1.001-1.10	1.05
Chlorophyll				
$P_{\max}$	Maximum potential growth rate of phytoplankton	day^{-1}	0.3-3.5	0.33
ϑ_p	Phytoplankton temperature multiplier	-	1.02-1.14	1.04
I_K I	Parameter for initial slope of P_I curve	$\mu Em^{-2}s^{-1}$	100-500	120

Table 5.2 Calibrated water quality parameters used for the DYRESM-CAEDYM model.

5.5 Simulation and results

Two year (2000-2001) time series of the daily average short wave radiation, cloud cover, vapour pressure, wind speed, inflow volume, inflow temperature and withdrawal volume are plotted respectively in (Figs. 2.19A, 2.19B, 2.20, 2.21, 2.23A, 2.23B and 2.24 in Chapter 2).

A moderate agreement has been found between the simulated and the observed temperatures measured at the Cabanes station close to the dam. For the year 2000 (Fig. 5.3) the agreement is especially good for the period from February to June, and during the autumn the maximum observed difference is 5ºC. However, during the stratification period from July to the end of September, the simulated temperature in July and August is higher than the observed one, especially in the epilimnion and thermocline, with maximum observed differences being 5ºC (Figs. 5.4C, 5.8C and 5.11A) In the bottom layer, though, the opposite occurs.

We have chosen four temperature profiles corresponding to Julian days 46, 117, 192 and 272, with each profile representing one season of the year. In (Fig. 5.4) it is clear that the simulated temperatures are higher then the observed ones, especially in the surface layer and in the stratification period, the difference reaching 7 degrees on Julian day 117, corresponding to the end of March, and on Julian day 272, corresponding to the end of September. Additionally, in the hypolimnion layer in the stratification period at a depth of 7m the difference is negative. A comparison between simulated and observed temperatures shows that the DYRESM-CAEDYM model cannot be accepted as a good tool to predict the evolution of the thermal cycle in the Boadella Reservoir, especially in the stratification period. Also, the increases in the modelled temperatures are probably due to the consideration of only one river arriving to the reservoir in simulation. Such a difference between the modelled and observed temperatures is probably also due to outflow.

The comparison of simulation temperatures in the Sau and Boadella reservoirs using the same model (DYRESM-CAEDYM) with the same simulation length reveals that the model gives better results for the Sau Reservoir (Figs. 4.4 and 4.9A in Chapter 4) than for Boadella (Figs. 5.4 and 5.8A).

The simulated dissolved oxygen concentration (Fig. 5.5) is in reasonable agreement with the field measurement. It indicates the depletion of dissolved oxygen in the hypolimnion and a higher concentration in the surface layer. In the surface layer in (Fig. 5.9A) and for the years 2000 and 2001, from the beginning of spring, it has been observed that the dissolved oxygen concentration in the field is a bit higher than the simulated value. This is probably due to an early spring bloom peak of algae, quite possibly other type of phytoplankton, in which the model cannot reproduce. However, in the summer, simulated DO concentration in the epilimnion was low than in the field by approximately (2mg/l) of difference. Regarding dissolved oxygen concentration in the bottom, (Figs. 5.6 and 5.9A) demonstrate that there was small deficit in DO concentration between simulated and field. Nevertheless, the lack of some bottom data could make the comparison somewhat hard to predict. Also the huge deficit found between the simulated and the field in the hypolimnion in the beginning of the mixing period (5mg/l) should be mentioned. This is probably due to the deeper hypolimnion not being totally mixed, in agreement with the low lake numbers found in (Fig. 3.1 in Chapter 3). All in all, one can estimate that DYERSM-CAEDYM gives good prediction of the dissolved oxygen concentration in the Boadella Reservoir in spite of certain differences between the simulated and the field values cited above. However, simulated dissolved oxygen was well adjusted to the field in the Sau Reservoir case (Figs. 4.6, 4.10A in Chapter 4) compared to the Boadella Reservoir (Figs. 5.6 and 5.9A).

Unfortunately, there is a lack of measured dissolved organic phosphorus. The field phosphorus profiles are unavailable for Julian days 46, 80, 117, 152, 172 and 192. For the remaining profiles, Julian days 215, 244, 272 and 292, the measured phosphorus is restricted to the threshold limit value as the phosphorus concentration is smaller than 0.1 mg/l. Hence, a comparison between the simulated and the field values will not be taken into consideration in this section.

Concerning chlorophyll, the simulation done by DYRESM-CAEDYM (Fig. 5.6) correctly indicates the existence of phytoplankton blooms at the water surface through the period early in the beginning of spring as observed in (Fig. 5.7A and 5.8A). However, the observed chlorophyll values in March and in August are higher ($2\,\mu g/l$) compared to the simulated ones, but in June the simulated values are higher than the observed ones. The maximum observed difference was about ($6\,\mu g/l$) (Fig. 5.6A). This difference is probably due to the existence of another or several other types of phytoplankton species

as diatoms which we have not considered.. Therefore, inclusion of S_i dynamics into CAEDYM may reduce the algal biomass peak via limitation by this third macronutrient which we do not take in consideration. Additionally it may be due to the restriction limit of one dimensional model. In general, calibration of the model to get a good fit to chlorophyll in the field is a bit difficult, especially when we model nutrient and chlorophyll. Consequently, the simulation of chlorophyll in the Boadella Reservoir is similar to that in the Sau Reservoir (Figs. 4.8A and 4.12A in Chapter 4).

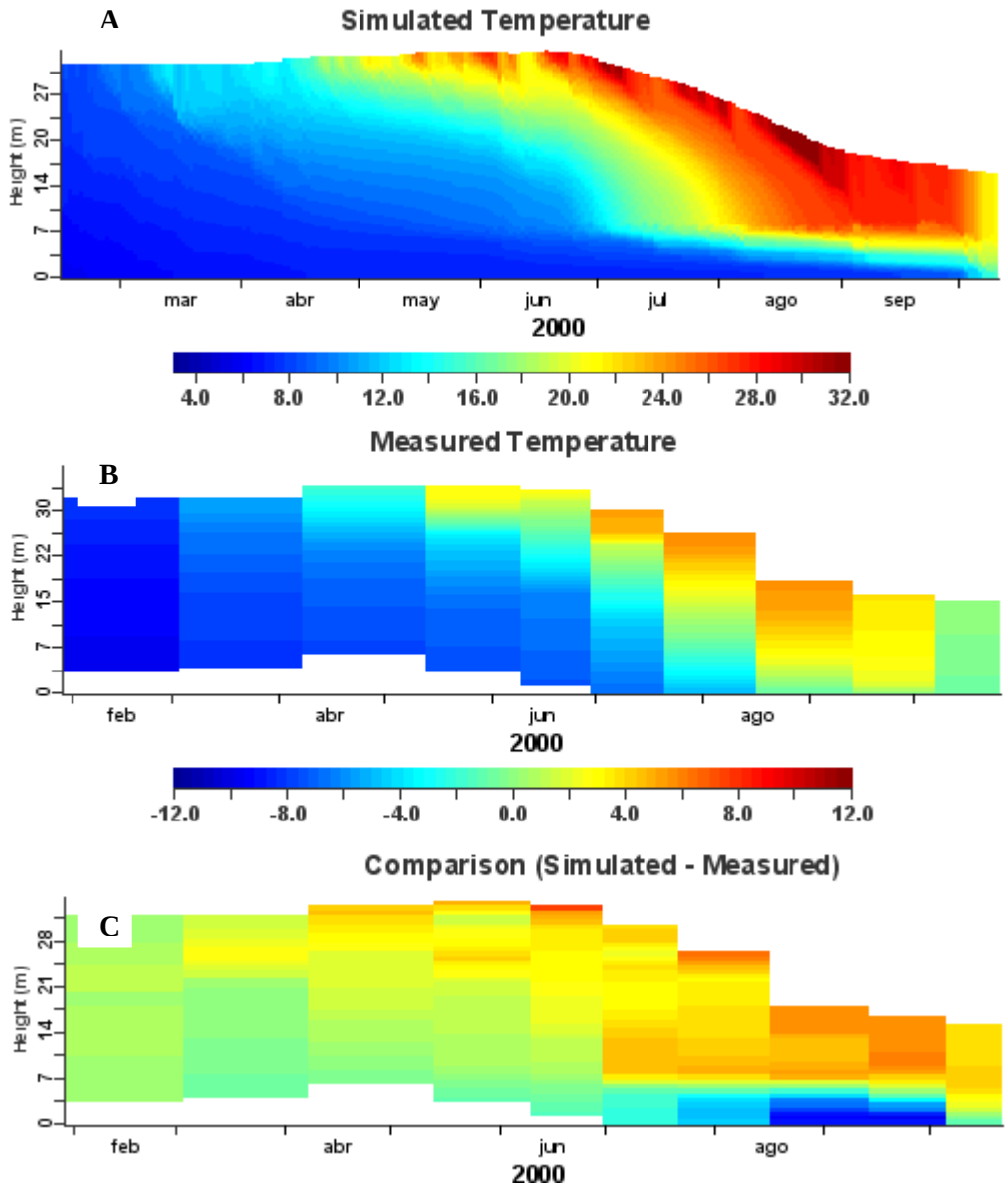

Figure 5.3 represents one year (2000) of simulated temperature (A) and of measured temperature (B) and the difference between simulated and measured temperatures (C).

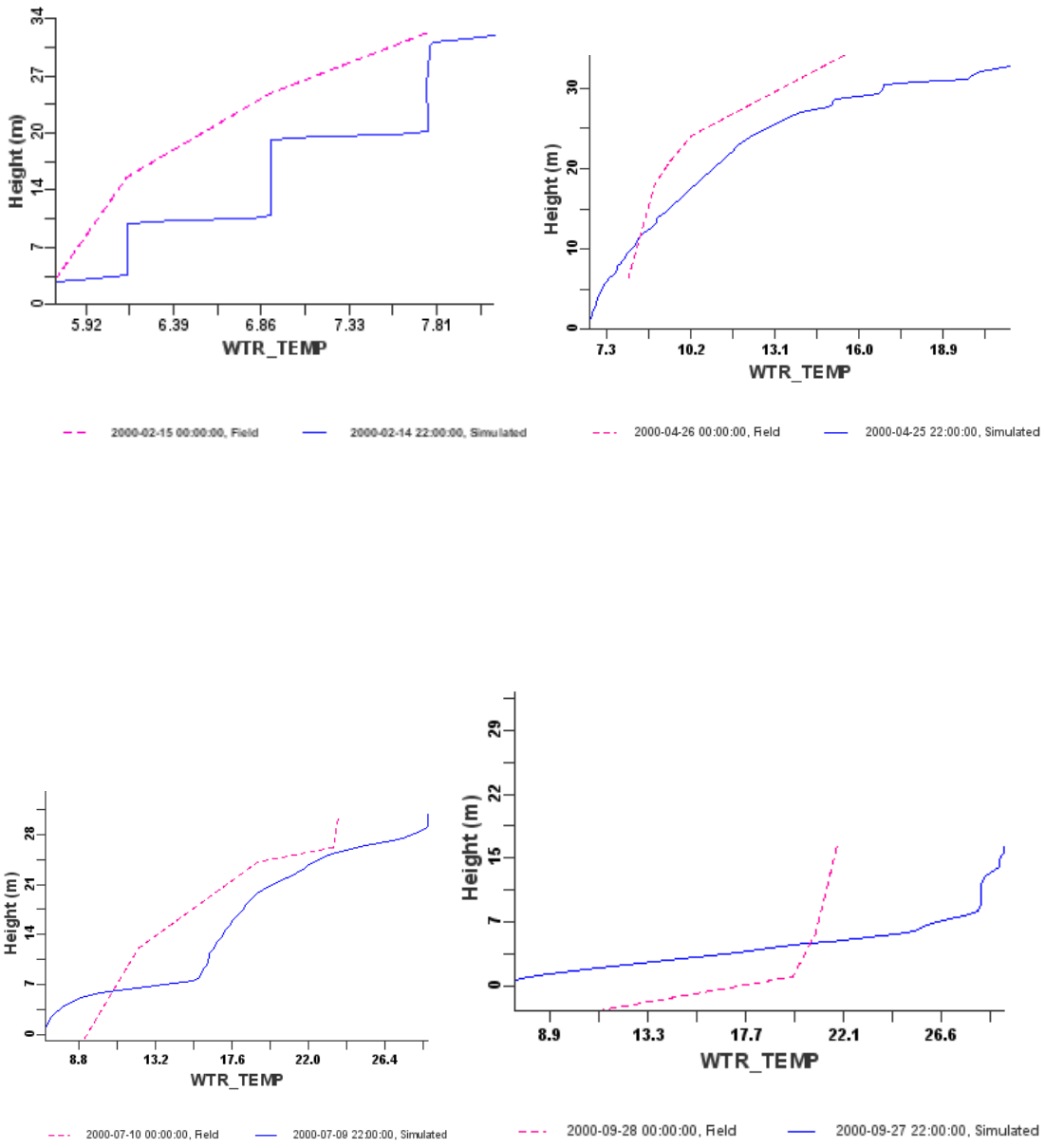

Figure 5. 4 Comparison of temperature profiles between observed and simulated results on Julian days 46, 117, 192 and 272 of the year 2000 (dashed line: observation, solid line: simulation).

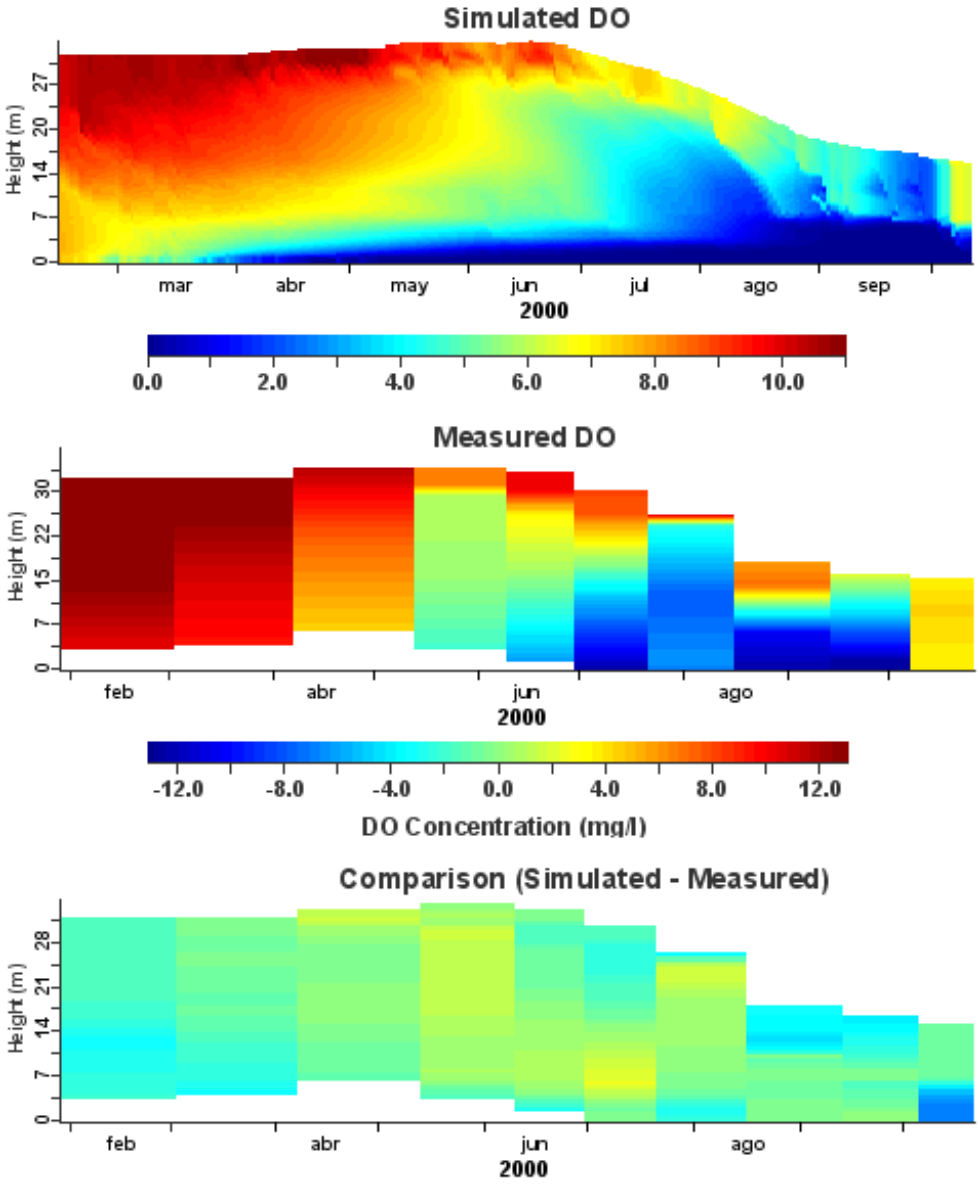

Figure 5.5 One year (2000) of dissolved oxygen values: simulated (A), measured (B) and comparison (C).

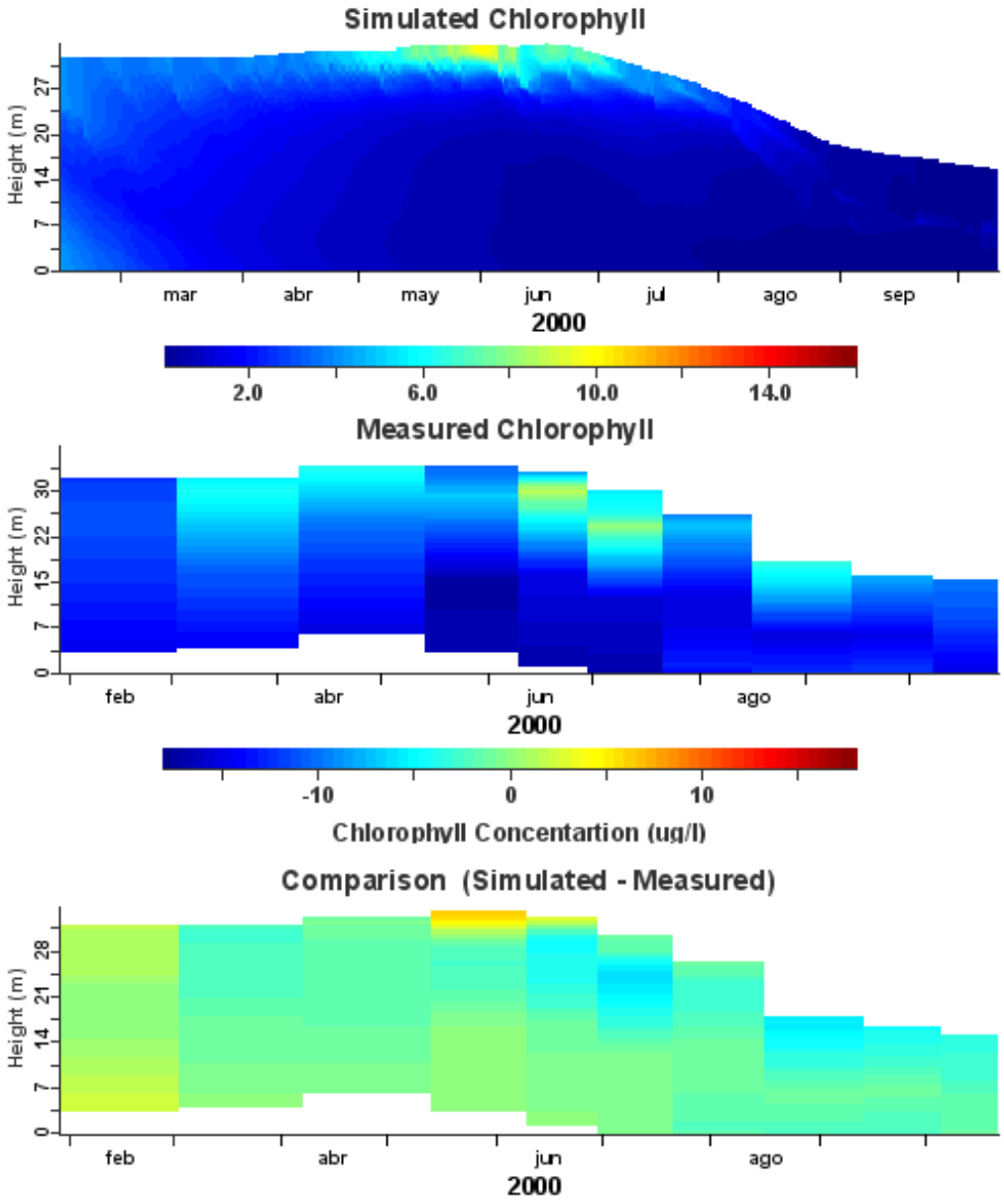

Figure 5.6 One year (2000) of chlorophyll values: simulated (A), measured (B) and a comparison (C).

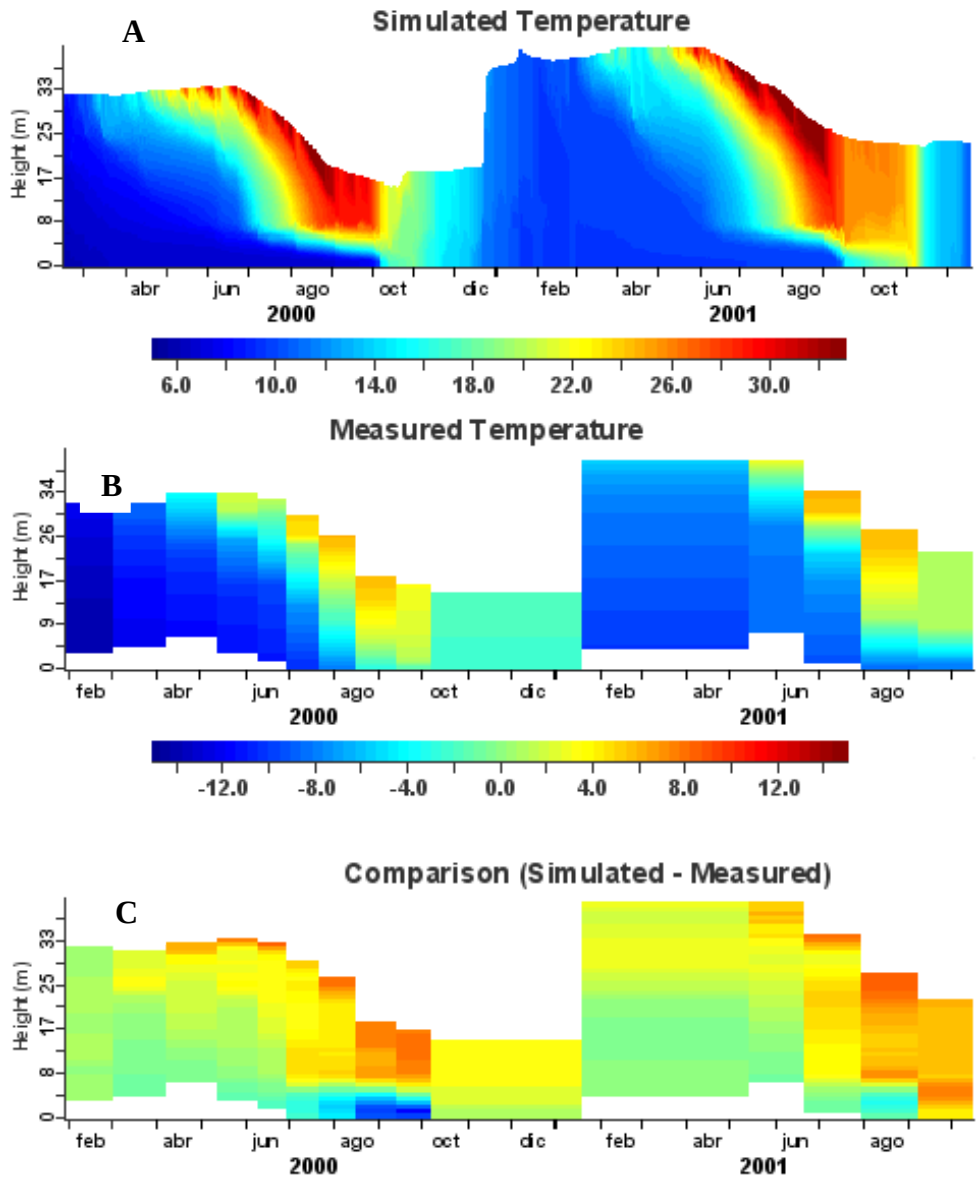

Figure 5.7 Two years (2000-2001) of simulated temperatures (A), measured temperatures (B) and a comparison (C).

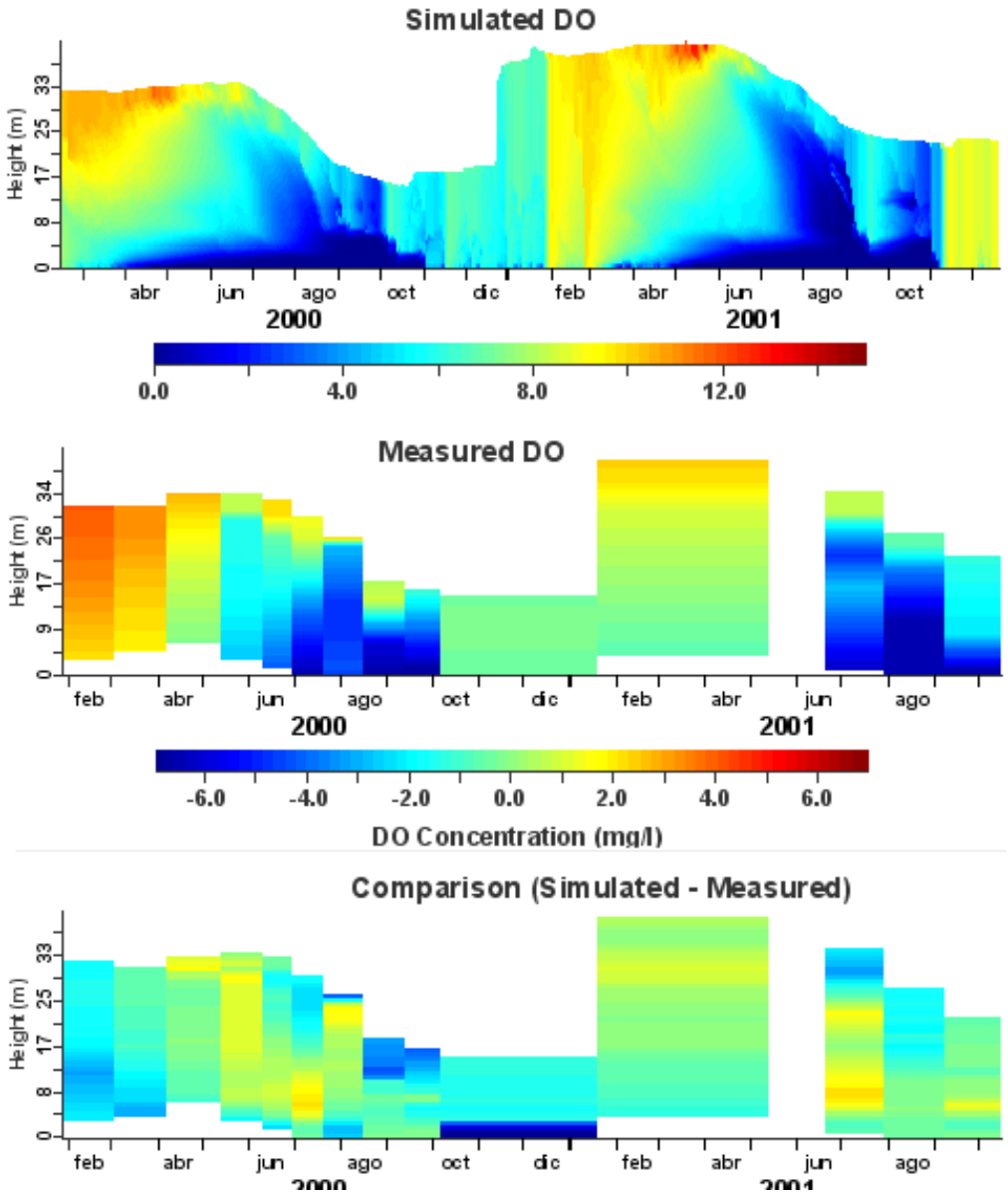

Figure 5. 8 Two years (2000-2001) of simulated DO (A), measured DO (B) and a comparison (C).

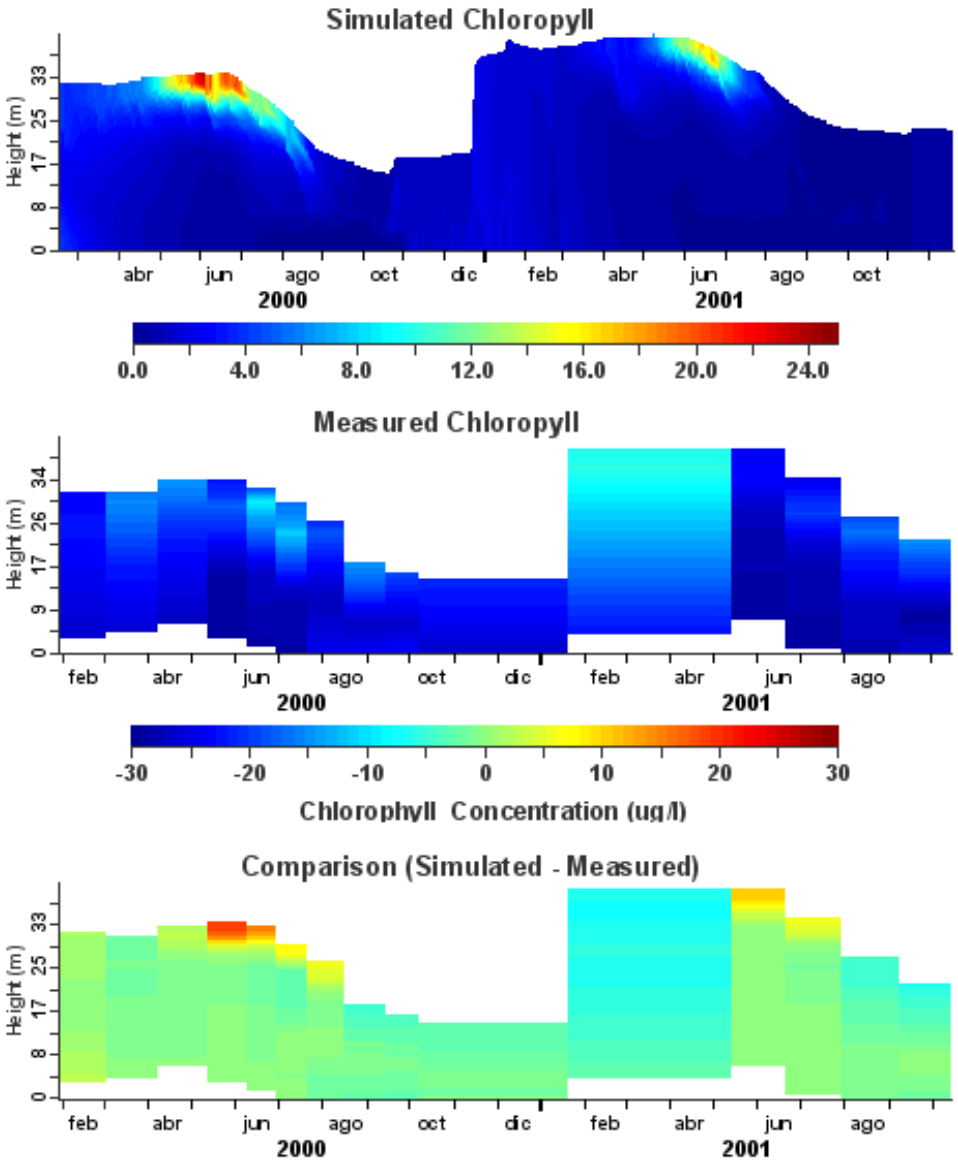

Figure. 5.9 Two years (2000-2001) of simulated chlorophyll (A), measured chlorophyll (B) and a comparison (C).

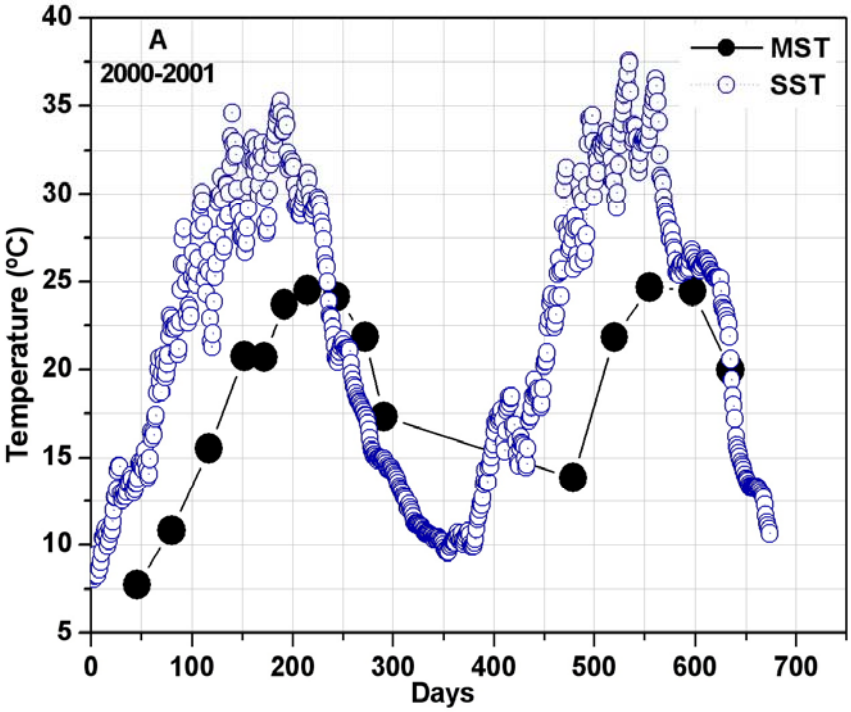
A
2000-2001
MST
SST
Temperature (ºC)
Days
40
35
30
25
20
15
10
5
0
100
200
300
400
500
600
700

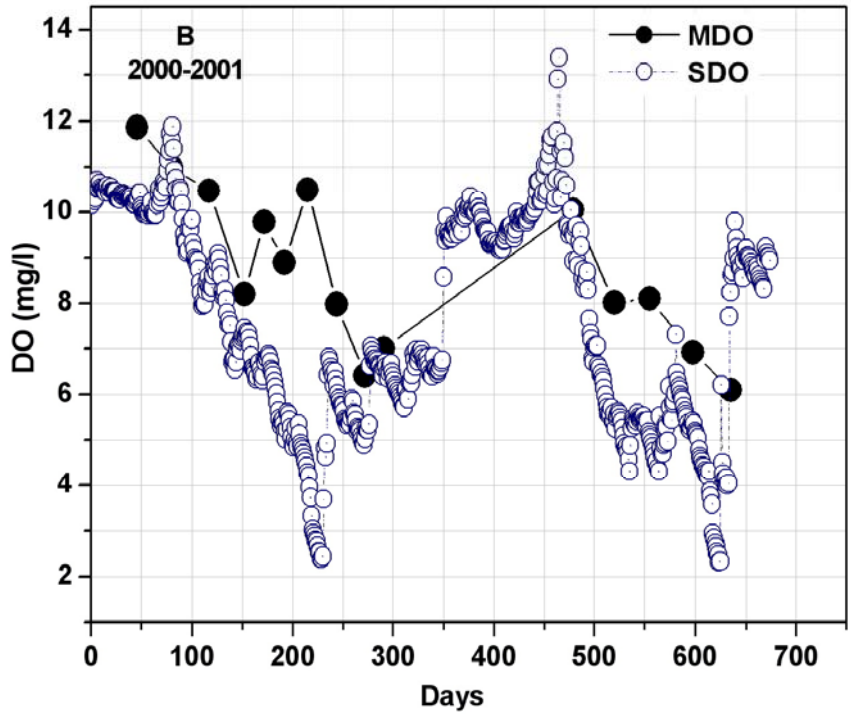
B
2000-2001
MDO
SDO
DO (mg/l)
Days
14
12
10
8
6
4
2
0
100
200
300
400
500
600
700

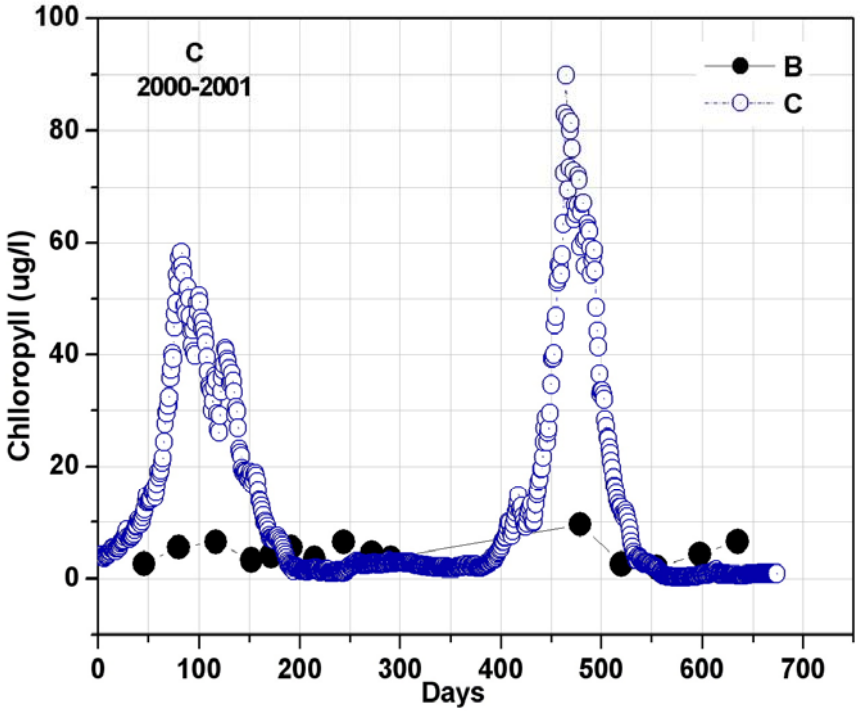

Figure 5.10 Comparison between water surface simulation (open circles) and observation (filled circles) of temperature (A), dissolved oxygen (B) and chlorophyll (C).

5.6 Conclusion

As it has been said about the Sau Reservoir in Chapter 4, the DYRESM-CAEDYM model requires daily inflow data for temperature and concentrations of dissolved oxygen, nutrients and chlorophyll. However, there was a lack of real measurement of these concentrations so it is worthwhile to admit such a hypothesis. In the chlorophyll case as it was done in Sau Reservoir our hypothesis is based on the idea of using variable reservoir profiles to deduce daily concentrations throughout the simulation period. So, the chlorophyll concentrations were considered as the long-term mean of the in-lake concentrations. However, in Boadella Reservoir there is sometimes a lack, even in the reservoir profiles and especially for dissolved inorganic phosphorous, so the comparison is difficult to speculate about it and the phosphorus inflow concentration were taken as those of Sau Reservoir.

Hence, after a long calibration process and validation we could say that the DYRESM-CAEDYM is truly a helpful tool for understanding hydrodynamic, nutrient and

phytoplankton dynamics. Also, the model generally produced relatively same tendency in temperature, dissolved oxygen and far a way tendency in chlorophyll case.
Unfortunately, this difference between simulated and observed values my be linked to many factors such as measuring input data accuracy, estimation of daily inflow water quality concentrations of nutrients from water quality profiles in reservoir. Likewise, neglecting some parameters like nutrient groundwater seepage used in the irrigation regions perimeters surrounding the catchments area of reservoir, additionally, some type of phytoplankton that has not been taken into account in our modelling but that could interfere and worsen the simulation. Finally, limitation of one dimensional assumption which might be influences such difference. Therefore, tow dimension 2D modelling would be of advantage especially when modelling chlorophyll.

Finally, one can conclude that combine model DYRESM-CAEDYM gives better simulation results for almost of parameters such as temperature, dissolved oxygen, a good tendency for dissolved organic phosphorous and small divergence in reproducing the seasonal variation of biomass of the phytoplankton in the Sau Reservoir than in the Boadella Reservoir. Apparently, the Sau Reservoir is well monitored and most of the data needed for simulation is available, while there is not any complete data for the Boadella Reservoir. However, for a future DYRESM-CAEDYM user may need such additional improvement to obtain a good simulation this will be subordinate to daily river inflow data. As it was mention by (Vidal et Om 1993), (Armengol et al. 1994), (Hmilton et al.1995), (Armengol et al. 1994) and (Armengol et al. 2003). Therefore, input data of river inflow should be primordial.

GENERAL CONCLUSIONS

Application of 1D hydrodynamic model linked to water quality model to different reservoirs, such as Sau and Boadella, shows that the principal external forces especially wind velocity and the river inflow were the major forces affecting the hydrodynamic. In order to apply the water quality model to the reservoirs, daily concentrations of dissolved oxygen, nutrients, and chlorophyll in the river inflow must be known; however, this was not the case for both reservoirs. It is therefore necessary to establish a hypothesis. Our hypothesis for the estimation of daily river water quality concentration was based on the available reservoirs water quality profiles. For every month's water quality profile we take the mean concentrations and use the most repeated one as the daily concentration constant over the simulation period. However, an important recommendation for future work on modelling the hydrodynamics and water quality of the Sau and Boadella reservoirs is to have more accurate and regular field data. The main conclusions of our work are described below.

- We have used non dimensional numbers (Lake number, Wedderburn number, Burger number, inflow number and outflow number) to characterize the dynamical regimes of the Sau and Boadella reservoirs. Both reservoirs have high lake numbers; this indicates that meteorological forces, especially wind velocity, were relatively small resulting in less momentum being transferred to the surface which causes less mixing in the surface layer. Notwithstanding, the Wedderburn numbers for both of the reservoirs are small; this means that the wind will induce higher vertical mode oscillations. The estimation of lake numbers and Wedderburn numbers are respectively depending on the centre of thermocline and diurnal water depth which are both difficult to estimate from observed water temperature profiles, additionally estimation of daily water temperature profiles from existing profiles is not a bad solution however doesn't reflect totally the reality. The Burger numbers are slightly larger than one, indicating that rotation effect is discarded.

  Regarding the inflow Froude numbers, those for the Sau and Boadella reservoirs are smaller than unity indicating that the inflow separates as an underflow or an

overflow. Finally, the outflow Froude numbers of Sau and Boadella are smaller than unity, feeding speculation that water is removed via a thin layer adjacent to the level of the outflow, making this a selective withdrawal. The estimation of non dimensional numbers such as lake number, wedderburn number, burger number and inflow/outflow numbers are useful tool for characterising the dynamical regime of reservoir.

- Application of DYRESM-CAEDYM to the Sau Reservoir gives a good simulation of thermal structure and dissolved oxygen but only a general view of trends in phosphorus and chlorophyll. It underpredicts the phosphorus in the hypolimnion; this is most likely because the effect of the suspended solids carried out by the river inflow. The chlorophyll is difficult to calibrate because of its dependency on temperature, dissolved oxygen and phosphorus. The model overpredicts the chlorophyll concentrations during the stratified period and underpredicts them in the mixed layer during the mixing period; this might be due to the limitation of the one dimensional model or some type of phytoplankton that has not been considered in our simulation. Our work based on our hypothesis for the estimation of daily river water quality concentration however, in future simulation might be improved rigorously if we depose observed daily inflow nutrient concentrations.

- Application of DYRESM–CAEDYM to the Boadella Reservoir reveals that the thermal structure is not as well predicted as in the Sau Reservoir, especially in stratification periods, probably due to fact that Boadella in this period is considered to be shallow (water depth=14m) so heat transfer occurs rapidly and the water column moves a large quantity of energy from the water surface to the bottom of the reservoir. Additionally, there are two rivers supplying Boadella reservoir, the Arnera and the Muga, with different water inflow temperatures which might cause such temperature differences between simulated and observed. It has to be noted that in our simulation we considered only one river. The dissolved oxygen, however, was well simulated and the chlorophyll is better simulated in comparison with the Sau Reservoir. The phosphorus is not considered due to the lack of observed data. It is therefore obvious that the

predictive capacity of the model was not maximized completely due to a lack of extensive field data.

- DYRESM-CAEDYM was calibrated and validated separately for the Sau and Boadella reservoirs Although it can be considered an adequate tool to simulate the hydrodynamic effect on the water quality in a long time scale

- The magnitude of contribution of the ground water to the water and nutrient budget of Sau and boadella reservoirs is unknown. Here, it has been neglected. Water quality variables such as nutrients concentrations were not available. Further improvements in representing groundwater contribution may be worth considering future developments for long-term simulations.

- Sau reservoir posses observed data sets relatively complete. However, a major particular deficiency was in the daily water quality data for the inflows. Lacking data were filled making some hypothesis of the nutrient determination such as phosphorus. Despite, model produced some interesting results which confirm that it is possible to successfully calibrate DYRESM-CAEDYM for its intended use to predict simulated temperature and dissolved oxygen, phosphorous, and chlorophyll. Whereas, for Boadella reservoir, the lack of measurement of nutrient of two rivers make it not be possible to evaluate a full performance of the model. As (Vidal et Om. 1993), (Armengol et al. 1994, 2003) and (Han et al. 2000) found after application of DYRESM to the Sau reservoir, how the river is the main factor controlling the thermal structure in the reservoir. In contrast, it appears that the simulated results for Boadella reservoir were sufficiently close to the few measured values especially for temperature, dissolved oxygen.

- A coupled hydrodynamic and ecological water quality model DYRESM-CAEDYM is the significant advance on previous models that seek to predict water quality in lakes and reservoirs. Thus, through applying DYRESM-CAEDYM to Sau and Boadella we have provided a starting point for predicting thermal structure, dissolved oxygen, phosphorus and chlorophyll. However, in future may be using such 2D model or 3D is worthy. For all possibilities of models and for future purposes, further monitoring of the catchment area, rivers

and reservoirs will be an advantage to produce high quality results which is subordinate to be done by close cooperation between modelers and field researchers. Aftermath it could be used to allow water resources managers to predict how will to respond to changes in water quality management regimes and environmental factors.

REFERENCES

Afres, W and L. Andreas. 2003. Small-scale Hydrodynamic in lakes
Ann.Rev.Fluid Mech. **35**: 373-412.

Amborosetti, W and L. Barbanti. 2001. Temperature, heat content, mixing and stability in Lake Orta: a pluriannual investigation. Limnol. **60**(1): 60-68.

Ambrosetti, W., L.Barbanti and N. Sala. 2003. Residence time and physical processes in lakes. Limnol. **62**(Suppl. 1): 1-15.

Aminot, A. And R. Kérouel. 2004. Dissolved organic carbon, nitrogen and phosphorus in the N-E Atlantic and the N-W Mediterranean with particular reference to non-refractory fractions and degradation. Deep-Sea Research. **I 51**: 1975-1999.

Amrosetti, W and L. Barbanti. 2002. Physical limnology of Italian lakes. 1. Relationship between morphometry and heat content. Limnol. **61**(2): 147-157.

Andradóttir, H. Ó and H. M. Nepf. 2000.Thermal mediation by littoral wetland and impact on lake intrusion depth. Water Ressources Research. **36**(3): 725-735.

Andrew, J. Tanentzap, D. P. Hamilton, and N. D. Yan. 2007. Calibrating the Dynamic Reservoir Simulation Model (DYRESM) and filling required data gaps for one-dimensional thermal profile predictions in a boreal lake. Limnol. Oceanogr.Methods. **5**: 484–494.

Antenucci, J. P and J. Imberger. 2003. The seasonal evolution of wind/internal wave resonance in Lake Kinneret Limnol. Oceanogr. **48**(5): 2055-2061.

Antenucci, J and A. Imerito. 2003 The CWR Dynamic Reservoir Simulation Model DYRESM. User Manual. Centre for Water Research. University of Western Australia.

Antenucci, J., and A. Imerito. 2002 The CWR Dynamic Reservoir Simulation Model DYRESM. Science Manual. Centre for Water Research. University of Western Australia.

Appt, J., J. Imberger, and H. Kobus. 2004. Basin-scale motion in stratified upper Lake Constance. Limnol.Oceanogr. **49**(3): 919-933.

Armengol, J., J. Toja, J., and A. Vidal. 1994. Seasonal rhythm and secular changes in Spanish reservoirs. In "Limnology Now: A Paradigm of Planetary Problems." (R. Margalef, ed.), 237-253. Elsevier science

Armengol, J., M. Comerma, J.C. Gracía, M. Romero, J.J. Rodriguez and A. Vidal 1999. Contribució al coneixement de l'ecologia acuática de l'embassament de Sau evoluciò de l'embassament al 1998. Aigües Ter de Llobregat. pp 66

Armengol, J., M. Comerma, J.C. Gracía, M. Romero, J.J. Rodriguez and A. Vidal 2000. Contribució al coneixement de l'ecologia acuática de l'embassament de Sau evoluciò de l'embassament al 1999. Aigües Ter de Llobregat. pp 118.

Armengol, J., J. Gracia, M. Comerma, M. Romero, J. Dolz, M. Roura, B. P. Han, A. Vidal and K. Simek. 1999. Longitudinal Processes in Canyon Type Reservoirs: The Case of Sau (N.E. Spain). Theoretical Reservoir Ecology and its Applications 313-345

Balistrieri, L., R.Tempel, L Stillings and L. Shevenell. 2006. Modelling spatial and temporal variations in temperature and salinity during stratification and overturn in Dexter pit lake, Tuscarora, Nevada, USA. Applied Geochemistry. **21** 1184-1203.

Bruce, L. C., D Hamilton, J. Imberger, G. Gal, M. Gophen, T. Zohary and K. D. Hambright. 2006 A numerical simulation of the role of zooplankton in C, N and P cycling in Lake Kinneret, Israel. Ecological Modelling.**193**. 412-436.

Carr, G. M., H.C. Duthie and W.D. Taylor. 1997. Models of aquatic plant productivity: a review of the factors that influence growth. Aquatic Botany. **59** 195-215.

Casmitjana, X., T. Serra, J. Colomer, C. Baserba and J. Pérez-Losada. 2003. Effects of the water withdrawal in the stratification patters of a reservoir. Hydrobiologia. **504**: 21-28.

Casamitjana, X., T. Serra, M. Soler, J. Colomer. 2002. A study of the evolution of the particle boundary layer in a reservoir, using laser particle sizing. Water Research **36**: 4293-4300.

Chan, T. U., D. P. Hamilton, B J. Robson, B. R, Hodges and Chris. Dallimore. 2002. Impacts of hydrological Changes on Phytoplankton Succession in the Swan River, Western Australia. Estuaries. **25**(68): 1406-1415.

Chao. X., Y. Jia, F. D. Shields Jr, S. S.Y. Wang and C. M. Cooper.2007. Numerical modelling of water quality and sediment related processes. Ecological modelling. **201**: 385-397

Chapelle, A., A. Ménesguen, JM. Deslous-Paoli, P. Souchu, N. Mazouni, A. Vaquer and B. Millet. 2000. Modelling nitrogen, primary production and oxygen in a Mediterranean lagoon. Impact of oysters farming and inputs from the watershed. Ecological Modelling **127:** 161-181.

Cobelas, M. A., A. Baltanás, J. L. Velasco and C. Rojo. 2002. Daily variations in the optical proprieties of small lake. Freshwater Biology **47**: 1051-1063.

Colomer, J., E. Roget and X. Casamitjana 1996. Daytime heat balance for estimating non-radiative fluxes of lake Banyoles, Spain. Hydrological Processes. **10**: 721-726.

Colomer, J., T. Serra, M. Soler and X. Casamitjana. 2002. Sediment fluidization events in a lake caused by large monthly rainfalls Geophysical research Letters. **29**, 0.1029/2001GL014299

Colomer, J., T. Serra, M. Soler, X. Casamitjana. 2003. Hydrothermal plumes trapped by thermal stratification Geophysical Research Letters **30**(21): 2092,

Comerma, M., J. C. Garc, M. Romero, J. Armengol, K. Šimek.2003. Carbon flow dynamics in the pelagic community of the Sau Reservoir (Catalonia, NE Spain). Hydrobiologia **504**: 87-98.

Dallimore, C. J., B. R. Hodges and J. Imberger. 2003 Coupling an Underflow Model to a Three-Dimensional Hydrodynamic Model. Journal of Hydraulic Engineering, ABCE. **748**

Dallimore, C. J., J. Imberger and B. R. Hodges. 2004 Modeling a Plunging Underflow Journal of Hydraulic Engineering. **130**(11): 1068-1076.

Dukowicz, J.K. 2000. Reduction of Density and Pressure Gradient Errors in Ocean Simulations. Journal of Physical Oceanography. **31**: 1915-1921

Duras, J and J. Hejzlar. 2001. The effect of outflow depth on phosphorous retention in a small, hepertrophic temperate reservoir with short hydraulic residence time International Rev. Hydrobiology **86**: 585-601.

Eckert, W., J. Imberger and A. Saggio. 2002. Biogeochemical response to physical forcing in the water column of a warm monomictic lake. Biogeochemistry. **61**: 291-307.

Elliott, J.A., A.E. Irish, and C.S Reynolds. 2001. The effects of vertical mixing on a phytoplankton community: a modeling approach to the intermediate disturbance hypothesis. Freshwater Biology. **46** (10): 1291-1297.

Etemad-Shahidi, A and J. Imberger. 2006. Diapycnal Mixing in the Thermocline of Lakes: Estimations by Different Methods. Environmental Fluid Mechanics. **6**: 227-240.

Ewing, T., T.R. Romero, J. Imberger, J. Antenucci and A. Deen. 2004. A real-time reservoir decision support system. (6th International conference on Hydro informatics World) scientific publishing Company, ISBN 981-238-787-0

Fernandes, R. L and J. Imberger. 2006. Bed roughness induced entrainment in a high Richardson number underflow. Journal of Hydraulic Research. **44**(6): 725-738.

Fischer, J. 1979. Modelling of water quality processes in lakes and reservoirs. Hydrological Sciences. **24**: 2-6.

Fleenor, W. E. 2001. Effects and Control of Plunging Inflows on Reservoir Hydrodynamics and Downstream Releases PhD thesis pp 160

Forty, J and J. Llebotz. 1996. Radiative transfer in the framework of extended irreversible thermodynamics J. Phys. **29**: 3427-3436.

Franke, U., K. Huter and K. Jöhnk, 1999, A Physical- biological Coupled Model for Algal Dynamics in Lakes. Bulletin of Mathematical Biology. **61**, 239-272.

Fricker, P.D and H.M. Nepf. 2000. Bathymetry, stratification, and internal seiche structure Journal of Geophysical research **105** (6) 14237-14251.

Fu, S. and B. R. Hodges. 2005. The Grid Scale Problem in Numerical Modeling of Flow Around Large Woody Debris in Rivers. University of Texas at Austin Graduate Student Research Conference. April 28, 2005

Gal, G., A. Parparov, U. Wagner and T. Rozenberg. 1999. Testing the impact of management scenarios on water quality using an ecosystems model. Ecological Modelling. **114**: 137-173.

Gal, G., J. Imberger, T. Zohary, J. P. Antenucci, A. Anis, and T. Rosenberg. 2003. Simulating the thermal dynamics of Lake Kinneret. Ecological Modelling. **162**(1-2): 69-86.

Gaedke, U. 1993. Ecosystem analysis based on biomass size distributions: a case study of plankton community in a large lake. Limnol. Oceanogr. **38**(1): 112-127.

Gelda, K. R. and S. W. Effler. 2002. Estimating oxygen exchange across the air–water interface of a hypereutrophic lake. Hydrobiologia. **487**: 243-254.

Gallerano, F., R. Ricci and P. Viotti. 1993. Analysis of the eutrophication trend in a deep lake. Ecological Modelling, **66**: 157-179.

Gemmrich, J. R and H.V. Haren. 2002. Internal wave band kinetic energy production flat vs. sloping bottom. Journal of Sea Research. **47**: 209-222.

Gunkel, G., J. Casallas. 2002. Limnology of an equatorial high mountain lake-Lago san Pablo Ecuador: The significance of deep diurnal mixing for lake productivity. Limnologica .**32**: 33- 43.

Haggard, B. E., P. A. Moore, T. C. Daniel and D. R. Edwards. 1999. Trophic Conditions and Gradients of the Headwater Reaches of Beaver Lake, Arkansas Proc. Okla. Acad. Sci. **79**: 73-84.

Han, B. Joan Armengol, J. Garcia, M Comerma, M. Roura, J. Dolz and M. Straskraba. 2000. The thermal structure of Sau Reservoir (NE: Spain): a simulation approach. Ecological Modelling. **125:** 109-122.

Hâkanson, L. 2005. The Importance of Lake Morphometry for the Structure and Function of Lakes. Internat. Rev. Hydrobiol. **90**(4): 433-461.

Hamilton, D and G. Schladow. 1995. Controlling the indirect effects of flow diversion on water quality in an Australian reservoir. Environment International, **21** (5): 583-590.

Hipsey, M. R., J. R. Romero, J. P. Antenucci and D. Hamilton. 2005. Computational Aquatic Ecosystem Dynamics Model: CAEDYM v2. Science Manual. Centre for Water Research. University of Western Australia.

Hodges, B. R. 1998. Heat budget and thermodynamics at a free surface. Centre for Water Research, the University of Western Australia, Ben Hodges working manuscript, June 9, 1998.

Hodges, B. R. 2000. Recirculation and the equilibrium displacement of the thermocline in a wind-driven stratified lake.5th International Symposium on Stratified Flows, Canada, July-10-13.

Hodges, B. R.2004. Accuracy Order of Crank-Nicolson Discretization for Hydrostatic Free- Surface Flow. Journal of Engineering Mechanics ABCE. **804.**

Hodges, B. R., J. Imberger, A. Saggio and K.B. winters. 2000. Modeling basin-scale internal waves in a stratified lake. Limnol Oceanogr. **45(7)**: 1603-1620.

Hodges, B. R and S. K. Delavan. 2004. Numerical Diffusion in Hydrostatic Models of Internal Waves. 17th ASCE Engineering Mechanics Conference, June 13-16, 2204, University of Delaware, Newark, DE, EM.

Hodges, B. R., J. Imberger, B. Laval and J. Appt. 2000. Modelling the Hydrodynamics of Stratified Lakes. Hydroinformatics 2000 Conference, Iowa Institute of Hydraulic Research, 23-27.

Hodges, B. R. and J. Imberger. 2001. Simple Curviline Method for Numerical Methods of Open channels. Journal of Hydraulic Engineering. **884**

Hodges, B. R., B. Laval and B M. Wadzuk. 2006. Numerical error assessment and a temporal horizon for internal waves in a hydrostatic model. Ocean Modelling **13**: 44-64.

Hodges, B. R. and R L. Street. 1998. Wave-Induced Enstrophy and Dissipation in a Sheared Turbulent Current. 13th Australian Fluid Mechanics Conference, Monash University, Melbourne, Australia, 13-18 December 1998. Editors: M.C.Thomson and K. Hourigan, **2**: 717-720

Hondzo, M and H. G. Stefan. 1996. Long-term lake water quality predictors.
Water research. **30** (12) 2835-2852.

Hurtado, J. V. Basin-Scale Hydrodynamics in a Mediterranean reservoir. Implications for the phytoplankton dynamics. PhD Theses. University of Girona. 133 pp.

Imberger, J. 1994. Transport processes in lakes. Limnology Now: A Paradigm of Planetary Problems." (R. Margalef, ed.) 99-193. Amsterdam: Elsevier science

Imberger, J. 2001. Characterizing the dynamical regimes of a lake
6th Workshop on physical Process in Natural Waters University of Girona: 77-92

Jellison, R and J. M. Melack. 1993. Meromixis in hypersaline Mono Lake, California.1- Stratification and vertical mixing during the onest, persistence, and breakdown of meromexis, Limnol.Oceanogr. **38**(5): 1008-1019.

Joaquim, P., E. Roget and X. Casamitjana. 2003. Evidence of High Vertical Wave-Number Behaviour in a Continuously Stratified Reservoir: Boadella, Spain. Hydraulic Engineering 737

Jorgensen, S. E. 1998. An improved parameter estimation procedure in lake modelling. Lakes & Reservoirs. Research and Management. **3**: 139-142.

Kagalou, I., G. Economidis, I. Leonardos and, C. Paploukas. 2006. Assessment of a Mediterranean a shallow lentic ecosystem (Lake Pamvotis, Greece) using benthic community diversity: Response to environmental parameters. Limnologica. **36**: 269-278.

Ken Mori, B. Q. Lap. 2007. A two-dimensional numerical model of wind-induced flow and water quality in closed water bodies. Paddy Water Environ. **5**:29-40.

Knauer, K., H. M. Nepf and H. F. Hemond. 2000. The production of chemical heterogeneity in Upper Mystic Lake. Limnol. Oceanogr. **45**(7): 1647-1654.

Kostic, S and G. Parker. 2003. Progradational sand-mud deltas in lakes and reservoirs. Part 1. Theory and numerical modelling. Journal of Hydraulic Research. **41**(2): 127-140.

Kulis, P S. and B.R. Hodges. 2005. Improved techniques for gravity Current Modelling. Proceeding of McMat 2005:2005 joint ASME/ASCE/SES Conference on Mechanics and Materials, June 1-3, 2005, Baton Rouge, Louisiana, USA

Kutser, T. 2004. Quantitative detection of chlorophyll in cyanobacterial blooms by satellite remote sensing. Limnol. Oceanogr. **49**(6): 2179-2189.

Laval, B., B. R. Hodges and J, Imberger. 2000. Numerical Diffusion in Stratified Lake Models. In proceedings of the Fifth International Symposium on Stratified Flows, Vancouver, Canada, July 7-11, 2000: 343-348

Laval, B., B. R. Hodges and J. Imberger. 2003. Reducing Numerical diffusion Effects with Pycnocline Filter. Journal of Hydraulic Engineering, ABCE. **216.**

Laval, B. E., J. Imberger and A. N. Findikakis. 2005. Dynamics of a large tropical lake: Lake Maracaibo. Aquat. Sci. **67**: 337-349.

Laval, B., J. Imberger, B. R. Hodges and R. Stocker. 2003. Modeling circulation in lakes: Spatial and temporal variations. Limnol Oceanogr **48(3)**: 983-994.

Lewis, D.M. 2005. A simple model of plankton population dynamics coupled with a LES of the surface mixed layer. Theoretical Biology **234** 565-591.

Lewis, D. M., J. D. Brookes and M. F. Lambert. 2004. Numerical models for management of Anabaena circinalis. Journal of Applied Phycology. **16**: 457-468.

Livingstone, D. M. 2003. Impact of secular climate change on the thermal structure of large temperate central European Lake. Climatic Change. **57**: 205-225.

Lonin, S. A and Y. S. Tuchkovenko. 2001. Water quality modelling for the ecosystem of the Cienagade Tesca coastal lagoon. Ecological Modelling. **144**: 279-293.

Lorke, A., B. Müller, M. Maerki and A. Wüest. 2003. Breathing sediments: The control of diffusive transport across the sediment–water interface by periodic boundary-layer turbulence. Limnol. Oceanogr. **48**(6): 2077-2085.

Lorke, A., K. Tietze, M. Halbwachs and A. Wüest. 2004. Response of Lake Kivu stratification to lava inflow and climate warming. Limnol. Oceanogr. **49**(3): 778-783.

Lorke, A.1998. Investigation of turbulent mixing in shallow lakes using temperature microstructure measurements Aquatic. Science. **60**: 210-219.

Lorke, A., L. Umlauf, T. Jonas and A.Wüest. 2002. Dynamics of Turbulence in Low-Speed Oscillating Bottom-Boundary Layers of Stratified Basins. Environmental Fluid Mechanics **2**: 291-313.

Marcé, R., C. Feijoó, E. Navarro, J. Ordoñez, J. Gomà and J. Armengol. 2007. Interaction between wind-induced seiches and convective cooling governs algal distribution in a canyon-shaped reservoir. Freshwater biology. **52**: 1336-1352.

Macintyre, S., J.O. Sickman, S.A. Goldthwait, and G.W. Kling. 2006. Physical pathways of nutrient supply in a small, ultraoligotrophic arctic lake during summer stratification. Limnol. Oceanogr. **51**(2): 1107-1124.

Macintyre, S., K. M. Flynn, R. Jellison and J. R. Romer. 1999. Boundary mixing and nutrient fluxes in Mono Lake, California. Limnol. Oceanogr. **44**(3): 512-529.

Macintyre, S., J.R. Romero and G. W. Kling. 2002. Spatial- temporal variability in surface layer deepening and lateral advection in an embayment of Lake Victoria, east Africa. Limnol. Oceanogr. **47**(35): 656-671.

Mackenzie, B.R and T. Kiørboe. 2000. Larval fish feeding and turbulence: A case for the downside Limnol. Oceanogr. **45**(1): 1-10.

Macintyre, S and R. Jellison. 2001. Nutrient fluxes from upwelling and enhanced turbulence at the top of the pycnocline in Mono Lake, California. Hydrobiologia. **466**: 13-29.

Mackay, M. D. 2005. Regional Climate Impacts of Small Lakes: A Sub-grid scale Lake Module for Class. 15th International Northern Research Basins Symposium and Workshop. Luleá to Kvikkjokk, Sweden, 29Aug.-2 Sept.2005

Marti, C. L and J. Imberger. 2006. Dynamics of the benthic boundary layer in a strongly forced stratified lake. Hydrobiologia **568**: 217-233.

Mcginnis, D. F., A. Lorke, A. Wüest, A. Stöckli and J.C. Little .2004. Interaction between a bubble plume and the near filed in a stratified lake. Water Resources Research. Vol. **40**

Menwade, V.M., D.R. Maidement and B. R. Hodges.2005. Geospatial Representation of river channels. Journal of Hydrologic Engineering, ABCE. **243.**

Millero, F.J. 2000. The Equation of State of Lakes. Aquatic Geochemistry. **6**: 1-17.

Moshfeghi, H., A. Etemad-Shahidi and J. Imberger. 2005. Modelling of bubble plume destratification using DYRESM. Journal of Water Supply: Reserch and Technology-AQUA **54**(1)**:** 37-46

Muhammetoglu, A. B and S. Soyupak. 2000. A three-dimensional water quality-macrophyte interaction model for shallow lakes. Ecological Modelling **133**: 161-180

Murdock, J. D. Roelke and F. Gelwick. 2004. Interaction between flow, periphton, and nutrients in a heavy urban stream: implications for stream restoration effectiveness Ecolological Engineering, **22**: 194-207.

Na, E. H and, S. S. Park. 2006. A hydrodynamic and water quality modeling study of spatial and temporal patterns of phytoplankton growth in a stratified lake with buoyant incoming flow. Ecological modelling **199**: 298-314

Nedoma, J., J. C. García, M. Cnmerma, K. Šimek, J. Armengol. 2006. Extracellular phosphates in a Mediterranean reservoir. Seasonal, spatial and kinetic heterogeneity. Freshwater Biology. **51**: 1264-1276.

Nepf, H. M., E. W. Koch. 1999. Vertical secondary flows in submersed plant-like arrays Limnol. Oceanogr. **44**(4), 1072-1080.

Okely, P., J. Imberger. 2007. Horizontal transport induced by upwelling in a canyon-shaped reservoir. Hydrobiologia. **586**: 343-355.

Ostrovsky, I., Y. Z. Yacobi, P. Walline and I. Kalikhman. 1996. Seiche-induced mixing: its impact on lake productivity. Limnol. Oceanogr. **41**(2): 323-332.

Palmer, M. R., H. M. Nepf, T. J. R. Pettersson and J. D. Ackerman. 2004. Observations of particle capture on a cylindrical collector: Implications for particle accumulation and removal in aquatic systems. Limnol. Oceanogr. **49**(1): 76-85.

Prandke, H and A. Stips. 1998. Test measurements with an operational microstructure turbulence profiler: Detection limit of dissipation rates. Aquat.sci.**60:** 191-209.

Priyantha, D. T. Asaeda, S. Saitoh and K. Gotoh. 1997. Modelling effects of curtain method on algal blooming in reservoirs Ecological Modelling **98**: 89-104.

Quesada, A., F. Jüttner, T. Zotina, A. P. Tolomeyev and A. G. Degermendzhy. 2002. Heterotrophic capability of a metalimnetic plankton population in saline Lake Shira (Siberia, Khakasia). Aquatic Ecology **36**: 219-227.

Rajar, R and M. Cetina. 1997. Hydrodynamic and water quality modelling: An experience. Ecological Modelling **101**: 195-207.

Rajar, R. M. Cetina and A. Sirca. 1997. Hydrodynamic and water quality modelling: case studies. Ecological Modelling **101**: 209-228

Ramírez, J. J and C. E. M. Bicudo. 2005. Diurnal and spatial (vertical) dynamics of nutrients (N, P,Si) in four sampling days (summer, fall, winter, and spring) in a tropical shallow reservoir and their relationships with the phytoplankton community. Braz. J. Biol, **65**(1): 141-157.

Reynolds, C. S. 1999. Modelling phytoplankton dynamics and its application to lake management. Hydrobiologia. **395/396**: 123-131.

Reichart, I and M. Simon. 1996. Horizontal variability of bacterioplankton growth dynamics in a large lake. Aquat. Microb. Ecol. **11**: 31-41.

Robertson, D. M. and J. Imberger. 1994. Lake Number, a Quantitative Indicator of Mixing Used to Estimate Changes in Dissolved Oxygen. Int Revue ges. Hydrobiol. **79**: 159-176.

Robson, B. J and D. P. Hamilton. 2004. Three-dimensional modelling of a Microcystis bloom event in the Swan River estuary, Western Australia Ecological Modelling. **174**: 203-222.

Roget, E., G. Salvude and F. Zamboni.1997. Internal seiche climatology in a small lake where transversal and second vertical modes are usually observed seiche. Limnology. Oceanogr. **42**(4d): 663-673.

Roget, E., I. Lozovatsky, X. Sanchez and M. Figueroa. 2006. Microstructure measurements in natural waters: Methodology and applications Progress in Oceanography **70**: 126-148.

Romero, J. R and J. M. Melack. 1996. Sensitivity of vertical mixing in a large saline lake to variations in runoff. Limnol. Oceanogr. **41**(5): 955-965.

Romero, J. R., C.P. dallimore, J.P. Antenucci, D.P, Hamilton, J. Imberger, D.A. Hora and A. Deen. Application of 1D and 3D Hydrodynamic Models Coupled to an Ecological Model to Two Water Supply Reservoirs. Sydney Catchment Authority, Penrith, NSW 2750: 307-312

Røy, H., M. Hüttel and B. B. Jørgensen. 2002. The role of small-scale sediment topography for oxygen flux across the diffusive boundary layer. Limnol. Oceanogr. **47**(3): 837-847

Romero, J.R., J.P. Antenucci and J. Imberger. 2004. One- and three-dimensional biogeochemical simulations of two differing reservoirs Ecological Modelling. **174**: 143-160.

Romero, J. R. and J. Imberger. 2003. Effect of a flood underflow on reservoir water quality: Data and three-dimensional modelling. Arch. Hydrobiol. **157** 11-25.

Rueda, F.J., E. Moreno-Ostos and J. Armengol. 2006. The residence time of river water in reservoirs. Ecological Modelling. **191**: 260-274.

Saiz, E., A. Calbet and E.Broglio. 2003. Effects of small-scale turbulence on copepods: The case of Oithona davisae .Limnol. Oceanogr. **48**(3): 1304-1311.

Salençon, M. J and J.M. 1997. Thébault. Modélisation d'écosystème Lacustre (Application á la retenue de Pareloup (Aveyron)) : 3-104

Salmaso, N., R. Mosello, L. Garibaldi, F. Decet, M.C.Brizzio and P. Cordella. 2003. Vertical mixing as a determinant of trophic status in deep lakes: a case study from two lakes south of the Alps (Lake Garda and Lake Iseo) Limnol. **62**(Suppl. 1): 33-41.

Sànchez, X and E. Roget. 2007. Microstructure measurements and heat flux calculations of a triple-diffusive process in lake within the diffusive layer convection regime. Geophysical research **112**, C02012

Schallenberg, M., U. Friedrich and C. W. Burns. 2001. Postulated responses of phytoplankton and bacteria to predict increase of inorganic suspended sediments in ologotrophic lakes. New Zealand journal of marine and freshwater research. **35:** 763-779.

Schladow, G. S and D. P Hamilton. 1997. Prediction of water quality in lakes and reservoirs: Part I- Model description. Ecological Modelling. **96**: 91-110.

Schladow, G. S and D.P. Hamilton. 1997. Prediction of water quality in lakes and reservoirs: Part II- Model calibration, sensitivity analysis and application.
Ecological Modelling **96**: 111-123.

Schmida, M., A.Lorkea, C. Dinkela, G. Tanyilekeb and A. Wüest. 2004. Double-diffusive convection in Lake Nyos, Cameroon. Deep-Sea Research I **51:** 1097-1111.

Serra, T., J. Colomer, C. Baserba, M. Soler and X. Casamitjana. 2002 Quantified distribution of diatoms during the stratified period of Boadella reservoir. Hydrobiologia **489**: 235-244.

Serra, T., J. Vidal, X. Casamitjana, M. Soler, J. Colomer. 2007. The role of surface vertical mixing in phytoplankton distribution in a stratified reservoir. Limnol. Oceanogr. **52**(2): 000-000

Serra,T., M. Soler, R. Julia, X. Casamitjana, J. Colomer. 2005. Behaviour and dynamics of a hydrothermal plume in Lake Banyoles, Catalonia, NE Spain. Sedimentology. **52**: 795-808.

Serra, T., T. Granata, J. Colomer, A. Stips, F. Møhlenberg and X. Casamitjana. 2003 The role of advection and turbulent mixing in the vertical distribution of phytoplankton. Estuarine, Coastal and Shelf Science **56**: 53-62.

Shipeng, F. and B. R. Hodges. 2005. Grid-Scale dependency of Subrid-Scale Structure effects in Hydraulic Models of Rivers and Streams. Proceeding of McMat2005:2005 joint ASME/ASCE/SES Conference on Mechanics and Materials, June 1-3, 2005, Baton Rouge, Louisiana, USA

Simona, M. 2003. Winter and spring mixing depths affect the trophic status and composition of phytoplankton in the northern meromictic basin of Lake Lugano Limnol., **62**(2): 190-206.

Soyupak, S., L. Mukhallalati, D. Yemien, A. Bayar and C. Yurteri. 1997. Evaluation of eutrophication control strategies for the Keban Dam Reservoir. Ecological Modelling **97**: 99-110

Stocker, R and J. Imberger. 2003. Horizontal transport and dispersion in the surface layer of a medium- sized lake. Limnol. Oceanogr. **48**(3): 971-982.

Straskraba, M and G. Hocking. 2002. The effect of theoretical retention time on the hydrodynamics of deep river valley reservoirs. International Review of Hydrobiology. **87** (1): 61-83.

Tada, K., S. Pithakpol, K. Ichemi and S. Montani. 2000. Carbon, nitrogen, phosphorous, and chlorophyll a content of large diatom, coscinodiscus wailesii and its abundance in the seto inland sea, Japan. Fisheries science. **66**: 509-514.

Tarela, P. A and A.N. Menéndez 1999 A model to predict reservoir sedimentation Lakes &reservoirs Research and Management

Tufford, D. L. and H. N. Mckellar. 1999. Spatial and temporal hydrodynamic and water quality modeling analysis of a large reservoir on the South Carolina (USA) coastal plain. Ecological Modelling **114**: 137-173.

Vidal, J., X. Casamitjana, J. Colomer and T. Serra 2005 The internal wave field in Sau reservoir: Observation and modeling of a third vertical mode. Limnol. Oceanogr. **50**(4):1326-1333.

Varus, S. J., R. H. Wynne and J. A. Foley. 1996. Measuring the sensitivity of south Wisconsin lake ice to climate variations and lake depth using a numerical model. Limnol. Oceanogr. **41**(5). 822-831

Wadzuk, B. M., B.R. Hodges. 2003. Comparing Hydrostatic and Non hydrostatic Navier-Stokes Models of Internal Waves. 16th ASCE Engineering Mechanics Conference, University of Washington, Seattle, electronic Proceedings

Wadzuk, B. M and B. R. Hodges. Model Bathymetry for Sinuous, Dendritic Reservoirs. 6th International workshop on Physical Processes in Natural waters, June 27- 29, Girona, Catalonia, Spain

Wadzuk, B. M and B. R. Hodges. 2004 .Isolation Of Non-Hydrostatic Regions with a Basin. 17th ASCE Engineering Mechanics Conference, June 13-16, 2004, University of Delaware, Newark, de EM 2004

White, L., B. R. Hodges. 2005. Filtering the signature of submerged large woody debris from bathymetry data. Journal of Hydrology. **309**: 53-65.

White, B. L and H.M. Nepf. 2003. Scalar transport in random cylinder arrays at moderate Reynolds number. J. Fluid Mech. **487**: 43-79.

Wiegand, R.C and V. Chamberlain. 1987. Internal waves of the second vertical mode in a stratified lake. Limnol. Oceanogr. **32**(1): 29-42.

Williams, C. S., Stephens and B. Waugh. 2005. Field calibration of a formula for entrance mixing of river inflows to lakes: Lake Taupo, North Island, New Zealand. Marine and Freshwater Research. **39**: 785-802.

Wolk, F., H. Yamazaki, L. Seuront and R.G. Lueck. 2002. A New Free-Fall Profiler for Measuring Biophysical Microstructure Atmospheric and oceanic technology. **19**: 780-793.

Wilson, B. W. 1972. Seiches in Advances in Hydrosciences, edited by V. T. Chow. Academic, San Diego, Calif. pp. 1-94.

Winterwerp, J.C. 1998. A simple model for turbulence induced flocculation of cohesive sediment. J. Hydraulic Res. **36**: 309-326.

Wüest, A. G., Piepke and D.C. Van Senden. 2000. Turbulent kinetic energy balance as a tool for estimating vertical diffusivity in wind-forced stratified waters. Limnol. Oceanogr. **45**: 1388-1400.

Yeates. P.S., J. Imberger. 2003. Pseudo two-dimensional simulations of internal and boundary fluxes in stratified lakes and reservoirs. Intl.J.River Basin Management. IAHR and INBO. **1** (4). 297-319.